UNIVERSIDADE FEDERAL DE SÃO CARLOS
CENTRO DE CIÊNCIAS EXATAS E DE TECNOLOGIA
DEPARTAMENTO DE QUÍMICA
PROGRAMA DE PÓS-GRADUAÇÃO EM QUÍMICA

SUPRAMOLECULAR SYNTHESIS AND CHARACTERIZATION OF NEW MULTICOMPONENT FORMS OF FLUCONAZOLE

Bolaji Charles Dayo Owoyemi*

Tese apresentada como parte dos requisitos para obtenção do título de DOUTOR EM CIÊNCIAS, área de concentração: QUÍMICA ANALÍTICA.

Orientador: Prof. Dr. Renato Lajarim Carneiro

* Bolsista CNPq

São Carlos - SP
2020

UNIVERSIDADE FEDERAL DE SÃO CARLOS

Centro de Ciências Exatas e de Tecnologia
Programa de Pós-Graduação em Química

Folha de Aprovação

Defesa de Tese de Doutorado do candidato Bolaji Charles Dayo Owoyemi, realizada em 30/06/2020.

Comissão Julgadora:

Prof. Dr. Renato Lajarim Carneiro (UFSCar)

Prof. Dr. Paulo de Sousa Carvalho Júnior (UFMS)

Prof. Dr. Marcello Garcia Trevisan (UNIFAL)

Prof. Dr. Tiago Venâncio (UFSCar)

Prof. Dr. Fillipe Vieira Rocha (UFSCar)

O presente trabalho foi realizado com apoio da Coordenação de Aperfeiçoamento de Pessoal de Nível Superior - Brasil (CAPES) - Código de Financiamento 001.
O Relatório de Defesa assinado pelos membros da Comissão Julgadora encontra-se arquivado junto ao Programa de Pós-Graduação em Química.

“Education is an investment essential to empowering individuals to reach their full potential and to make their own positive impact on the world.”

– Connie Loo

“The more that you read, the more things you will know, the more that you learn, the more places you’ll go.”

– Dr. Seuss

To the blessed memory of my honest and loving dad….

Victor Adedayo Owoyemi

ACKNOWLEDGEMENT

My most appreciation goes to God Almighty for the gift of life and grace for making everything possible. My warmth appreciation goes to my parents Victor Adedayo and Philomena for their love, support, and the guidance through life. To my sisters Dr. Ifeloju and Omolola, and their spouses especially Dr. Segun Folarin. Also, to my nice and nephews; Afolabi, Samuel, Paulo and Ololade. I thank you all for your affection and unconditional love. To my fiancé Franciele and her family for their affections, care and love towards me. I appreciate you all.

Special thanks and appreciation go to my supervisor Prof. Dr. Renato Lajarim Carneiro, for the knowledge and teachings that I received during these years of academic development. Obviously, the trust and confidence you bestowed upon me was the courage that pushed me through the thick and thin. Apparently, you defined my academic career that would not have been possible without you.

I appreciate my friends and colleagues of the GQA, LABBES and LABIE, both present and past like Jorgito Armando, Federico, Marcão, Cecília, Benedito, Wallace and my good friends in LIEC; Francisco and Mario. It will be unjust to forget your assistances and academic advice that are important contributions.

Special thanks go to Egnr. Adeleke Adegbemile, for his support, his fatherly advice and importantly for his role in my academic pursuits. Thanks to my mentors, especially, Dr. Shayo Olubosede for his contributions towards my academics.

To my friends; Banky, Sunday, Aguda, Olumide, Pat, Deji, Bayo, Segun, Zac, Olamide, Elijah, Isaac, Amos, Cedrick and others I am not chanced to mention. These people have always been there with open arms to talk, encourage, vent and laugh at everything I do. God bless you all.

My appreciation goes to the Professors in the Department of Chemistry, for training me towards attaining important life lessons. I am very grateful for your assistance and scientific advice/discussions. Also, to all the functionaries and especially the secretaries; Luciani, Ariane and Cristina, for their attention.

Finally, I appreciate goes to the National Council for Scientific and Technological Development (CNPq) for the scholarship opportunity granted to study in Brazil.

LIST OF ABBREVIATIONS

AAS	Aspirin
AIDS	Acquired Immune-Deficiency Syndrome
API	Active Pharmaceutical Ingredient
ANVISA	Brazilian Health Regulatory Agency
BCS	Bio-pharmaceutics Classification System
CA	Cluster Analysis
CAF	Caffeine
CCD	Charged-Coupled Device
CE	Crystal Engineering
CIF	Crystallographic Information Files
CSD	Cambridge Structural Database
DSC	Differential Scanning Calorimetric
EMA	European Medicines Agency
FLZ	Fluconazole
FTIR	Fourier-Transform Infrared Spectroscopy
GI	Gastrointestinal tract
GRAS	Generally Recognized as Safe
IBP	Ibuprofen
IL	Ionic Liquid
IR	Infrared Spectroscopy
LED	Light Emitting Diodes
NCE	New Chemical Entity

NMR	Nuclear Magnetic Resonance Spectroscopy
NSAID	Non-Steroidal Anti-Inflammatory Drug
PC	Principal Component
PCA	Principal Component Analysis
TGA	Thermogravimetric Analysis
USFDA	United States Food and Drug Administration
UV-Vis	Ultraviolet-visible Spectrophotometry
WHO	World Health Organization
XRD	X-ray Diffraction
5FC	5-Fluorocytosine

LIST OF TABLES

LIST OF FIGURES

ABSTRACT

SUPRAMOLECULAR SYNTHESIS AND CHARACTERIZATION OF NEW MULTICOMPONENT FORMS OF FLUCONAZOLE

Active Pharmaceutical Ingredient (API) is the therapeutic constituent that defines the pharmacological properties and performance of the drug. Their qualities vary due to their respective physicochemical and pharmacological properties/parameters like solubility, dissolution rate, bioavailability and stability. Orally administered must present adequate parameters for an effective absorption into the systemic circulation for an optimal pharmacological response. Crystal engineering is an established route through which the problematic physicochemical and pharmacological properties of an API is optimized and re-addressed by using a new solid form, which is reached via supramolecular synthesis through synthon interactions of an API and a conformer molecule. Therefore, the selection of complementary API/coformer for the design of multicomponent structures via intermolecular interactions is achieved using tools like multicomponent screening wizard of MERCURY program and the pKa rule. This thesis presents a reproducible crystallization route for the synthesis of new pharmaceutical cocrystals and a salt of fluconazole (FLZ), an antifungal multifunctional drug. The selected coformers were the dicarboxylic acids adipic, dipicolinic, oxalic, fumaric and malic, which showed strong intermolecular interactions like O−H···N and O−H···O (hydrogen bond) between FLZ molecule and the dicarboxylic acid. Herein, we reported four new pharmaceutical cocrystal forms; (1:1:1) fluconazole-fumaric acid monohydrate, (1:1) fluconazole-malic acid, (1:1) fluconazole-dipicolinic acid and (1:1) fluconazole-adipic acid. In addition, a stable (1:1) fluconazolium oxalate salt was synthesized through protonation (H^+) of API, i.e. a FLZ cation with an oxalate anion through N^+–H···O^- ionic bond and O–H···O hydrogen bond. All these new structures present better solubility compared to the commercialized form. The combination of spectroscopy techniques (Raman/FTIR) and principal component analysis (PCA) was employed as tool for visualizing and screening the spectra obtained from the products of the supramolecular synthesis, therefore, facilitate the discrimination of physical mixtures of API and coformers from

new desired crystal structures. The structural properties characterizations of all these reported structures was performed using X-ray diffraction (powder and single crystal), Spectroscopy (Raman and FTIR) and thermal analysis (DSC, TGA, and HSM). UV-vis spectrophotometry was employed for the determination of aqueous solubility of new crystalline structures. The results in this thesis will be present as the published papers, and annexed at the end of this thesis: Annex I – Fluconazolium oxalate: synthesis and structural characterization of a highly soluble crystalline form, CrystEngComm, 21, 1114 - 1121, 2019; Annex II – Fluconazole: Synthesis and Structural Characterization of Four New Pharmaceutical Cocrystal Forms, Crystal Growth & Design, 19, 648 - 657, 2019.

RESUMO

SÍNTESE SUPRAMOLECULAR E CARACTERIZAÇÃO DE NOVAS FORMAS MULTICOMPONENTES DE FLUCONAZOL

O Ingrediente Farmacêutico Ativo (API) é o constituinte terapêutico que define as propriedades farmacológicas e o desempenho de uma droga. Suas qualidades variam devido as suas respectivas propriedades físico-químicas e farmacológicas e parâmetros como a solubilidade, taxa de dissolução, biodisponibilidade e estabilidade. A administração oral deve apresentar parâmetros adequados para uma absorção eficaz na circulação sistêmica para obter uma resposta farmacológica ótima. A engenharia de cristais é uma rota estabelecida através da qual as propriedades físico-químicas e farmacológicas desfavoráveis de uma API são otimizadas e modificadas utilizando uma nova forma sólida, a qual é obtida via síntese supramolecular através das interações entre síntons de um API e de uma molécula coformadora. Portanto, a seleção de API/coformador complementares para o design de estruturas multicomponentes por meio de interações intermoleculares é obtida usando ferramentas como o assistente de triagem multicomponente do programa MERCURY e a regra do pKa. Esta tese apresenta rotas de cristalização reprodutíveis para a síntese de novos cocristais e um sal de fluconazol (FLZ), um fármaco antifúngico. Os coformadores selecionados foram os ácidos dicarboxílicos adípico, dipicolínico, oxálico, fumárico e málico, os quais formaram fortes ligações intermoleculares através de interações como O−H···N e O−H···O (ligações de hidrogênio) entre o FLZ e os ácidos dicarboxílicos. Aqui, relatamos quatro formas farmacêuticas de cocristal; (1:1:1) ácido fumárico-fluconazol monohidrato, (1:1) ácido málico-fluconazol, (1:1) ácido dipicolínico-fluconazol e (1:1) ácido adípico-fluconazol. Além disso, um sal estável de oxalato de fluconazol (1:1) foi sintetizado por meio da protonação do API, isto é, um cátion FLZ e ânion oxalato através da ligação iônica N^{+}–H···O^{-} e de hidrogênio O–H···O. Todas essas novas estruturas apresentam melhor solubilidade em relação à forma comercializada. A combinação de técnicas de espectroscopia (Raman / FTIR) e análise de componentes principais (PCA) foi empregada como ferramenta para

visualizar e rastrear os espectros obtidos a partir dos produtos da síntese supramolecular, facilitando a discriminação de misturas físicas de API e coformadores de novas estruturas cristalinas desejadas. As caracterizações das propriedades destas novas estruturas foram realizadas por difração de raios-X (pó e monocristal), espectroscopia (Raman e FTIR), análise térmica (DSC, TGA e HSM). A espectrofotometria UV-vis foi utilizada para avaliação da solubilidade aquosa das novas estruturas cristalinas. Os resultados desta tese estarão presentes como artigos publicados e anexados ao final desta tese: Anexo I – Fluconazolium oxalate: synthesis and structural characterization of a highly soluble crystalline form, CrystEngComm, 21, 1114 - 1121, 2019; Anexo II – Fluconazole: Synthesis and Structural Characterization of Four New Pharmaceutical Cocrystal Forms, Crystal Growth & Design, 19, 648 - 657, 2019.

SUMMARY

CHAPTER 1

INTRODUCTION

1. Introduction

1.1. Pharmaceutical industry and drugs

Pharmaceutical industries are licensed (authorized) and assigned with the responsibility to research, develop, and market approved quality drugs products that meet stated standard and requirements of governmental agencies like the United States Food and Drug Administration (USFDA),[1] European Medicines Agency (EMA),[2] Brazilian Health Regulatory Agency (ANVISA)[3] and World Health Organization (WHO) guidelines for drugs.[4] Therefore, development/manufacturing of drugs with quick/effective therapeutic responses for maintaining health, preventing and curing infections/diseases are the objectives of the pharmaceutical industry.[5] Generally, medicines contain active pharmaceutical ingredient (APIs) and excipients that are added to the API during formulation processes to enhance therapeutic efficiency, improve crystalline drug flowability, and aid vitro stability/expected shelf life.[6]

Unfortunately, more than 40% of new chemical entities (NCEs) formulated by pharmaceutical industries, especially drugs for oral administration, present low therapeutic response due to physicochemical and pharmacokinetic property, mainly low aqueous solubility, slow dissolution rate and low permeability that causes low bioavailability.[7]

The introduction Bio-pharmaceutics Classification System (BCS)[8] in 1995 by Amidon et al., as an excellent scientific framework for classifying drug substances based on their aqueous solubility and permeability was excellent.[9] Governmental agencies and stakeholders like FDA, EMA, ANVISA and WHO, quickly adopt it as guideline for drug classification by considered the highest dose that have direct effect on the in vivo drug pharmacokinetic performances.[10] FDA made available BCS-biowaiver guidelines for Classes I/III drugs for the purposes of validating and release new pharmaceutical products (CDER/FDA, 2000).[11] This approach excludes in vivo bioequivalence studies considering that it provides an alternate for in vivo bioequivalence when the drug substance(s) in test and reference products are identical.[12]

However, the BCS model classify pharmaceutical drugs into four classes (Figure 1.1) and presents/elucidates the pharmacokinetics of drug process in the gastrointestinal (GI) tract. Hence, the criteria/basis for establishing a drug as highly soluble drugs/highly permeable depends on two conditions. (1) The highest dose strength must be soluble in less than 250 ml water and over a pH range of 1 to 7.5; and (2) the absorption in humans must be higher than 90% of an administered dose, based on mass-balance or intravenous dose comparison.[13]

BCS CLASS I High Solubility High Permeability	**BCS CLASS II** Low Solubility High Permeability
BCS CLASS III High Solubility Low Permeability	**BCS CLASS IV** Low Solubility Low Permeability

FIGURE 1.1–The Bio-pharmaceutical Classification System (BCS) for drugs.

As mentioned earlier, many approved and marketed pharmaceutical drugs like Carbamazepine,[14] Ritonavir[15] and Furosemide[16] present low aqueous solubility and are classified to the BCS classes II or IV of drugs. Therefore, the formulation of low solubility drugs for oral delivery among other drug property issues is a challenge for pharmaceutical industry.

1.2 Pharmaceutical polymorphism

Crystal materials (such as APIs) have the tendency to exist in more than one crystalline forms.[17] Hence, in terms of regulatory approval, the crystalline forms of an active ingredient is limited to polymorphs, salt, stoichiometric solvate and hydrate, and cocrystal forms (Figure 1.2).[18] However, APIs have the tendency to become solvates/hydrates by interacting/bonding with solvent/water molecule(s), or form a

salt through proton transfer, or multicomponent cocrystal forms through interactions with coformer(s) that are usually FDA approved substances Generally Recognized as Safe (GRAS).[19] Therefore, the inclusion of solvent/water molecule(s) in the molecular structure of a cocrystal will change their solid-state structure and physicochemical properties, such as dissolution profile and thermal stability.

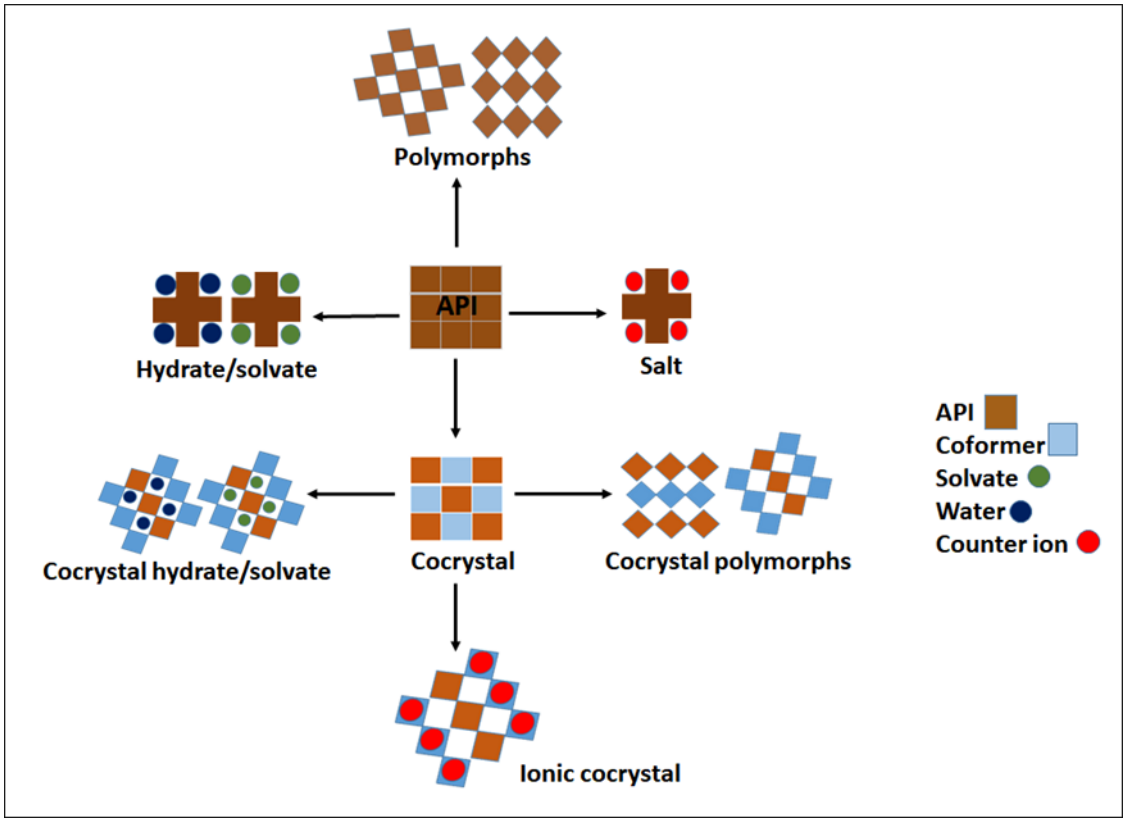

FIGURE 1.2 – Different classes of crystalline solid system into which an API can exist.[20]

Crystal materials with less desired physical property may be readdressed and rechanneled into other desired crystalline stable states. The tendency of a crystalline material such as API to exist in different phases of the solid form with same chemical composition, but observable diversities in structure arrangement and potentially differences in their properties is termed polymorphism.[21] The multiplicity of structures or forms is either enantiotropic (reversible) or monotropic (nonreversible) in solid-

state, in addition, the more stable polymorph will show slower dissolution profile than less stable forms, which are more soluble.[22] This phenomenon became important to the formulation scientists/researchers in the pharmaceutical industries and research institutes/centers because it presents the opportunity to alter/reduce undesired properties such as dissolution profile, bioavailability and stability of API at low cost.[23]

Polymorphs frequently occurs extemporaneously in most crystalline solid materials, such as pharmaceutical materials, minerals, metals and proteins complexes. The polymorphism (not including salts or cocrystals) may occur due to: the crystal packing/molecular arrangement (packing polymorphism); the existence of different conformers of the same molecule (conformational polymorphism); the effect of hydration/solvation that is referred as pseudo-polymorphism or better as solvomorphism, since different solvates will present varying chemical formulae.[24]

Polymorphism unveil advanced understanding of the importance of structural variations due to molecular packing and especially the possibility of interconversion among polymorphic forms, that can influence every aspect of the solid state properties of drugs. However, more than 50% of active ingredients are observed to present more than one polymorphic form in the Cambridge Structural Database (CSD).[25] McCrone (1965) humorously commented that the discovery of polymorphs is correlated with the energy and time invested into researching for the compound.[26] Therefore, polymorphic studies/research is a crucial and important pharmaceutical industry activity because a particular polymorph can present a particular property, which is not present in the other forms. In many cases, a polymorph form of a drug can suffer crystalline transition for a more stable form, promoting changes in the drug efficacy, in the bioavailability and may even exhibit toxicity.[27] Nevertheless, the most stable polymorph (thermodynamically) is preferred for making marketed formulations to prevent polymorphic transformation that may occur during drug manufacturing and post manufacturing processes (delivery and storage).[28] Chloramphenicol,[29] Ranitidine hydrochloride (GSK's Zantac®)[30], Fluconazole[31], Cefdinir[32], Carbamazepine[14], and Diflunisal[33] are examples of pharmaceutical drugs with two or more reported polymorphic forms.[34]

1.3 Crystallization and Co-crystallization techniques

In “general chemistry”, crystallization is a separation/purification process and technique through which solid phase of pure crystallinity is obtained from saturated solutions.[35] This process just like recrystallization[36] is a route/channel through which the physicochemical/particle properties of a crystalline solid material, such as purity, particle size, crystal shape, solubility, form stability, and degree of agglomeration is addresses through polymorphism or the incorporation of coformer substance(s) or solvent molecule(s).[37] The “industrial crystallization” is a complex processing technique for specific solid crystal formation under carefully controlled conditions, to yield pure and homogenous form of the corresponding product.[38] In the pharmaceutical industries, products passed through process development of crystallization process that enables the initial designing, modelling, process control, and final product analysis using analytical tools.[39] Herein, the process and conditions leading to the desired product yield is monitored, controlled and optimized when necessary, to upgrade the properties and qualities of the solid product.[40]

Co-crystallization technique[41] is defined in the context of crystal engineering[42] concept as a well-designed approach for modification and optimization of the physicochemical property issues of crystalline materials (APIs) such as low solubility/bioavailability, and instability through intermolecular interactions like hydrogen bond (X–H···Y)[43], dipole forces[44], π-π interactions[45] and ionic bonds[46] between selected API and coformer(s).[47] Interestingly, co-crystallization process presents diverse advantages of generating array of solid-state forms with stable and physically improved properties in cocrystal forms.[48] Furthermore, co-crystallization offers the potential flexibility for designing novel pharmaceutical cocrystal and resolve crystallization problems even when traditional approaches such as salt formation fails.[49] However, other drug delivery approaches for enhancing the dissolution profile of an API, like amorphous solid dispersions[50], nanoparticle[51] and lipid-based[52] approaches have proven to optimize the above-mentioned drug issues.[53] Even though these methods increases dissolution profile of the APIs, they not assure a sufficient bioavailability and stability for all cases.[54] While the co-crystallization process involves weak interactions between API and coformer(s) for

cocrystal formation, the formation of a salt involves strong ionic interaction that requires proton (H^+) transfer between oppositely charged counterions, and can be predicted using the pKa rule.[55]

Although different co-crystallization techniques, such as, supercritical and compressed fluids techniques,[56] melting and slurry cocrystallization,[57] and ultrasound-assisted technology[58] are described/discussed in the literature, the mechanochemical and solution-based crystallization/cocrystallization methods[59] sketched in Figure.1.3 are the prevalent, most reliable and commonly used methods for cocrystal/salt synthesis.[60] The solvent evaporation techniques can be fast/slow evaporation,[61] cooling crystallization and antisolvent precipitation approach.[62] Herein, stoichiometric ratio(s) of API and coformer(s) is dissolve in a suitable solvent that will evaporate. The API/coformer(s) are expected to undergo intermolecular interactions such as hydrogen bonding and pi-pi interactions between their functional groups, thereafter, producing a thermodynamically favored cocrystal product (high quality and purity).[63]

The mechanochemical methods are solid-state grinding technique or neat grinding, and liquid-assisted or solvent-drop grinding techniques.[64] These methods involves mixing/crushing of stoichiometric amount of API/coformer(s) with and without solvent. The neat grinding technique reducing the API/coformer particle size and increases their specific surface area for intermolecular interaction, improving the efficiency compared to the cocrystallization through dissolution.[65] Even when the solution based method fails to present evidence of intermolecular interactions, the neat grinding technique is reported to present evidence of cocrystal, e.g., *caffeine-trifluoroacetic acid*[66] and *pterostilbene-caffeine cocrystals*[67] were obtained by grinding.[68] The solvent assisted grinding method offers catalytic modification to neat grinding by adding drops of solvent to the grinding process. The inclusion of solvent present advantageous increase in cocrystallization rate and performance, it also controls polymorph production with improved crystallinity, and aid the selective synthesis of polymorphic forms of cocrystals.[69]

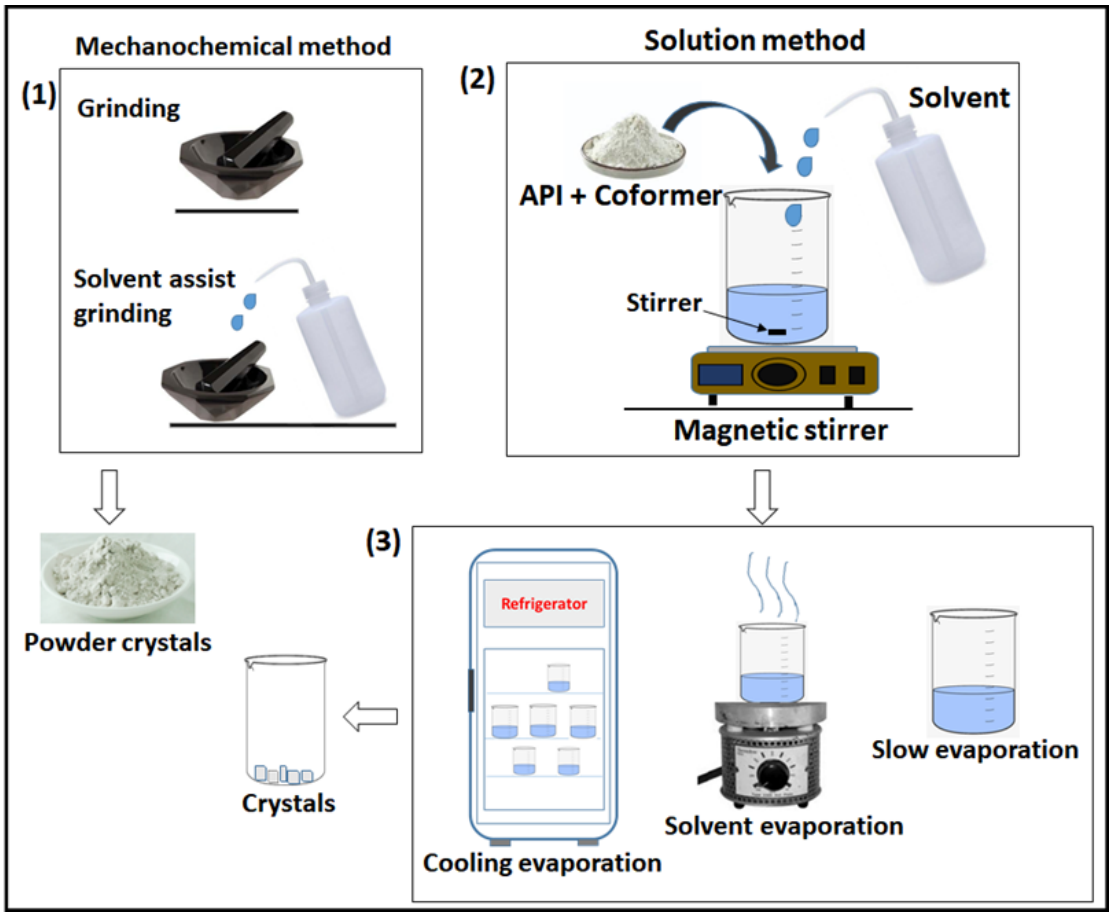

FIGURE 1.3 – Cocrystallization/salt synthesis techniques.

The limitations of neat and liquid-assisting grinding techniques is observed in its small-scale techniques that require high-energy consumption and present a low performance in terms of product purity.[70] In addition, many times, these methods fail to yield crystals suitable for the structural characterization analysis.

The Figure 1.4 present a novel (1:1) drug-drug cocrystal involving 5-Fluorocytosine[71] (5FC) – an antifungal drug – and Aspirin[72] (AAS) – a non-steroidal anti-inflammatory drug – designed and synthesized by our research group. Interestingly, this cocrystal was obtained through the mechanochemical methods (solid-state grinding/liquid-assisted grinding techniques), and synthesized through slow solvent evaporation method. Therefore, it serves as a typical example of

pharmaceutical cocrystal that is producible by both mechanochemical and solution methods.

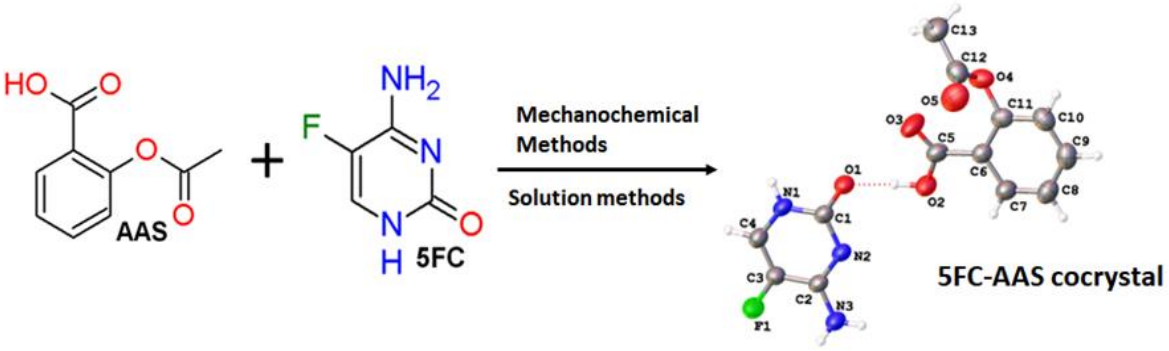

FIGURE 1.4 – 5-Fluorocytosine (5FC) and Aspirin (AAS) cocrystal.

1.4 Cocrystal and pharmaceutical cocrystals

Cocrystals[73] are established class of well-designed single-phase crystalline material in which the molecular and/or ionic compounds are present in a definite stoichiometric ratio, and bonded together by intermolecular interactions.[74] This definition was accepted after a series of debate and speculations at an organized Indo-US Bilateral Meeting in Delhi, India, titled "*The Evolving Role of Solid State Chemistry in Pharmaceutical Science"* attended by 46 scientists/stakeholders.[75]

Although initial emphasis in the hydrogen bonding in cocrystal design (Etter[76]), the deep intuitive understanding and insight on the application of supramolecular synthon concept/approach for hydrogen bond architecture, prediction and formation in polar functionalities was proposed/established by Desiraju.[77] Thus, in addition to his work, pharmaceutical cocrystal[78] (a subclass of cocrystals) was established and defined as a distinct class of pharmaceutical crystalline materials in which the less desired physicochemical properties of an API could be optimized by lattice rearrangement through weak intermolecular interaction with a coformer.[79] Thus, the physical properties of crystalline materials depends on their molecular packing, and alterations of this molecular packing usually promote a direct effect on these properties. Hence, different forms of pharmaceutical crystals,

such as cocrystals, hydrates[80] and solvates[81] can present better or worst properties when compared to the an API.[82]

Cocrystals are classified into either molecular or ionic cocrystal based on the nature of coformers according to Duggirala and coworker.[83] The ionic cocrystal is obtained from a stoichiometric ratio of an API and ionized coformers in a charge assisted hydrogen bonds and/or ion dipole bonds, while a neutral or non-ionized coformer dictates the commonly reported molecular cocrystal formation.[84]

It is however important to comment about the increasing of commercial pharmaceutical cocrystal and the recent development of drug-drug pharmaceutical cocrystals.[85] Important drugs such as Entresto® (*sacubitril-valsartan*) for the treatment heart failure,[86] Lexapro® (*escitalopram-oxalate*) for the treatment of depression and anxiety,[87] and Depakote® (*valproate sodium-valproic acid*) for the treatment of seizure disorders, manic depression, and to prevent disorders,[88] are examples of drug-drug pharmaceutical cocrystal that was approved by FDA.[89]

The design of 5-Fluorocytosine (5FC)[71] and Aspirin (AAS)[90] cocrystal, and cocrystals of Fluconazole (FLZ)[91] with non-steroidal anti-inflammatory drugs (NSAIDs)[92] like Aspirin, Caffeine (CAF)[93] and Ibuprofen (IBP),[94] will fits perfectly as drug-drug pharmaceutical cocrystals of important APIs.[95] Although cocrystals suffers limitations in the scale-up process and general classification by FDA as “intermediate medicinal products”, regarding the coformer as an excipient,[60] the application of cocrystals for drug formulations remains an ongoing promising development in the pharmaceutical industry/research institutes.[96]

1.5 Crystal Engineering and Supramolecular chemistry

The term “crystal engineering” (CE) was coined in 1955 by Pepinsky,[97] and later implemented by Schmidt during his photodimerisation reactions study.[98] CE is defined as the design and synthesis of molecular solid-state structures with desired properties, through the understanding and use of intermolecular interactions such as hydrogen bonding and coordination bonding, thus, within the conceptual and theoretical understanding of supramolecular synthon and secondary building unit.[99] That is, the molecular self-assembly that involves the direct interaction between

complementary hydrogen bond, metal-ligand interactions observed in organometallic and coordination compounds, halogen bonds and intermolecular forces such as pi...pi and Au...Au interactions are the basis of crystal engineering.[100]

In 1995 Gautam Desiraju, a leading stakeholder in crystal engineering field, coined the term "*supramolecular synthon*" to describe the building blocks of organic structures for ordering specific groups in the solid state.[77] Desiraju define crystal engineering as "*the understanding of intermolecular interactions in the context of crystal packing and the utilization of such understanding in the design of new solids with desired physical and chemical properties.*"[42] He further emphasized the potentials of CE concepts as a design strategy for molecular crystal structures in pharmaceutical multicomponent system and in metal organic species.[101] Interestingly, CE has broadened considerably and continue to incorporate many aspects/application of solid-state supramolecular chemistry such as the spatial molecular organization, variations in the strength of intermolecular forces like hydrogen bond (X-H•••Y), dipole forces, pi-pi interactions and the ionic bonds.[102]

Crystal engineering relies on non-covalent organization of molecules and ions i.e. molecular self-assembly through design of desired multicomponent structures and this is achieved using weak intermolecular interactions that can be categorized into the following classes, considering their relative strength (Figure 1.5).

(1) Electrostatic interactions (1-40 kcal/mol) are forces that electric charges exert on each other and is based on the coulombic attraction of ions/molecules with full permanent charges such as: ion-ion (non-directional), ion dipole and dipole-dipole interactions (directional) are examples of these ionic interactions (Figure 1.5-a-c). In addition, hydrogen bonds (Figure 1.5-e) and halogen bonds are other two examples of electrostatic interactions that supramolecular chemists usually use for achieving strong bonding.[103] The hydrogen bond is a partial intermolecular bonding interaction between a lone pair on an electron rich donor atom (Dn), and the antibonding molecular orbital of a bond between hydrogen (H) attached to a more electronegative acceptor atom (Ac) like nitrogen (N), oxygen (O), or fluorine (F) in a Dn–H···Ac fashion. This bond is stronger than van der Waals forces, and weaker than covalent

or ionic bonds. Likewise, weaker “non-classical” H-bonds (~1 kcal/mol) involving donor other than N, O, or F and/or acceptor Ac with electronegativity approaching that of hydrogen (less electronegative) exist, and carbon (C) as a good example.[104]

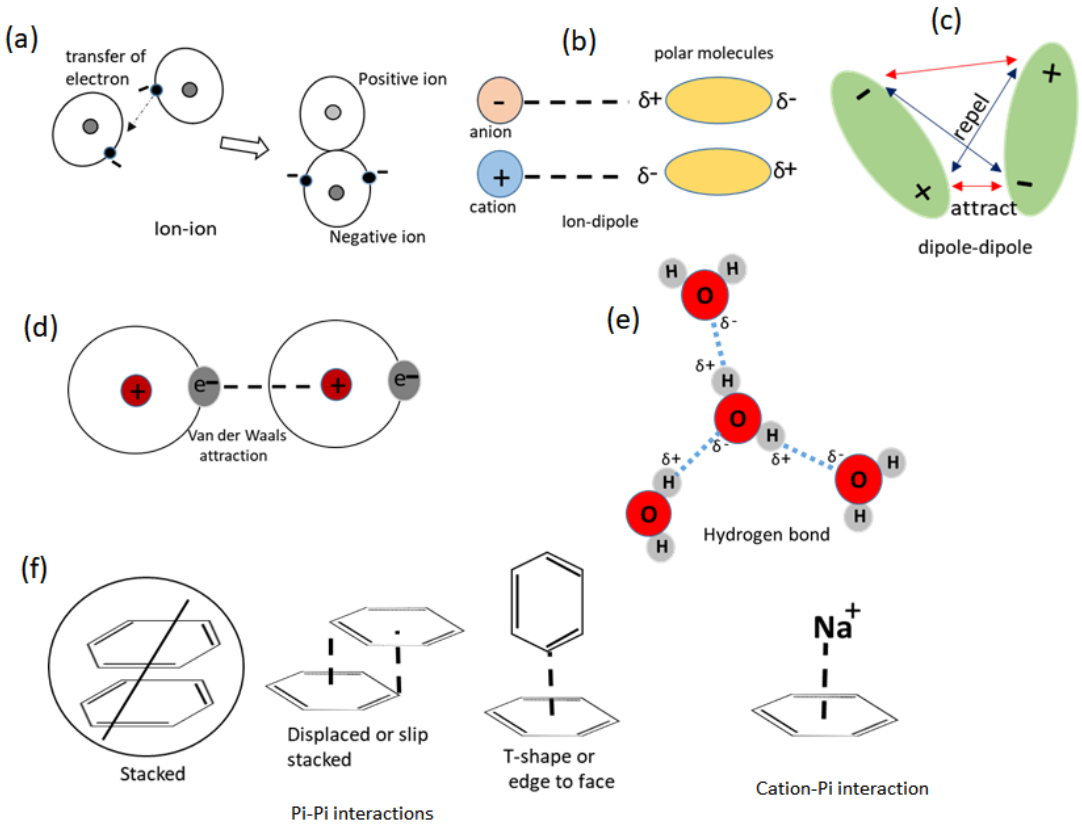

FIGURE 1.5 – Types of non-covalent interaction.

(2) Van der Waals forces are promoted by permanent or induced dipoles and a special class of electrostatic interactions that consist of three types; dipole-dipole interactions (Keesom force), dipole-induced dipole interactions (Debye force) and induced dipole induced dipole interactions (London dispersion forces, Figure. 1.5-d).[99] They are topographically dependent, i.e., the stronger the contact between two particles the greater is the Van der Waals force of attraction.[105] Pi–pi stacking force (Figure. 1.5-f) is another type of Van der Waals force where electrostatic attractive forces occur in aromatic ring systems. The pi-effect is linked with the interactions of molecules with pi-systems of conjugated molecules. Herein, the interactions occur

in different format like “face-to-face‟, “edge-to-face‟ or in an “offset‟ manner. Also, cation–pi interaction between face of an electron-rich pi system such as benzene, ethylene, acetylene and an adjacent cation such as Li^+ and Na^+, have demonstrated to be useful non-covalent bonds in molecular recognition.[106]

(4) Hydrophobic effect is the force that promote separation of non-polar molecules in an aqueous solution. It presents the tendency for nonpolar substances to aggregate in an aqueous solution and exclude water molecules.[107]

However, the ionic bond in salt formation results from replacement of part or all of the replaceable acid hydrogen (nH^+, n = 1, 2 ,3....) of an acid by a metal or a radical acting like a metal as presented in Figure 1.6. This process is predictable via the multicomponent screening tools (molecular complementarity) available in the Mercury program of the Cambridge Structures Database, and using the pKa rule; i.e., (ΔpKa = pKa (base) – pKa (acid), when ΔpKa ≥ 3, that salt will be produced). Hence, salt (ionic bond via electron (H^+) transfer) is different from multicomponent cocrystal forms (weak intermolecular interactions) on this regard.[82]

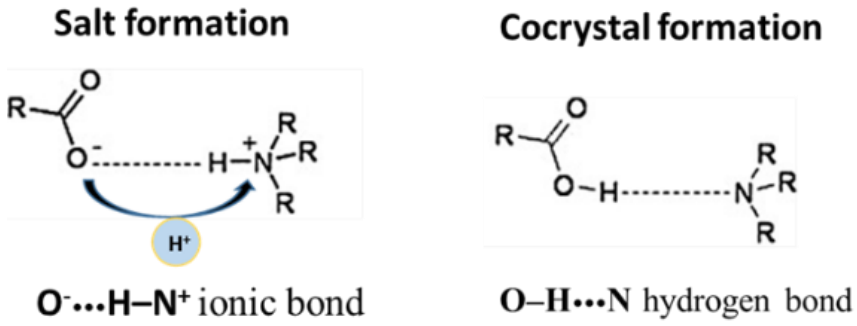

FIGURE 1.6 – Salt and cocrystal formation through ionic and hydrogen bond.

In crystal engineering, hydrogen bond is the most important intermolecular non-covalent force by virtue of its directionality, specificity and biological relevance. The fundamental principles and objectives of crystal engineering have made easier to develop strategies that employ hydrogen bonding as a tool for designing and incorporating predictable structural aggregates into crystalline materials, also allowing to explore reasonable correlations between their molecular structures,

morphology, and physicochemical properties.[108] The CE concept is employed in many researches to optimize the less desired properties of APIs belonging to the BCS class II/IV in the solid state, thus resulting into different stable multicomponent cocrystal and salt forms of the selected APIs.[109] The challenges of CE remains its insufficient scalability, the unpredictability of crystals morphology and reaction path.

Supramolecular chemistry[110] as a discipline is concerned with the study of molecular recognition and self-assemblage via intermolecular bonds, and entails complete understanding of the factors responsible for varied dimensions observed with “supermolecules”, complexes and molecular assemblies.[102] Therefore, in line with crystal engineering concept, the prerequisite for non-covalent bonding is the intermolecular association through supramolecular synthon interactions, which represent the molecular building unit and starting point for non-covalent bonding in all CE syntheses.[77]

The contributions of Jean-Marie Lehn,[111] Charles J. Pedersen[112] and Donald J. Cram[113] to supramolecular chemistry,[114] that is, host–guest supramolecular assemblies, was appreciated and awarded the Nobel Prize in chemistry in 1987.[115] In his words, Lehn define supramolecular chemistry *“as the chemistry of the intermolecular bond, covering the structures and functions of the entities formed by the association of two or more chemical species.”*[111] In few words, he defined it as *“the chemistry beyond the molecule”* or *“the chemistry of non-covalent bond”*.[116]

In supramolecular chemistry, synthons are the recognized molecular unit of functionalities that establish or initiate motifs/patters of “host–guest” network in a non-covalent interactions to produce a complex or supramolecular entity.[117] However, the probability of designing a particular synthon interaction depends on the presence of multiple interaction site for complementary non-covalent interaction, steric complementarity, medium effects, high selectivity and sensitivity, and free energy for formation of non-covalent interactions. Nevertheless, synthon can be homo or heterosynthon depending dimer interactions they present as shown in Figure 1.7.[118] The carboxylic acid and imides dimers synthon in (a) are examples of

homosynthon interaction, while the carboxylic acid-pyridine (b) are good examples of heterosynthon dimers respectively.[119]

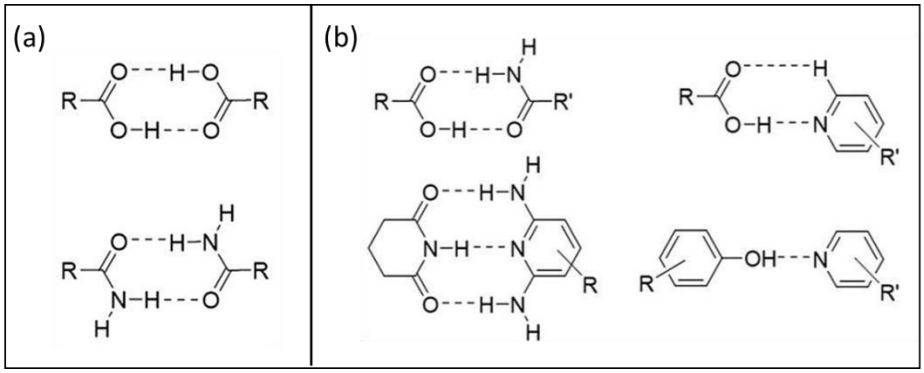

FIGURE 1.7 - Supramolecular synthons adopted by imides and carboxylic acids showing (a) homosynthon and (b) heterosynthon interaction.

The possibility of modeling or designing a desired cocrystal structure through API/coformer hydrogen bond synthon dimer interaction can be evaluated/checked using the Mercury software of the Cambridge crystallographic database. The competition between homosynthon and heterosynthon was set up using their frequency of occurrence as a percentage of the number of structures in which the functional group is present. Interestingly, the result indicated that motif search observed for heterosynthon structures outnumbered homosynthon, thus indicating the higher probability (likelihood) of obtaining a structure through heterosynthon motif.[120]

In supramolecular chemistry, the significance of non-covalent interactions like hydrogen bond and coordination bond are established and demonstrate to affect physicochemical and biological properties of supramolecules and coordination complexes in the solid state.[121] Crystal-engineering concept and other retrosynthetic approach to organic synthesis in the solid state absolutely relies on supramolecular chemistry (non-covalent interactions) as a powerful tool to design and synthesize improved drug forms.[122] Hence, supramolecular chemistry and crystal engineering disciplines continues to enjoy growth, expansion and publicity through important international scientific journals like *CrystEngComm* from the Royal Society of Chemistry and *Crystal Growth and Design* from the American Chemical Society.

1.6 Screening and Characterization techniques/tools

Screening is an important procedure for investigating the feasibility of reactions through designed hit and trial approach that identify desired conditions and coformers from complex numbers of evaluated samples, using designed and selective approaches that consider the most desired results thereby saving time and experimental costs.[123]

In crystal engineering, screening techniques have proven to be an important and useful tool in crystallization processes for predicting, identifying, and detecting desired conditions, especially in some complex crystallization processes such as in cocrystal screening. Therefore, in cocrystallization/salt synthesis, screening provide an insight into the feasibility of achieving intramolecular interactions or ionic bond prior to the crystallization or co-crystallization process.[124]

However, different screening methods and approaches such as hydrogen-bond[125] and supramolecular propensity simulation using MERCURY[126] software from the Cambridge Structural Database (CSD),[127] pKa based model,[128] Lattice energy calculation,[129] Hansen solubility parameter,[130] and the virtual cocrystal screening (molecular electrostatic potential surfaces-MEPS),[131] have been reported.[132] In addition, the combination of multivariate analysis such as the principal component analysis (PCA) and cluster analysis (CA)[133] with analytical tool like Raman/FTIR spectroscopy for screening was considered effective for detecting new cocrystals, polymorphs, and differentiate between similar multicomponent forms.[134] Also, this combination aids better screening/selection of different supramolecular synthesis routes from complex cocrystallization experiments that lead to robust cocrystal and salt formation in this thesis report.[135]

Screening may be classified as “pre- or post-screening” processes based on the instant of crystallization activities. The “pre-screening” activities involves finding suitable components and conditions for achieving improved solid-state properties, while “post-screening” activities involve the investigation for evidences of intermolecular interactions and construction of new multicomponent materials.[136] The aforementioned cocrystal and salt screening approaches like hydrogen-bond propensity and pKa-based model provide insight on experimental feasibility and

outcome of selected experimental conditions such as API/coformer and solvent selection, and crystallization methods. However, the “post-screening” activities include the cocrystal/salt screening and characterization that is achieved through different known approaches and use of analytical equipment such as Raman/FT-IR spectroscopy and X-ray diffraction studies.

The Figure 1.8 shows the stages and events/processes performed for the cocrystal/salt screening and characterization, starting from the pre-screening (stage 1), to screening (stage 3), and post-screening processes (stage 4). These stages of events are the important methodologies that are in line with the crystal engineering concept for API optimization, and was applied in the course of this research work.

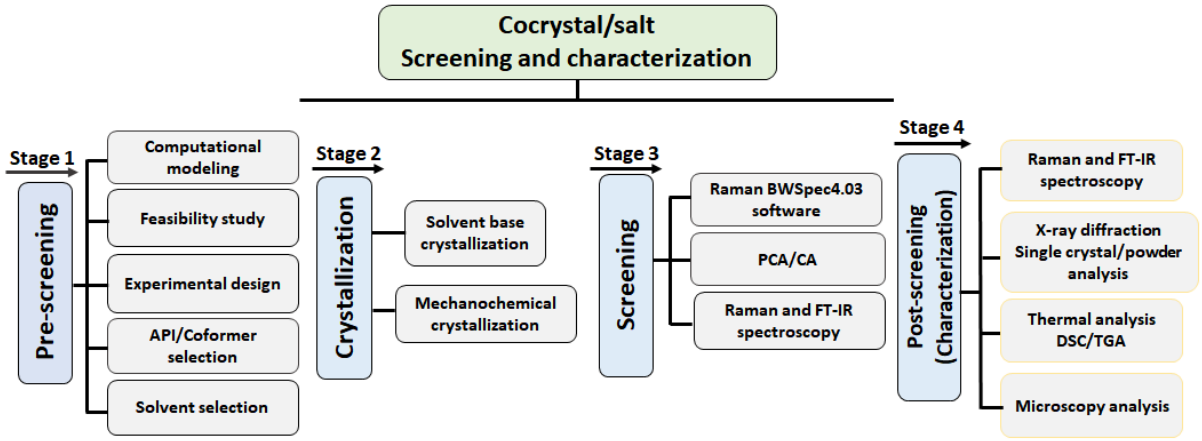

FIGURE 1.8 - Screening and characterization stages for cocrystal/salt synthesis.

Therefore, this employed solid-state screening and characterization methods and techniques will result into the synthesis and detection of multicomponent forms and polymorphs of the API with optimized physicochemical and pharmacokinetic properties like physical stability, aqueous solubility, dissolution rate, bioavailability, phase homogeneity, morphology, formulation performance, and processability.[137]

In addition, screening and characterization activities can detect evidences of phenomenon like polymorphism in solid-state materials,[138] and generate/present the

complete information and resolution on molecular structure patterns using the most sophisticated software such as the multivariate tool (principal component analysis) that is capable to provide visual discrimination for intermolecular interactions, detect polymorphs and the formation of new multicomponent structures.[139]

1.6.1 Principal component analysis (PCA).

Principal component analysis (PCA) is a multivariate analysis method that uses orthogonal transformation to reduced data of high dimensionality into linearly uncorrelated variables called the principal components (PCs) thereby unveiling latent variations within the decomposed dataset and indiscriminately presents their projections in linear space.[140] PCA is the basis for most multivariate methods, and it aims to find the direction of greater dispersion within data in the space of the studied variables, based on the hypothesis testing that the greatest variability contains the most relevant information.[141]

The PCA is able to pick/contain the most relevant information in a reduced number of new variables, discriminating (discarding) irrelevant data describe within the system. The reduction of variables is obtained when there is collinearity between the variables in the data matrix, if there is correlation and presence of the same information in some variables. The application of PCA to recognize patterns, select samples, build multivariate calibration models and obtain a quick and easy view/projection of similar traits in groups/samples or anomalies is observed in the reduced variables.[142]

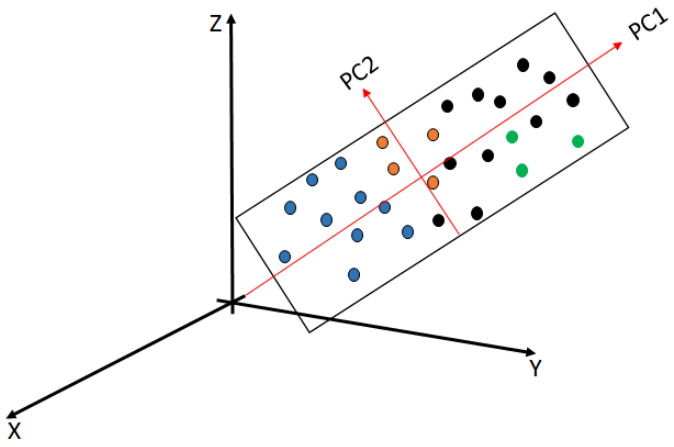

FIGURE 1.9 - Graphical representations of Principal Component Analysis.

The PCA methodology is based on the transformation of the coordinates of the original variables of a data matrix (samples x variables) in a new axis of orthogonal variables, that is, not correlated. The new axis, known as the principal component (PC), explains the greater amount of information in the data obtained as illustrated by Figure 1.9. Herein, the transformation of a data set that presents values for three original variables: x, y and z. This distribution is easily explained in a new two-dimensional space projection formed by the new variables (PC1 and PC2, with PC2 being orthogonal to PC1), reducing the number of factors analyzed, without losing relevant information in the set.

Mathematically, the PCA obtains a relationship between the original data (**X**) and the data obtained in this new dimension of variables from the weights given by each variable (**P**) and sample projection in the new dimension of variables (**T**) according to the equation 1.1 that expresses the PCA in a matrix terms:

$$\mathbf{X} = \mathbf{T}\mathbf{P}^{\mathbf{T}} + \mathbf{E} \qquad \textbf{(1.1)}$$

Herein, the PCA decomposes the original data matrix, **X** (*n,m*) into two new matrices **T** (*n,d*) and $\mathbf{P}^{\mathbf{T}}$ (*d,m*) alongside with the matrices of residual E (*n,m*) as described in Figure 1.10. Herein, *n* is the number of samples (rows), *m* is the number

of variables (columns) of the original matrix, and *d* is the number of PCs calculated for the model.[143]

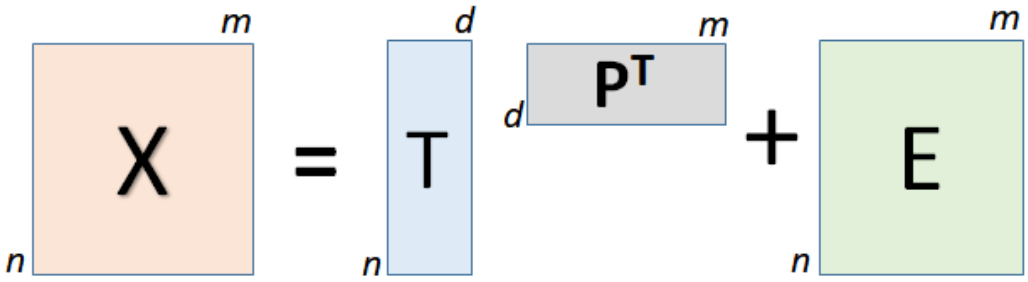

FIGURE 1.10 – Schematic decomposition of data matrix **X.**

The equation 1.2 is better simplified and written as:

$$\mathbf{X} = \mathbf{t}_1\mathbf{p}_1^T + \mathbf{t}_2\mathbf{p}_2^T + \ldots + \mathbf{t}_d\mathbf{p}_d^T \qquad (1.2)$$

where PCA decomposes **X** as the sum of the product of $\mathbf{t}_i$ and $\mathbf{p}_i$, where *d* is the rank of the matrix **X.** Herein, *d* must be less or equal to the smaller dimension of X, i.e., $d \leq \min(m,n)$. The $\mathbf{t}_i$, $\mathbf{p}_i$ pairs are ordered by the amount of variance they capture. The $\mathbf{t}_i$ vectors are known as *scores* that present observation on how samples in the new axis system relates to each other, and each sample will have a score value for each PC. Since, every column of **T** or row of $\mathbf{P}^T$ are orthogonal to each other (Figure 1.10), that is, we have $\mathbf{p}i^T\mathbf{p}j = 0$ and $\mathbf{t}i^T\mathbf{t}j = 0$, for $i \neq j$. The $\mathbf{p}_i$ vectors are known as *loadings* and contain information on how the variables relates to each other in the principal component (PC).[144] Each element of the matrix P is mathematically equal to the cosine of the angle between the axis of each original variable and the PC. The closer to ± 1, the greater the influence that the variable has on the description of the main component for an average-centered data matrix. Since the PCA model is truncated after *k* components, the extra/remaining variance factors are added into the residual matrix E, according equation 1.3:

$$\mathbf{X} = \mathbf{t}_1\mathbf{p}_1^T + \mathbf{t}_2\mathbf{p}_2^T + \ldots + \mathbf{t}_k\mathbf{p}_k^T + \mathbf{E} \quad (1.3)$$

The residual matrix (matrix E) is the amount of information not relevant or not explained by the main components. Generally, in spectroscopic data, the residual matrix is attributed to the unwanted noised factors obtained alongside the analysis.[145]

In this way, PCA can be effectively combined with important analytical methods and tools/instruments that generates an extraordinary amount of high-quality data, such as Raman, FT-IR, and NIR spectrophotometer, X-ray diffractiometer, and mass spectrometer, in order to help in the screening and characterization process.[146] Hence, multivariate tools like PCA have demonstrated its potentials as a strong data processing/decomposing tool for understanding complex data systems, and thereby serving as an analytical screening, modeling, predicting and quantification tool.[147]

In crystal engineering and especially in crystallization processes, PCA enables the decomposition of complex spectra data set for the simultaneous visualization of scores/loadings plot projections, better understanding the crystallization result, and aids better selection of different synthesis routes leading to robust and homogenous cocrystals/salt synthesis.

As an example, the PCA scores plot of 100 processed Raman spectra and 6 selected screened spectra obtained from different stoichiometric combinations of fluconazole and adipic acid (FLZ-ADP) is presented in the Figure 1.11 A and B, respectively. Herein, Figure 1.11-A shows the PC1 (43.04%) and PC2 (22.27%) that explain trends/variations in the model and class/group samples according to their purity/contaminants, while Figure 1.11-B present the Raman spectra of the best PCA assist-selected supramolecular routes. Herein, the best routes will be the ones that generate different spectra when compared with the conformer and API. This spectral evaluation of the dataset is easily achieved utilizing PCA, which will find differences in functionalities/groups vibration modes of the crystallization products.

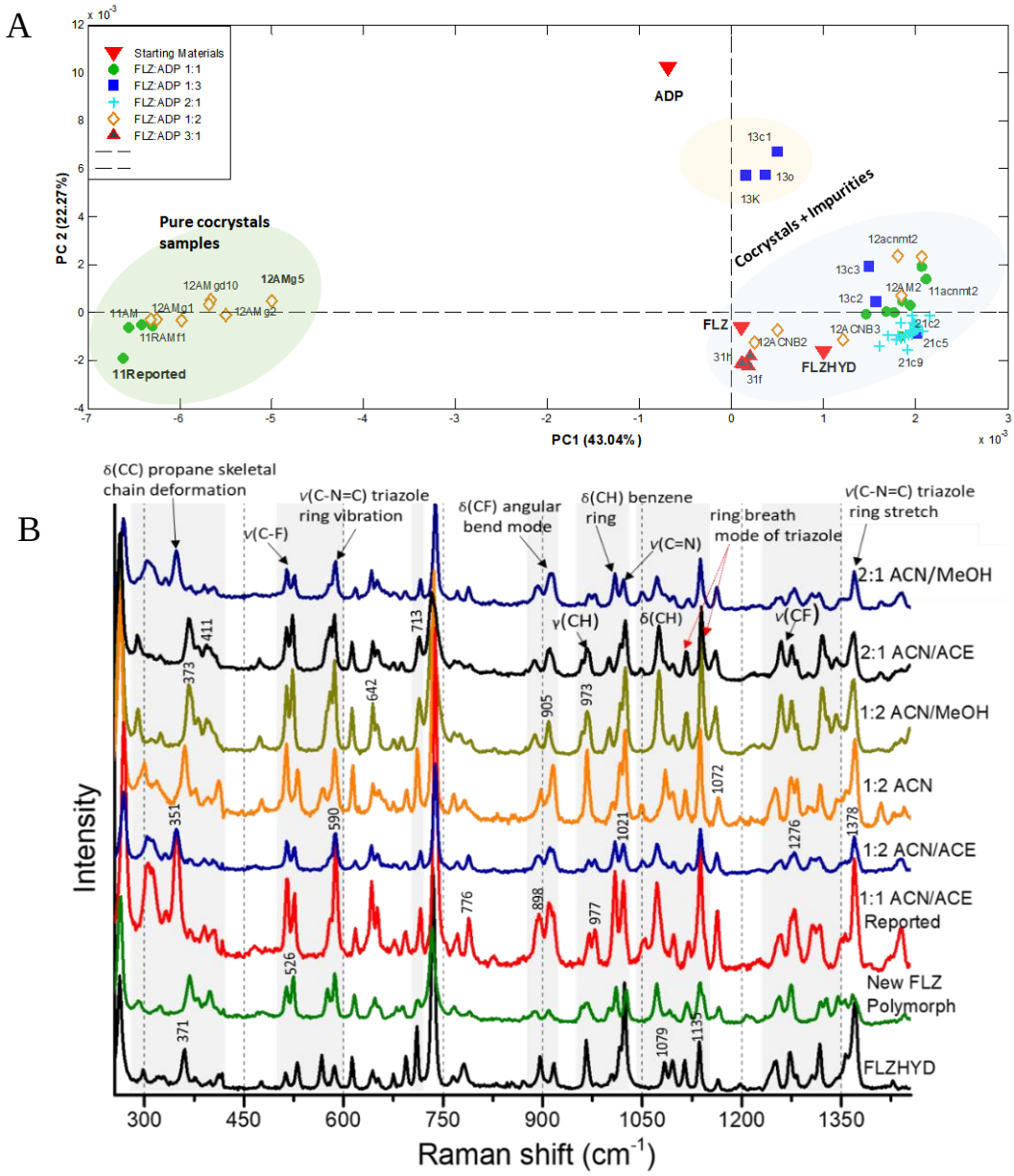

FIGURE 1.11 - (A) PCA score plots for crystallization process (B) Raman spectra of different supramolecular synthesis route selected through PCA screening.

1.6.2 Raman Spectroscopy.

Raman spectroscopy is a molecular spectroscopic technique that utilizes the interaction of radiation and matter to induce light scattering phenomenon that occur from the absorption, emission, or scattering of photons, and presents qualitative

measurements of the characteristic vibrational modes of functionalities observed and present in the compounds.[148] In this way, the Raman spectroscopy generates data on the molecular structure and some important physical information regarding the determined compound through lower frequency modes/vibrations. Therefore, it is serves as a characterization technique (similar and complementary to infrared spectroscopy), to identify substances (or set of compounds) from a spectral pattern ("fingerprint"), or for quantitative or semi-quantitative measurements analysis of wide range of materials.[149]

Raman spectroscopy provide intra- and inter-molecular vibrational information of specific molecular vibrations modes, and for this reason it can be used as a "fingerprint" technique for identification of materials. Hence, conformational properties and phenomenon like polymorphism and the nature of intermolecular interactions are mostly identified by using the vibrational information. Since Raman spectroscopy generates spectral data set from the result of various screening tests, this technique can be combined with multivariate tools like PCA to serve as analytical screening and characterization tool to analyze the results of complex crystallization processes.[150]

In Raman scattering (Figure 1.12), a laser photon of energy hv_0 interacts with electron cloud of the molecule generating a distortion in the electron cloud and scattering the incident radiation with a higher or lower energy. This electron cloud distortion promotes a polarization of the bond that are shortly excited to a higher energy state called "virtual state". Here, the excited molecule have extremely short lifespan in this unobservable intermediate electronic/quantum state and changes in the energy and geometry of the electron clouds is observed without interfering with affecting core electrons of the molecule. For radiation scattering effects, the photon of energy (hv_0) that interacts with molecule needs **not** to have equal energy as the energy differences between the two states. The scattered photons can be result of an elastic (Rayleigh scattering, incident and scattered photon have some energy hv_0) or inelastic (Stokes and anti-Stokes scattering, where scattered photon present lower or higher energy, respectively $-h(v_0 \pm v_v)$). The elastic scattering occurs when scattered photons have the same energy and, therefore, the same wavelength as

the incident photons. Inelastic scattering is a fraction of about 1/10000000 of photons that have a higher or lower energy in relation to the incident photon, and scatter at different frequency than the incident photon.[151]

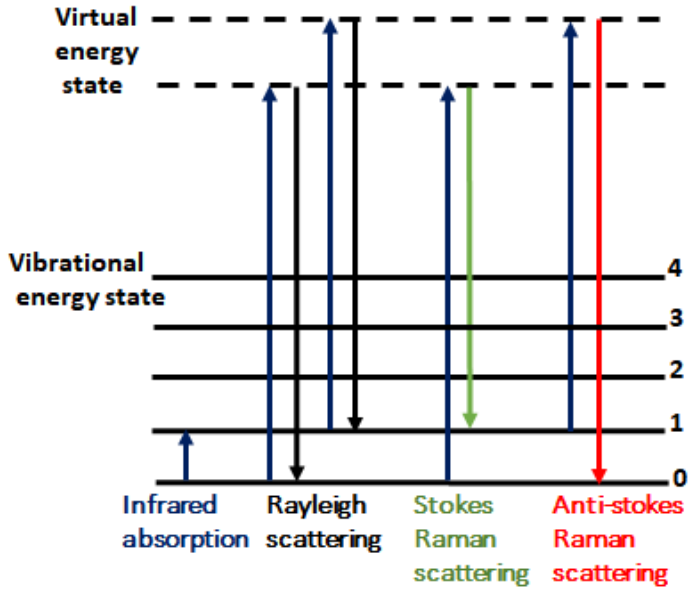

FIGURE 1.12 – Energy-level diagram showing the states in Raman/IR spectra.

While Rayleigh scattering produce no exchange of energy between incident and scattered photons, higher vibrational energy is obtained in the case of Stokes - $h(v_0 - v_v)$ and lower vibrational energy in the anti-Stokes scattering $-h(v_0 + v_v)$. This indicates that the wavelength of the scattered light depends of the difference of energy among different vibrational states. Chandrasekara Venkata Raman proved the Raman effect and won the Nobel Prize in Physics in the year 1930.[152]

Raman spectrometers allow the acquisition of several spectra in a short time, improving their sensitivity, especially the signal to noise ratio. Different types of lasers with wavelengths ranging from 200 to 1064 nm are used as radiation sources, such as lasers in the UV-visible region (argon or krypton ions) that generate large Raman scattering but promote fluorescence in some molecules, which is very undesirable in Raman spectroscopy. Another example is the lasers in the near infrared region like the diode Nd:YAG with emission at 1064 nm, that generates low Raman scattering but is virtually free of fluorescence.[153]

In the Raman spectrum, it is conventional to use 'Raman Shift (cm^{-1})' as the abscissa axis and the “Scattering Intensity” in the ordinate. The Raman Shift is obtained by converting the difference of energy between the incident and scattered photons to cm^{-1}. Therefore, peaks always have the same Raman Shift value regardless of the wavelength of the incident radiation, because the difference of energy between the incident and scattered photon will be always the difference among two vibrational states. It is noteworthy that the wavenumber was selected as a reference measure for the practicality of correlate the peaks present in a Raman spectrum with the infrared spectrum, such that a C=C stretch in a molecule will present a Raman Shift value very close to the wavenumber of its infrared spectrum, thus facilitating the characterization of the peaks.[154]

Most Raman spectroscopy are coupled with optical microscope usually with the charged-coupled device (CCD) camera, the laser employed at the source is focused through the microscope lenses, with possibility to target selected single points in the sample. This approach allows a spatial analysis of the sample, both visually (through the microscope) and by spectral representation (Fig. 1.13-A). Therefore, it is possible to obtain chemical information from specific points within the sample or even an spectroscopic image (hyperspectral analysis), where each pixel has a Raman spectrum linked to it, being used in several fields of analysis, such as imaging, homogeneity studies, and characterization of pharmaceutical materials.[155]

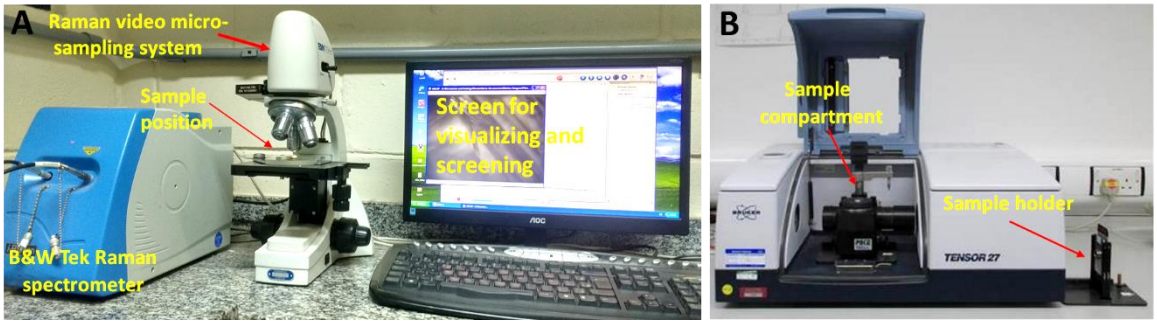

FIGURE 1.13 – Photos of (A) Raman spectrometer setup (B) FTIR spectrometer device.

1.6.3 Fourier-transform infrared (FTIR) spectroscopy

Like Raman, ultraviolet-visible, NMR and other spectroscopy techniques, the infrared (IR) spectroscopy is a powerful technique that exploits the absorption of infrared light by functionalities in molecules. When IR of specific frequencies (energy) matches the frequencies of infrared active bonds in a molecule, the radiation is absorbed. The measurement/processing of the wavelength and intensity of the absorbed IR by sample is presented in the form of spectra, using the Fourier transform conversion, an inbuilt mathematical and data processing computer software that convert signals into the sample's IR spectra.[156]

The IR spectroscopy technology was improved by the development of the Fourier Transform method and the performance of an FTIR is superior to that of conventional IR instruments. The principles of IR spectroscopy based on infrared absorption by matter when infrared radiation of specified energy passes through an interferometer and channeled through sample, movable mirror inside the apparatus alters the distribution of the light that passes through the interferometer. The recorded signal (interferogram) represents light output as a function of mirror position. The data-processing technique (Fourier transform) turns this raw data to a spectrum, i.e., the obtained signal at the detector is transformed into a spectrum representing the molecular “fingerprint” of the sample. Therefore, the absorption peaks correspond to the frequencies of vibrations between the bonds of the atoms of the sample.[157]

FTIR (Fig. 1.13-B) serves as characterization tool for investigating/detecting the absorption and vibrational modes of molecules or bonded atoms rather than solid-state properties. It has been one of the most widely used methods for investigating polymorphism and to observe the thermodynamic details such as transition point and number of components existing in samples.[158] Nevertheless, Raman, FTIR and other spectroscopy techniques like NMR, UV-Vis are strong complementary techniques for both qualitative and quantitative analysis.

IR spectroscopies are divided in three: near-, mid- and far- infrared. The higher-energy ‘’near-IR’’ approximately 14000–4000 cm^{-1} (0.7–2.5 μm wavelength) can excite overtones (harmonic molecular vibrations) and combination of vibrations. The

mid- infrared, approximately 4000–400 cm^{-1} (2.5–25 μm) may be used to study the fundamental vibrations and associated rotational-vibrational energy. The far infrared, approximately 400–10 cm^{-1} (25–1000 μm), lying adjacent to the microwave region, has low energy and may be used for rotational spectroscopy and to analyze inorganic compounds, due to the low frequency of vibration of bonds between heavy atoms.[159]

Raman spectroscopy provides vibrational information about bands that are weak or inactive in FTIR, such as the stretching vibrations of functional groups like C=C, C≡C, C≡N, N=N, C-S, O-O, and medium to strong skeletal vibrations of symmetrical molecules/groups. Likewise, the FTIR provides absorption information about Raman inactive/weak vibrational modes (polar functionalities) such as the C-O, N-O and O-H (obviously, not in all Raman inactive molecules). However, Raman spectrometers are capable of covering lower wavenumbers like 100 cm^{-1} or lower, whereas most spectra provided by FTIR stop at 400 or 200 cm^{-1}. For these reasons, Raman and FTIR spectroscopy serve as complementary tools/techniques to cover wider wavenumbers range and provide information on the fundamental vibrations bands of functionalities that are either Raman or FTIR active.[160]

1.6.4 X-ray diffraction (XRD)

X-ray diffraction analysis is an important crystallographic characterization tool for molecular structure identification and resolution. It differentiates between solid material forms especially the crystalline, amorphous, and semi crystalline materials. It is a principal tool for polymorphic identification, analysis of material purity and crystallinity. Single-crystal XRD (SCXRD) can estimate the chemical composition, find the absolute configuration and determine some properties of materials. It generate information about the packing of atoms/molecules and full structural details (geometrical parameters) such as molecular connectivity, bond lengths and angles.[161] Unlike molecular spectroscopy that provide information on the vibrational modes of functionalities when they interact with radiation, the X-ray diffraction and crystallography studies provide complete and undisputed information on the elastic scattering of X-ray photons by atoms in a periodic lattice.[162]

In XRD equipment, X-rays are produced in a tube when high-velocity electrons decelerate as a consequence of an impact on a metal target (commonly copper or molybdenum) in an evacuated enclosure. Also intense X-rays are produced in synchrotron rings, in which electrons moving at relativistic speed are contained by magnetic fields.[162]

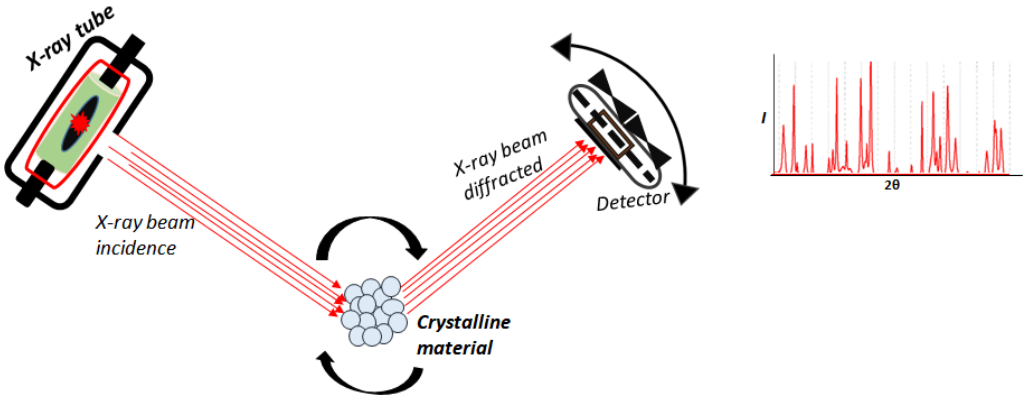

FIGURE 1.14 – A sketch of X-ray interaction with crystal to generate diffractions.

Therefore, when these X-rays interact with electrons clouds of the positioned crystal sample as demonstrated in Figure 1.14, the measurement of electron density within a unit cell of the crystalline system is obtained via scattered X-rays that present the same frequency as the incident beam. These scattered X-rays are collected on detector as diffractions patterns. Each atom in the crystal serves as a center for wave scattering, and thus, the magnitude and phase of the waves added by atoms to the interference pattern is a function of their respective atomic numbers and positions (*x, y, z*) in relation to each other.

Historically, in 1912, Max von Laue (a German physicist) discovered the X-ray phenomenon while studying the interaction between light and crystalline solids and he observed that crystals could act as diffraction grating for X-rays. Herein, he suggested that electromagnetic radiation of shorter wavelength is needed to observe crystalline solids and proposed that X-rays might have a wavelength comparable to the unit-cell spacing in crystals. He further demonstrated mathematically the diffraction of incident beams through laws that connects the scattering angles and

the size and orientation of the unit-cell spacing in the crystal, and established that X-rays are electromagnetic in nature through the interaction of X-rays beam with crystalline materials. Max von Laue was awarded the Nobel Prize in Physics in 1914.[163]

However, subsequent work by Sirs William and Lawrence Bragg established theories on crystal structure by the means of X-ray diffraction and discovered the precise three dimensional crystal structures of molecular solids. The Bragg proved that an incident electromagnetic radiation (X-rays) with a wavelength similar to an inter-planar distance (d) in crystal planes (of the order of 1Å), results in X-rays being scattered and presenting constructive (Figure 1.15) and destructive interference. The scattered monochromatic x-rays in phase will present constructive interference when the additional distance travelled by the radiation is a multiple of the X-ray wavelength.[164] This condition is expressed in equation 1.4 by Bragg's law, where θ is the incident angle, d is the distance between the planes, λ is the wavelength and n is a integer number, as follow:

$$n\lambda = 2d \sin \theta \qquad (1.4)$$

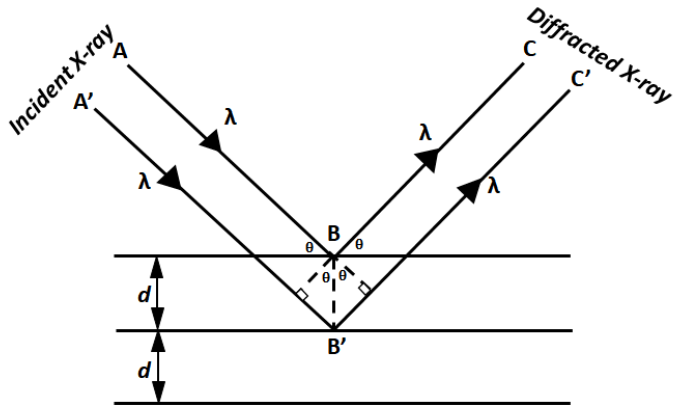

FIGURE 1.15 - Bragg diffraction of X-rays by crystal planes.

The X-ray powder diffraction pattern of a crystalline material is the plot of the diffraction intensity as a function of 2θ value (or equivalently, d spacings) and may be considered to be the fingerprint of the crystal. Nevertheless, the value of the d

spacings reflects the dimensions of the unit cell, while the contents of the unit cell and the arrangement of atoms/molecules therein presents the intensities.[165]

The unit cell (Figure 1.16 a) is often reduced to sub-units known as the asymmetric unit, where each asymmetric unit is related to others by symmetry elements (rotation, reflection, inversion and so on), to form the complete crystal structure. The planes within a set of asymmetric units are parallel and equidistant (interplanar distance known as d-spacing) and are labelled by integer values which are mathematically related to the unit cell parameters called the Miller indices (h,k,l). In crystallography, the Miller indices form a notation system for planes in crystal lattice (Bravais), i.e., an infinite array of discrete points generated by a set of discrete translation operations described in three dimensional space.[166]

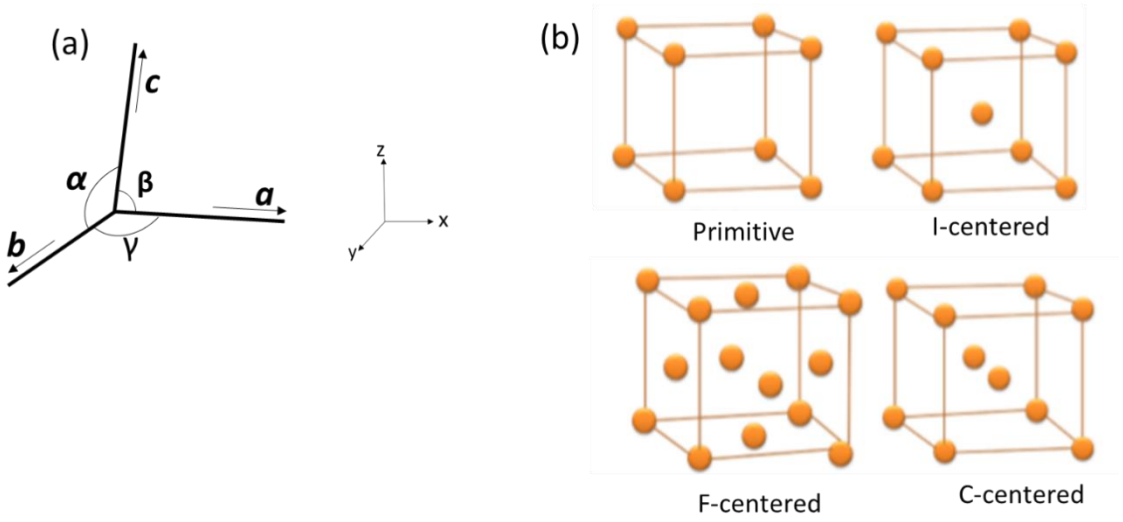

FIGURE 1.16 - (a) Sketch of a unit cell in three-dimensional parameters (b) The four of the fourteen Bravais lattice.

A crystal structure is assigned to a space group that represents its symmetry elements within the system using the combination of possible symmetry elements, the seven crystal systems and the fourteen types of unit cells or Bravais lattices (Table 1.1). The possible symmetry elements include inversion, rotation, reflection, screw axes and glide planes. Figure 1.16b shows the common four of the fourteen

Bravais lattice. Therefore, only 230 different space groups are available into which a crystal structure can possibly be assigned.

TABLE 1.1 – Showing the relationship between different crystal systems, unit cell and Bravais types.

Crystal System	Restriction on Unit Cell Parameter	Possible Bravais Types
Cubic	a = b = c α = β = γ = 90°	P, I, F
Hexagonal	a = b ≠ c α = β, γ = 120°	P
Trigonal	a = b = c α = β = γ ≠ 90°	R
Tetragonal	a = b ≠ c α = β = γ = 90°	P, I
Orthorhombic	a ≠ b ≠ c α = β = γ = 90°	P, I, F, C
Monoclinic	a ≠ b ≠ c α = γ = 90°, β ≠ 90°	P, C
Triclinic	a ≠ b ≠ c α ≠ β ≠ γ ≠ 90°	P

The molecular structure determination is achieved using single crystal methods.[167] Traditionally, the powder XRD is used for the qualitative identification of individual polymorphic phases, phase purity, and percentage crystallinity of a sample, while the single crystal method provides undoubtable details on molecular and crystal structure. However, these methods are employed complementarily to generate detailed structural information.[168] Nevertheless, the single crystal XRD serves as the ultimate crystallographic data source for complete structure determination and structure refinement software such as CrysAlisPro,[169] F2

(SHELXTL-97),[170] Olex2,[171] ORTEP-3,[172] WinGX[173] and MERCURY[174] are used for data integration, corrections, model refinement, crystal structure analysis and visualization, and preparation of the crystallographic information files (CIF).

1.6.5. Differential scanning calorimetric (DSC)

Thermal techniques generally provide quantitative information about the material thermal behaviors such as melting point, heat capacity, heat of fusion/transition, relative stability of polymorphic forms, and determination of phase transition energies. The methods are based on the principle that phase changes in the physical state of materials or even chemical reactions/decomposition are accompanied by the liberation or absorption of heat (exothermic and endothermic events).[175]

The differential scanning calorimetric (DSC) is a thermal analysis technique that detects the temperatures and heat flows caused by changes in heat capacity or by endothermic and exothermic processes of materials as a function of time and temperature. This technique serves as an important screening and characterization tool for studying and monitoring materials thermal properties, especially to differentiate between polymorphic materials.[176]

Figure 1.17 shows a typical chamber in a “heat flow” DSC, a temperature-controlled furnace that contain two cells for the sample and the inert reference material. The pan made of Al, Cu, Au, Pt, alumina, or graphite is selected to avoid reactions with samples, while the thermocouple measures the temperature flowing into both cell. However, the cells are heated (or cooled) at a controlled heating (or cooling) rate. The DSC account for difference in the heat energy required to increase the temperature of both sample and reference when they are heated cooled at the same rate.[177]

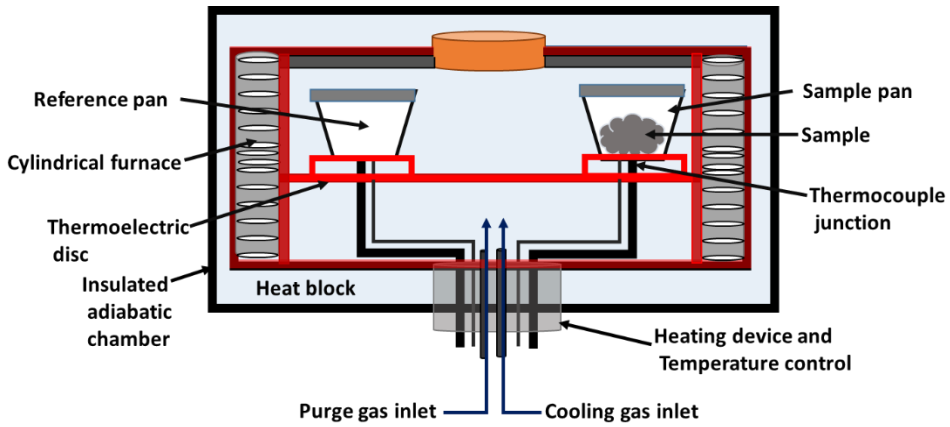

FIGURE 1.17 – Schematic diagram of a typical chamber setup in a “heat flow” DSC.

Generally, the temperature program for a typical DSC is designed to allow the sample temperature to increase linearly as a function of time. Therefore, when a sample undergo physical transformation such as phase transition, crystallization, or melting, more or less heat will be required to flow into the sample compared to the reference material to maintain both at the same temperature. Therefore, thermal event i.e., exothermic or endothermic transitions, thus depending on the thermal properties of the sample, is measured as a function of temperature or time.

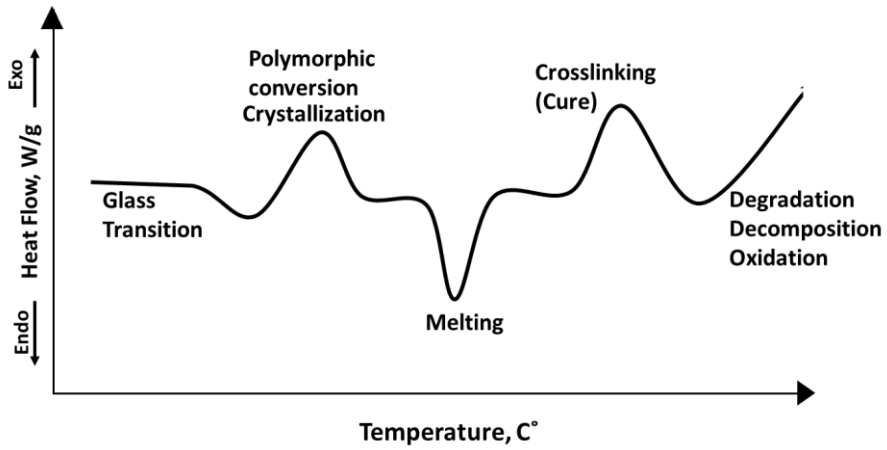

FIGURE 1.18 – DSC curve showing thermal events.

Figure 1.18 shows a typical DSC heating transition (heat flow) for endothermic and exothermic transition and the information that is obtained in the direction of heat flow when performing DSC analysis. DSC is used to ascertain the melting point (melting temperature), differentiate polymorphic forms and thermal stability of different multicomponent cocrystal/salt forms synthesized in this project.[24]

1.6.6 Thermogravimetric Analysis (TGA)

Thermogravimetric analysis (TGA) is a method that measures the amount and rate of change in the material weight as a function of temperature or time under a controlled atmosphere. This equipment determines the composition of materials by predicting their thermal stability at every increase in the temperature, and it determines material weight loss or gain due to the decomposition, oxidation, or dehydration. Based on this, it provides information about physical phenomena, such as second-order phase transitions, including vaporization, sublimation, absorption, adsorption, and desorption. Also, information about chemical phenomena including chemisorption, desolvation (especially dehydration), decomposition, and solid gas reactions (e.g., oxidation or reduction) are obtained.[178]

Unlike the DCS that detects the heat flows (energy variation) in thermal events, the TGA device is used mainly to measure the mass loss of a material as a function of temperature. These techniques are used complementarily as characterization tools for the determination of thermal stability, composition of multicomponent systems, and moisture/volatile content.[177]

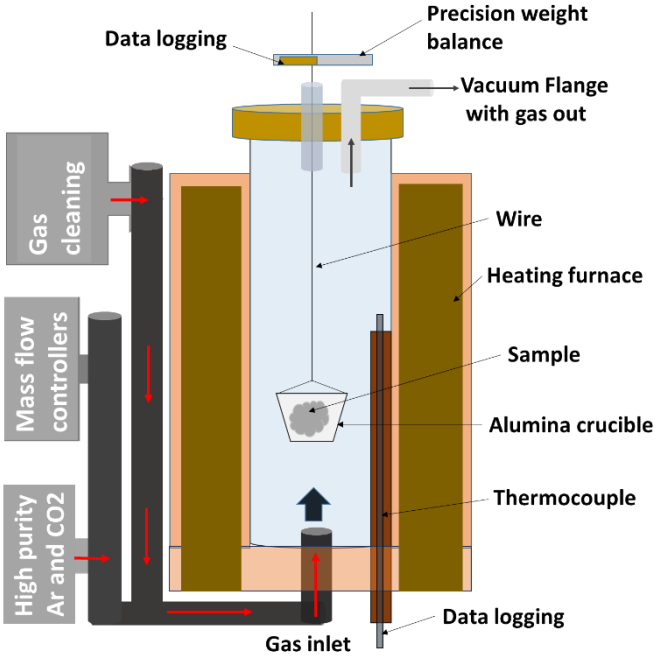

FIGURE 1.19 – Schematic diagram of a typical TGA chamber.

Figure 1.19 shows a typical TGA chamber with the sample placed in a pan suspended by the thermally isolated balance that accurately monitors the changes in the mass of the sample. Likewise, the heating rate and material weight change are continuously monitored over the entire thermal analysis period, while the temperature-scanning rate and the purge gas flow-rate can be changed. This analysis is achieved through gradual raising of temperature and plotting the sample's weight against temperature. For that, it is used computer programs to control the instrument and to process the data temperature vs. weight, as presented in Figure 1.20. Herein, the characteristics of the sample changes due to loss of volatiles (such as moisture), decomposition, and oxidation.[179]

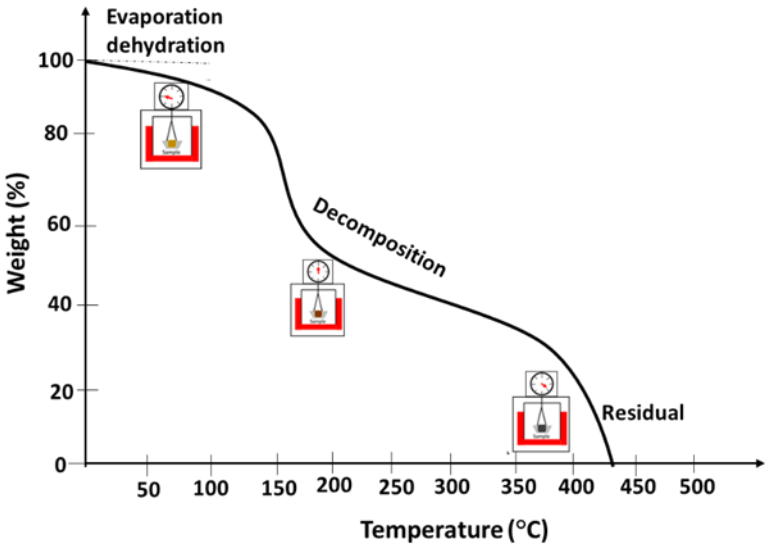

FIGURE 1.20 – A TGA curve indicating stages of thermal events.

1.6.7 Optical/Hot-Stage Microscopy

Hot-stage microscopy (HSM) is an analytical technique that combines the best properties of microscopy and thermal analysis to enable the comprehensive study and characterization of the physical properties of solid-state materials as a function of temperature and time.[180] It generates information (visual/video) about particle size and particle morphology, visual monitoring of thermal changes to obtain valuable information on material purity and melting point, recrystallization, decomposition and other transformations during heating.[181] In addition, USM provides information on phase transformations (solid-solid or solid-liquid), like evaporation, sublimation, evidences of molecular interactions (crystal growth), and the study of polymorphic transitions.[182]

This thermo-optical technique is credited to Ludwig/Adelheid Kofler (founders of the Innsbruck group), Otto Lehman, and Maria Kuhnert-Brandstätter.[24] Maria Kuhnert-Brandstätter worked extensively using HSM for the solid-state characterization of pharmaceutical compounds and this technique with other thermal devices have become a well-established screening and characterization tool.[183]

FIGURE 1.21 – A photo of an Optical/Hot-Stage Microscopy setup.

The Figure 1.21 shows the picture of an optical hot-stage photomicroscope (polarizing microscope) setup with programmed temperature controller. The staged compartments include the optical video-enhanced microscope, polarizer, hot-stage chamber, computer with image manipulation software, and high-resolution color digital camera that offers even greater possibilities for the characterization of materials. Herein, heating temperature from 0.1 °C/min up to ~350 °C is applied thermoelectrically, and cooling is achieved through high-pressure pumps or purge gas. The system allows the control of the heating process and observation of thermal events as high-resolution photomicrography. The generated data is imported into a computer to provide a real-time presentation of the temperature dependent transitions. The Figure 1.22 shows typical photomicrograph images obtained from HSM, collected at different temperatures and magnification using crossed polarizers.[184]

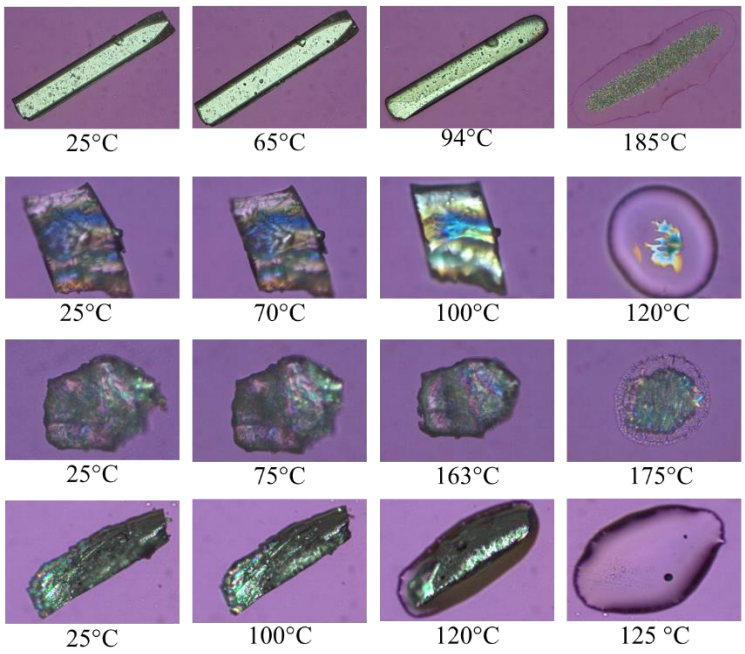

FIGURE 1.22 - Images obtained from HSM.

1.6.8 UV Spectrophotometry

Aqueous solubility plays important role in the pharmacokinetic properties of pharmaceutical materials and especially the bioavailability parameters.[185] The use of UV Spectrophotometer for solubility determination is based on the principle that molecules containing bonding and non-bonding electrons can absorb energy in the form of ultraviolet or visible light to excite these electrons to higher anti-bonding molecular orbitals. Hence, it presents an efficient method for the identification and quantification of the amount (quantity) of a solute in solution, especially, in the quality control of drugs. This concept is based on the Beer-Lamberts law that establish the relationship between light absorption and solute concentration under suitable conditions.[177]

Figure 1.23 shows a UV light source with an initial intensity (I_o) passing through a solution in a cuvette of length (*l*) and the intensity (I) after some light absorption by the sample. The ratio of (I/Io) is the transmittance (T), and is usually

expressed as percentage transmittance (%T). Thus, the absorbance (A), which is based on the transmittance, is expressed as follows:

$$\mathbf{A = - \log 10\ T = -\log 10\ (I/Io).} \quad (1.5)$$

$$\mathbf{1/T = 10(A)} \quad (1.6)$$

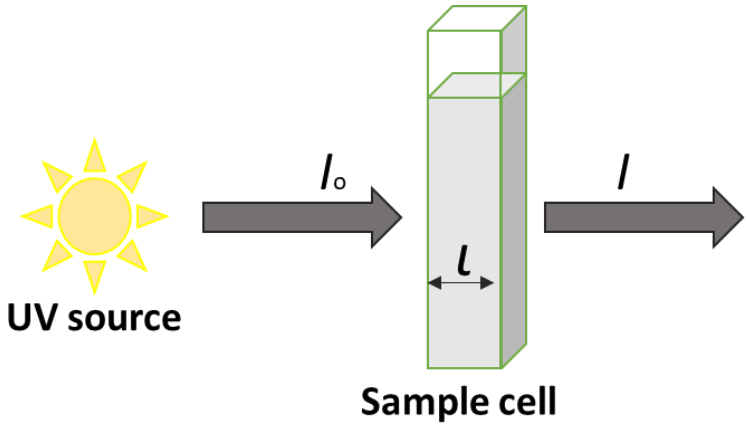

FIGURE 1.23 - UV light absorption by a sample.

The Figure 1.24 shows the basic parts of a typical UV spectrophotometer with a radiation source like Tungsten filament (300–2500 nm), deuterium arc lamp, which is continuous over the ultraviolet region (190–400 nm), Xenon arc lamp, which is continuous from 160 to 2,000 nm; or more recently, light emitting diodes (LED) for the entire visible wavelengths (390-780 nm). The monochromator filters degenerated light and only a short band (single wavelength) passes through the samples/reference where specific wavelengths are absorbed by the sample. The detector can be a photomultiplier tube, photodiode, photodiode array or charge-coupled device (CCD).[186]

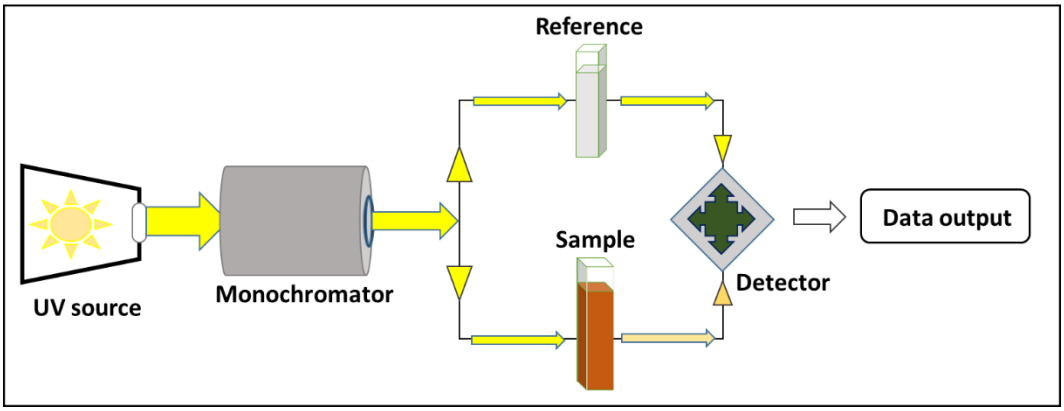

FIGURE 1.24 - The basic parts of a UV spectrophotometer.

1.7 Fluconazole

Fluconazole[91] (2-(2,4-difluorophenyl)-1,3-bis(1H-1,2,4triazole-1-yl)-propan-2-ol) is a first-generation triazole antifungal medication reported to be a slightly soluble multifunction drug sold as Diflucan® for preventing and curing fungal infections such as *candidiasis*,[187] *blastomycosis,*[188] *coccidiodomycosis,*[189] *pityriasis versicolor,*[190] *cryptococcosis,*[191] *histoplasmosis,*[192] and *dermatophytosis*.[193] It an important drug against *candidiasis* infection for immunocompromised patients with advanced acquired immune-deficiency syndrome (AIDS),[194] cancer patients undergoing some chemotherapy or radiation therapy treatment,[195] and patients with high infections risk following organ transplantation.[196]

Pharmacologically,[197] FLZ presents potential and competence to destroy yeast and fungal cell membranes like other imidazole- and triazole-class antifungals, by inhibits the synthesis of ergosterol, the component in the fungal cell membrane.[198] However, FLZ continuous usage is required to achieve the appropriate dosage concentration required for an effective biological activity due to its low aqueous solubility issue.[199]

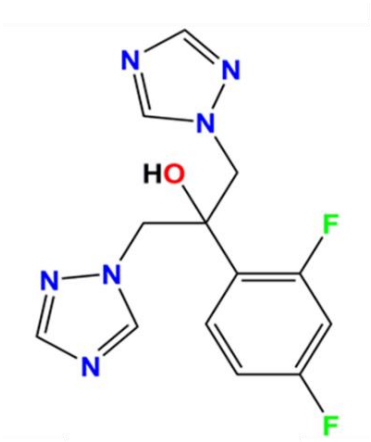

FIGURE 1.25 – Molecular structure of Fluconazole.

The Figure 1.25 presents the chemical structure of FLZ that differs from earlier azole antifungals such as ketoconazole[200] in that FLZ structure contains a triazole ring instead of an imidazole ring, and serves for systemic treatment because of their improved safety and predictable absorption when administered orally compared to other azole antifungal that are topically administered.[201] However, the bioavailability of FLZ is as high as 90%, and the plasma protein binding is very low (12%).[202] It was observed to present low solubility, about 4-5 mg/L at 25 °C for its polymorphs,[203] and will require about 50-400 mg for plasma concentration via continuous oral administration.[204]

However, due to the low aqueous solubility observed with this multifunction drug, there is a need to improve this property. Hence, different research and studies have reported successful breakthroughs with the syntheses of different multicomponent solid forms and polymorphs of FLZ.[205] The work of Alkhamis et al., detailed a report/summary on the syntheses of different multicomponent solid forms of FLZ, including solvates, salt and polymorphs.[31] In this contribution, four pharmaceutical cocrystals, a salt and a polymorph of FLZ with improved physicochemical properties such as aqueous solubility and stability were synthesized and characterized in line with the CE methodology.[203] These cocrystals and salt present improved and higher equilibrium solubility in different folds when compared to the reported solubility of commercialized FLZ forms. Interestingly, this

thesis presents the first structurally reported salt of the antifungal drug fluconazole with the highest reported solubility.

CHAPTER 2

AIM AND OBJECTIVES

2 AIMS AND OBJECTIVES

2.2 Aims

The discovery and development/manufacturing of therapeutically effective drugs is a challenging, expensive, and complex process to the pharmaceutical industries, in that, pharmaceutical industries seek high therapeutic and clinical potential drugs with preferable pharmacokinetic and physicochemical properties. Unfortunately, high percentage of important commercialized drugs present low therapeutic activity due to less desired physicochemical and pharmacokinetic property issues, such as low aqueous solubility, low bioavailability and chemical instability.

This research aims to optimize the pharmacokinetic and physicochemical properties of active pharmaceutical ingredients (APIs) belonging to the Biopharmaceutical Classification System (BCS) class II and IV, through the understanding of intermolecular interactions in the context of crystal engineering (CE) concept to design and synthesize new multicomponent solid-state functional structures, such pharmaceutical cocrystals and salts.

2.3 Objectives

The objectives of this research (thesis) are in line with the crystal-engineering concept for improving physicochemical properties APIs. Therefore, towards achieving our ultimate aim, the following are the objectives of this work:

(1) To design the selections of API/coformer(s) that present high possibility of achieving intermolecular interactions (hydrogen bond propensities) using the multicomponent screening wizard of MERCURY program of the CSD package and the supramolecular synthon interactions;

(2) To design simple crystallization experimental for synthesize new and physicochemically improved solid forms of APIs, in the forms of cocrystals/salt, with emphasis on their solubility and stability, using crystal engineering concept;

(3) To develop an efficient analytical method for screening/monitoring phases of supramolecular interactions such as different polymorphic phases, obtained from complex crystallization processes using the Raman/FTIR spectroscopy (vibrational and absorption modes) with a multivariate tool (PCA) as a complementary tools for data analysis.

(4) To recommend the importance of multivariate analysis (analytical data analysis) into crystal engineering concepts as a reliable tool/methodology for screening, monitoring and detecting new supramolecular synthesis routes, and especially the screening of new polymorphic phases.

(5) To perform structural property characterization for all obtained structure using Raman/FTIR spectroscopy, X-ray diffraction (powder/single crystal), thermal analysis; Differential scanning calorimeter, thermogravimetric analysis and optical/hot-Stage microscopy, using UV spectrophotometry to determine their equilibrium solubility.

CHAPTER 3

REPORTED RESULTS IN THE MANUSCRIPTS

According to the rules of the *Programa de Pós-Graduação em Química* of *Universidade Federal de São Carlos*, the Ph.D. candidate can present and use his published papers, which bring the obtained results during the thesis development, for the thesis defense. To do that, the sum of the impact factors of the published papers need to be higher than 6.0.

In this way, the obtained results and conclusions will be presented as papers in Annexes.

Annex I brings the first paper, *Fluconazolium oxalate: synthesis and structural characterization of a highly soluble crystalline form*, published in the journal CrystEngComm, volume 21, pages 1114 to 1121, 2019. Impact factor: 3.382.

Annex II brings the second paper, *Fluconazole: Synthesis and Structural Characterization of Four New Pharmaceutical Cocrystal Forms*, published in the journal Crystal Growth & Design, volume 19, pages 648 to 657, 2019. Impact factor: 4.153.

CHAPTER 4

CONCLUSIONS AND FUTURE PERSPECTIVE

4 CONCLUSIONS AND FUTURE PERSPECTIVE

4.1 Conclusions

This doctorate thesis re-presents the importance and potentials of crystal engineering as a dependable, established, and rapidly expanding discipline that aid the optimization of less desired physicochemical and pharmacokinetic properties of active pharmaceutical ingredients like solubility, dissolution rate and bioavailability. This practice of crystal lattice modification through design/screening, intermolecular interactions, supramolecular synthesis, monitoring and evaluation, quantification, and characterization result into novel (optimized form) multicomponent solid forms of previous APIs, which is eligible for patency approval under standard (regulations) and requirements of drug control governmental agencies.

However, considering the FDA directive 2001/83/EC reports and reflection paper published by EMEA that new generic medicinal products can contain APIs that deviate from the originator, and therefore, the polymorphic forms of the mentioned API variations are suitable for a generic application. It is however justifiable to say that the four (4) new cocrystals of fluconazole, the oxalate salt of fluconazole, the imidazolium hydrated salt of Diclofenac and the new polymorph of FLZ reported in this report stand the chance to be candidates for generic drugs. In as much as salts and pharmaceutical cocrystals are classified alongside polymorphs of an API, they are therefore eligible candidates for generic applications as laid out in Article 10 (2) (b) of directive 2001/83/EC.

In addition, the potential advantages of employing chemometric tool; principal component analysis (PCA), tool to monitor, visualize, detect and investigate the molecular properties of materials through decomposition of Raman/FTIR vibrational modes (data analysis) was rewarded with a new polymorph of FLZ as reported herein. Therefore, the credibility of this combination is its ability/potential to detect latent trends in complex crystallization processes and aid the selection of desired supramolecular synthesis routes compared to the conventional method of spectra superimposition.

4.2 Future perspective

In this thesis, crystal engineering and supramolecular chemistry present the opportunity to redefine the physicochemical and indirectly the pharmacokinetic properties of less desired APIs through non-covalent intermolecular interactions that manipulates crystal lattice arrangement without altering their therapeutic/biological activities, thus resulting into new and physicochemically improved pharmaceutical cocrystals/salts forms with patentability right under legal guidelines. Likewise, the application/combination of chemometric tools such as PCA for analytical purposes was demonstrated and justified.

The recent FDA directive 2001/83/EC and reflection by EMA suggested that new generic medicinal products can contain APIs that deviate from the originator, and therefore, the polymorphic forms of the said API are suitable for a generic application. In as much as pharmaceutical cocrystals are classified alongside polymorphs of an API, the former and likes (hydrates/solvates) are therefore eligible candidates for generic applications as explained in the Article 10 (2)(b) of directive 2001/83/EC, and the compliance of agencies like EMA and ANVISA as suggested in their recent reflections. In addition, the approval of biowaiver approach, serves the advantages of using salts, polymorphs, cocrystals and their diversities in generic pharmaceutical products. However fixed dose combinations of important APIs like *Combivir* (lamivudine-zidovudine)[206] and *Dovato* (dolutegravir-lamivudine)[207] for HIV and HIV-1 infections respectively, *Tukysa* (tucatinib, trastuzumab and capecitabine)[208] for HER2-positive breast cancer, to mention a few, have recently been approved.

Considering the aforementioned developments, the future perspectives and trends in the application crystal engineering and supramolecular chemistry will focus on the advantages and benefits of multidrug chemotherapy scheme that aim at using existing synergistic interactions between (related/selected) APIs to design/achieve pharmaceutical multidrug cocrystals and salts with optimized properties for diverse multi-actions therapy against resistance strains of diseases/infections

.

REFERENCES

1. Yong, C.; Kaplan, D. S.; Gray, A.; Ricles, L.; Kwilas, A.; Brubaker, S.; Arcidiacono, J.; Xu, L.; Chang, C.; Robinson, R., Overview of the US Food and Drug Administration Regulatory Process. In *Principles of Regenerative Medicine*, Elsevier: 2019; pp 1345-1365.
2. Morais, J. A. G.; Lobato, M. d. R., The new European Medicines Agency guideline on the investigation of bioequivalence. *Basic & clinical pharmacology & toxicology* **2010,** *106* (3), 221-225.
3. SANITÁRIA, I. E. V., ANVISA–AGÊNCIA NACIONAL DE VIGILÂNCIA SANITÁRIA.
4. Teixeira, T.; Kweder, S. L.; Saint-Raymond, A., Are the European Medicines Agency, US Food and Drug Administration, and Other International Regulators Talking to Each Other? *Clinical Pharmacology & Therapeutics* **2020,** *107* (3), 507-513.
5. Fisher, A. C.; Lee, S. L.; Harris, D. P.; Buhse, L.; Kozlowski, S.; Yu, L.; Kopcha, M.; Woodcock, J., Advancing pharmaceutical quality: an overview of science and research in the US FDA's Office of Pharmaceutical Quality. *International journal of pharmaceutics* **2016,** *515* (1-2), 390-402.
6. (a) Schweitzer, S. O.; Lu, Z. J., *Pharmaceutical economics and policy: perspectives, promises, and problems*. Oxford University Press: 2018; (b) Caliari, T.; Ruiz, R. M., Brazilian pharmaceutical industry and generic drugs policy: Impacts on structure and innovation and recent developments. *Science and Public Policy* **2014,** *41* (2), 245-256.
7. G de la Torre, B.; Albericio, F., The pharmaceutical industry in 2018. An analysis of FDA drug approvals from the perspective of molecules. *Molecules* **2019,** *24* (4), 809.
8. Löbenberg, R.; Amidon, G. L., Modern bioavailability, bioequivalence and biopharmaceutics classification system. New scientific approaches to international regulatory standards. *European journal of pharmaceutics and biopharmaceutics* **2000,** *50* (1), 3-12.
9. Kasim, N. A.; Whitehouse, M.; Ramachandran, C.; Bermejo, M.; Lennernäs, H.; Hussain, A. S.; Junginger, H. E.; Stavchansky, S. A.; Midha, K. K.; Shah, V. P., Molecular properties of WHO essential drugs and provisional biopharmaceutical classification. *Molecular pharmaceutics* **2004,** *1* (1), 85-96.
10. Cardot, J.-M.; Arieta, A. G.; Paixao, P.; Tasevska, I.; Davit, B., Implementing the biopharmaceutics classification system in drug development: reconciling similarities, differences, and shared challenges in the EMA and US-FDA-recommended approaches. *The AAPS journal* **2016,** *18* (4), 1039-1046.
11. Davit, B. M.; Kanfer, I.; Tsang, Y. C.; Cardot, J.-M., BCS biowaivers: similarities and differences among EMA, FDA, and WHO requirements. *The AAPS journal* **2016,** *18* (3), 612-618.
12. Karam, R., Biowaivers: Criteria and requirements. *Prepared by Dr. Mazen Kurdi* **2015**, 1-11.
13. Benet, L. Z., The role of BCS (biopharmaceutics classification system) and BDDCS (biopharmaceutics drug disposition classification system) in drug development. *Journal of pharmaceutical sciences* **2013,** *102* (1), 34-42.
14. Rustichelli, C.; Gamberini, G.; Ferioli, V.; Gamberini, M. C.; Ficarra, R.; Tommasini, S., Solid-state study of polymorphic drugs: carbamazepine. *Journal of pharmaceutical and biomedical analysis* **2000,** *23* (1), 41-54.
15. Bauer, J.; Spanton, S.; Henry, R.; Quick, J.; Dziki, W.; Porter, W.; Morris, J., Ritonavir: an extraordinary example of conformational polymorphism. *Pharmaceutical research* **2001,** *18* (6), 859-866.
16. Özdemir, N.; Ordu, S.; Özkan, Y., Studies of floating dosage forms of furosemide: in vitro and in vivo evaluations of bilayer tablet formulations. *Drug development and industrial pharmacy* **2000,** *26* (8), 857-866.
17. Vishweshwar, P.; McMahon, J. A.; Bis, J. A.; Zaworotko, M. J., Pharmaceutical co-crystals. *Journal of pharmaceutical sciences* **2006,** *95* (3), 499-516.
18. Bernstein, J.; Reutzel-Edens, S., Polymorphs, salts, solvates, co-crystals. **2019**.
19. Healy, A. M.; Worku, Z. A.; Kumar, D.; Madi, A. M., Pharmaceutical solvates, hydrates and amorphous forms: A special emphasis on cocrystals. *Advanced drug delivery reviews* **2017,** *117*, 25-46.
20. Schultheiss, N.; Newman, A., Pharmaceutical cocrystals and their physicochemical properties. *Crystal growth and design* **2009,** *9* (6), 2950-2967.
21. Brittain, H. G., Polymorphism in pharmaceutical solids. *Drugs and the pharmaceutical sciences* **1999,** *95*, 183-226.
22. Das, D.; Engel, E.; Barbour, L. J., Reversible single-crystal to single-crystal polymorphic phase transformation of an organic crystal. *Chemical Communications* **2010,** *46* (10), 1676-1678.
23. Alsirawan, M. B.; Paradkar, A., Impact of the Polymorphic Form of Drugs/NCE s on Preformulation and Formulation Development. *Innovative Dosage Forms: Design and Development at Early Stage* **2019**, 1-47.

24. Bernstein, J.; Bernstein, J. M., *Polymorphism in molecular crystals*. Oxford University Press: 2002; Vol. 14.
25. Kersten, K.; Kaur, R.; Matzger, A., Survey and analysis of crystal polymorphism in organic structures. *IUCrJ* **2018,** *5* (2), 124-129.
26. Dunitz, J., Phase changes and chemical reactions in molecular crystals. *Acta Crystallographica Section B: Structural Science* **1995,** *51* (4), 619-631.
27. Cruz-Cabeza, A. J.; Reutzel-Edens, S. M.; Bernstein, J., Facts and fictions about polymorphism. *Chemical Society Reviews* **2015,** *44* (23), 8619-8635.
28. Morris, K. R.; Griesser, U. J.; Eckhardt, C. J.; Stowell, J. G., Theoretical approaches to physical transformations of active pharmaceutical ingredients during manufacturing processes. *Advanced drug delivery reviews* **2001,** *48* (1), 91-114.
29. Censi, R.; Di Martino, P., Polymorph impact on the bioavailability and stability of poorly soluble drugs. *Molecules* **2015,** *20* (10), 18759-18776.
30. Thakuria, R.; Thakur, T., 5.13-Crystal Polymorphism in Pharmaceutical Science. Elsevier: Oxford, UK: 2017; pp 283-309.
31. Caira, M. R.; Alkhamis, K. A.; Obaidat, R. M., Preparation and crystal characterization of a polymorph, a monohydrate, and an ethyl acetate solvate of the antifungal fluconazole. *Journal of pharmaceutical sciences* **2004,** *93* (3), 601-611.
32. Cabri, W.; Ghetti, P.; Pozzi, G.; Alpegiani, M., Polymorphisms and patent, market, and legal battles: cefdinir case study. *Organic process research & development* **2007,** *11* (1), 64-72.
33. Pallipurath, A. R.; Civati, F.; Sibik, J.; Crowley, C.; Zeitler, J. A.; McArdle, P.; Erxleben, A., A comprehensive spectroscopic study of the polymorphs of diflunisal and their phase transformations. *International journal of pharmaceutics* **2017,** *528* (1-2), 312-321.
34. Bhatia, A.; Chopra, S.; Nagpal, K.; Deb, P. K.; Tekade, M.; Tekade, R. K., Polymorphism and its Implications in Pharmaceutical Product Development. In *Dosage Form Design Parameters*, Elsevier: 2018; pp 31-65.
35. Mullin, J. W., *Crystallization*. Elsevier: 2001.
36. Mao, W., Recrystallization and grain growth. *Handbook of Aluminum* **2003,** *1*, 211-258.
37. Patole, T.; Deshpande, A., Co-crystallization-a technique for solubility enhancement. *Int J Pharm Sci Res* **2014,** *5* (9), 3566.
38. Myerson, A., *Handbook of industrial crystallization*. Butterworth-Heinemann: 2002.
39. Fujiwara, M.; Nagy, Z. K.; Chew, J. W.; Braatz, R. D., First-principles and direct design approaches for the control of pharmaceutical crystallization. *Journal of Process Control* **2005,** *15* (5), 493-504.
40. Braatz, R. D., Advanced control of crystallization processes. *Annual reviews in control* **2002,** *26* (1), 87-99.
41. Kotak, U.; Prajapati, V.; Solanki, H.; Jani, G.; Jha, P., Co-crystallization technique its rationale and recent progress. *World J Pharm Pharm Sci* **2015,** *4* (4), 1484-508.
42. Desiraju, G. R., Crystal engineering: a holistic view. *Angewandte Chemie International Edition* **2007,** *46* (44), 8342-8356.
43. Bosch, E., Role of sp-C− H---N Hydrogen Bonding in Crystal Engineering. *Crystal growth & design* **2010,** *10* (8), 3808-3813.
44. Custelcean, R., Anions in crystal engineering. *Chemical Society Reviews* **2010,** *39* (10), 3675-3685.
45. Khavasi, H. R.; Azizpoor Fard, M., π− π interactions affect coordination geometries. *Crystal growth & design* **2010,** *10* (4), 1892-1896.
46. Aakeröy, C. B.; Champness, N. R.; Janiak, C., Recent advances in crystal engineering. *CrystEngComm* **2010,** *12* (1), 22-43.
47. Desiraju, G. R., Crystal and co-crystal. *CrystEngComm* **2003,** *5* (82), 466-467.
48. Desiraju, G. R., Crystal engineering: A brief overview. *Journal of chemical sciences* **2010,** *122* (5), 667-675.
49. Good, D. J.; Rodriguez-Hornedo, N., Solubility advantage of pharmaceutical cocrystals. *Crystal Growth and Design* **2009,** *9* (5), 2252-2264.
50. Yang, J.; Grey, K.; Doney, J., An improved kinetics approach to describe the physical stability of amorphous solid dispersions. *International journal of pharmaceutics* **2010,** *384* (1-2), 24-31.
51. Mukherjee, S.; Ray, S.; Thakur, R., Solid lipid nanoparticles: a modern formulation approach in drug delivery system. *Indian journal of pharmaceutical sciences* **2009,** *71* (4), 349.

52. Semalty, A.; Semalty, M.; Rawat, B. S.; Singh, D.; Rawat, M., Pharmacosomes: the lipid-based new drug delivery system. *Expert opinion on drug delivery* **2009,** *6* (6), 599-612.
53. Chien, Y., *Novel drug delivery systems*. CRC Press: 1991.
54. McNamara, D. P.; Childs, S. L.; Giordano, J.; Iarriccio, A.; Cassidy, J.; Shet, M. S.; Mannion, R.; O'Donnell, E.; Park, A., Use of a glutaric acid cocrystal to improve oral bioavailability of a low solubility API. *Pharmaceutical research* **2006,** *23* (8), 1888-1897.
55. Cruz-Cabeza, A. J., Acid–base crystalline complexes and the p K a rule. *CrystEngComm* **2012,** *14* (20), 6362-6365.
56. Kompella, U. B.; Koushik, K., Preparation of drug delivery systems using supercritical fluid technology. *Critical Reviews™ in Therapeutic Drug Carrier Systems* **2001,** *18* (2).
57. Lu, E.; Rodríguez-Hornedo, N.; Suryanarayanan, R., A rapid thermal method for cocrystal screening. *CrystEngComm* **2008,** *10* (6), 665-668.
58. Tiwari, B. K., Ultrasound: A clean, green extraction technology. *TrAC Trends in Analytical Chemistry* **2015,** *71*, 100-109.
59. Karimi-Jafari, M.; Padrela, L.; Walker, G. M.; Croker, D. M., Creating cocrystals: a review of pharmaceutical cocrystal preparation routes and applications. *Crystal Growth & Design* **2018,** *18* (10), 6370-6387.
60. Rodrigues, M.; Baptista, B.; Lopes, J. A.; Sarraguça, M. C., Pharmaceutical cocrystallization techniques. Advances and challenges. *International journal of pharmaceutics* **2018,** *547* (1-2), 404-420.
61. Douroumis, D.; Ross, S. A.; Nokhodchi, A., Advanced methodologies for cocrystal synthesis. *Advanced drug delivery reviews* **2017,** *117*, 178-195.
62. Sanjay, A. N.; Manohar, S. D.; Bhanudas, S. R., Pharmaceutical cocrystallization: A review. *India: Journal of Advanced Pharmacy Education & Research* **2014,** *4* (4).
63. Bysouth, S. R.; Bis, J. A.; Igo, D., Cocrystallization via planetary milling: enhancing throughput of solid-state screening methods. *International journal of pharmaceutics* **2011,** *411* (1-2), 169-171.
64. Lin, S.-Y., Mechanochemical approaches to pharmaceutical cocrystal formation and stability analysis. *Current pharmaceutical design* **2016,** *22* (32), 5001-5018.
65. Friscic, T.; Jones, W., Recent advances in understanding the mechanism of cocrystal formation via grinding. *Crystal Growth and Design* **2009,** *9* (3), 1621-1637.
66. Trask, A. V.; van de Streek, J.; Motherwell, W. S.; Jones, W., Achieving polymorphic and stoichiometric diversity in cocrystal formation: Importance of solid-state grinding, powder X-ray structure determination, and seeding. *Crystal growth & design* **2005,** *5* (6), 2233-2241.
67. Schultheiss, N. C.; Bethune, S. J., Pterostilbene cocrystals. Google Patents: 2013.
68. Sonawane, A., Insights of Dosage form Design: Polymorphs and Cocrystals. *Asian Journal of Biomedical and Pharmaceutical Sciences* **2013,** *3* (27), 1.
69. Bowmaker, G. A., Solvent-assisted mechanochemistry. *Chemical Communications* **2013,** *49* (4), 334-348.
70. Friščić, T.; Trask, A. V.; Jones, W.; Motherwell, W. S., Screening for inclusion compounds and systematic construction of three-component solids by liquid-assisted grinding. *Angewandte Chemie International Edition* **2006,** *45* (45), 7546-7550.
71. Block, E. R.; Bennett, J. E., Pharmacological studies with 5-fluorocytosine. *Antimicrobial agents and chemotherapy* **1972,** *1* (6), 476-482.
72. Awtry, E. H.; Loscalzo, J., Aspirin. *Circulation* **2000,** *101* (10), 1206-1218.
73. Dunitz, J. D., Crystal and co-crystal: a second opinion. *CrystEngComm* **2003,** *5* (91), 506-506.
74. Bond, A. D., What is a co-crystal? *CrystEngComm* **2007,** *9* (9), 833-834.
75. Rogers, R. D., Crystal Growth & Design Around the World in 2012. ACS Publications: 2012.
76. Bernstein, J.; Davis, R. E.; Shimoni, L.; Chang, N. L., Patterns in hydrogen bonding: functionality and graph set analysis in crystals. *Angewandte Chemie International Edition in English* **1995,** *34* (15), 1555-1573.
77. Desiraju, G. R., Supramolecular synthons in crystal engineering—a new organic synthesis. *Angewandte Chemie International Edition in English* **1995,** *34* (21), 2311-2327.
78. Qiao, N.; Li, M.; Schlindwein, W.; Malek, N.; Davies, A.; Trappitt, G., Pharmaceutical cocrystals: an overview. *International journal of pharmaceutics* **2011,** *419* (1-2), 1-11.
79. Shan, N.; Zaworotko, M. J., The role of cocrystals in pharmaceutical science. *Drug discovery today* **2008,** *13* (9-10), 440-446.
80. Khankari, R. K.; Grant, D. J., Pharmaceutical hydrates. *Thermochimica acta* **1995,** *248*, 61-79.

81. Griesser, U. J., The importance of solvates. *Polymorphism in the pharmaceutical industry* **2006**, 211-233.
82. Aitipamula, S.; Banerjee, R.; Bansal, A. K.; Biradha, K.; Cheney, M. L.; Choudhury, A. R.; Desiraju, G. R.; Dikundwar, A. G.; Dubey, R.; Duggirala, N., Polymorphs, salts, and cocrystals: what's in a name? *Crystal growth & design* **2012,** *12* (5), 2147-2152.
83. Smith, A. J.; Kim, S.-H.; Duggirala, N. K.; Jin, J.; Wojtas, L.; Ehrhart, J.; Giunta, B.; Tan, J.; Zaworotko, M. J.; Shytle, R. D., Improving lithium therapeutics by crystal engineering of novel ionic cocrystals. *Molecular pharmaceutics* **2013,** *10* (12), 4728-4738.
84. Kelley, S. P.; Narita, A.; Holbrey, J. D.; Green, K. D.; Reichert, W. M.; Rogers, R. D., Understanding the effects of ionicity in salts, solvates, co-crystals, ionic co-crystals, and ionic liquids, rather than nomenclature, is critical to understanding their behavior. *Crystal growth & design* **2013,** *13* (3), 965-975.
85. Thakuria, R.; Sarma, B., Drug-drug and drug-nutraceutical cocrystal/salt as alternative medicine for combination therapy: a crystal engineering approach. *Crystals* **2018,** *8* (2), 101.
86. Fala, L., Entresto (Sacubitril/Valsartan): first-in-class angiotensin receptor neprilysin inhibitor FDA approved for patients with heart failure. *American Health & Drug Benefits* **2015,** *8* (6), 330.
87. Garnock-Jones, K. P.; McCormack, P. L., Escitalopram. *CNS drugs* **2010,** *24* (9), 769-796.
88. Robbins, M. R., Pharmacologic Management of Patients with Neurologic Disorders. In *Contemporary Dental Pharmacology*, Springer: 2019; pp 69-84.
89. Pudipeddi, M.; Serajuddin, A. T.; Shah, A. V.; Mufson, D., 11 Integrated Drug Product. *Drug Discovery and Development* **2019**, 223.
90. Hankey, G. J.; Eikelboom, J. W., Aspirin resistance. *The Lancet* **2006,** *367* (9510), 606-617.
91. Grant, S. M.; Clissold, S. P., Fluconazole. *Drugs* **1990,** *39* (6), 877-916.
92. Day, R. O.; Graham, G. G., Non-steroidal anti-inflammatory drugs (NSAIDs). *Bmj* **2013,** *346*, f3195.
93. Sawynok, J., Pharmacological rationale for the clinical use of caffeine. *Drugs* **1995,** *49* (1), 37-50.
94. Rainsford, K., Ibuprofen: pharmacology, efficacy and safety. *Inflammopharmacology* **2009,** *17* (6), 275-342.
95. Vemuri, V. D.; Lankalapalli, S., Insight into Concept and Progress on Pharmaceutical Co-Crystals: An Overview. *INDIAN JOURNAL OF PHARMACEUTICAL EDUCATION AND RESEARCH* **2019,** *53* (4), S522-S538.
96. Karagianni, A.; Malamatari, M.; Kachrimanis, K., Pharmaceutical cocrystals: new solid phase modification approaches for the formulation of APIs. *Pharmaceutics* **2018,** *10* (1), 18.
97. Jona, F.; Shirane, G.; Pepinsky, R., Dielectric, X-Ray, and Optical Study of Ferroelectric Cd 2 Nb 2 O 7 and Related Compounds. *Physical Review* **1955,** *98* (4), 903.
98. Schmidt, G., Photodimerization in the solid state. *Pure and Applied Chemistry* **1971,** *27* (4), 647-678.
99. Desiraju, G. R.; Vittal, J. J.; Ramanan, A., *Crystal engineering: a textbook*. World Scientific: 2011.
100. Aakeröy, C. B.; Seddon, K. R., The hydrogen bond and crystal engineering. *Chemical Society Reviews* **1993,** *22* (6), 397-407.
101. Braga, D.; Grepioni, F.; Desiraju, G. R., Crystal engineering and organometallic architecture. *Chemical reviews* **1998,** *98* (4), 1375-1406.
102. Desiraju, G. R., *The crystal as a supramolecular entity*. John Wiley & Sons: 2008; Vol. 18.
103. Desiraju, G. R., Hydrogen bridges in crystal engineering: interactions without borders. *Accounts of chemical research* **2002,** *35* (7), 565-573.
104. Arunan, E.; Desiraju, G. R.; Klein, R. A.; Sadlej, J.; Scheiner, S.; Alkorta, I.; Clary, D. C.; Crabtree, R. H.; Dannenberg, J. J.; Hobza, P., Definition of the hydrogen bond (IUPAC Recommendations 2011). *Pure and applied chemistry* **2011,** *83* (8), 1637-1641.
105. (a) Ganguly, P.; Desiraju, G. R., Van der Waals and polar intermolecular contact distances: Quantifying supramolecular synthons. *Chemistry–An Asian Journal* **2008,** *3* (5), 868-880; (b) Fowkes, F. M., Donor-acceptor interactions at interfaces. *The Journal of Adhesion* **1972,** *4* (2), 155-159.
106. Martinez, C. R.; Iverson, B. L., Rethinking the term "pi-stacking". *Chemical Science* **2012,** *3* (7), 2191-2201.
107. Southall, N. T.; Dill, K. A.; Haymet, A., A view of the hydrophobic effect. ACS Publications: 2002.
108. Bhattacharya, S.; Peraka, K. S.; Zaworotko, M. J., The Role of Hydrogen Bonding in Co-crystals. In *Co-crystals*, 2018; pp 33-79.
109. Sarmah, K. K.; Nath, N.; Rao, D. R.; Thakuria, R., Mechanochemical Synthesis of Drug-Drug and Drug-Nutraceutical Multicomponent Solids of Olanzapine. *CrystEngComm* **2020**.
110. Lehn, J.-M., Supramolecular chemistry. *Science* **1993,** *260* (5115), 1762-1764.

111. Lehn, J. M., Supramolecular chemistry—scope and perspectives molecules, supermolecules, and molecular devices (Nobel Lecture). *Angewandte Chemie International Edition in English* **1988,** *27* (1), 89-112.
112. Pedersen, C. J., The discovery of crown ethers (Noble Lecture). *Angewandte Chemie International Edition in English* **1988,** *27* (8), 1021-1027.
113. Cram, D. J., The design of molecular hosts, guests, and their complexes (Nobel lecture). *Angewandte Chemie International Edition in English* **1988,** *27* (8), 1009-1020.
114. Desiraju, G.; Krishnamohan Sharma, C., Crystal engineering and molecular recognition. Twin facets of supramolecular chemistry. *The Crystal as a Supramolecular Entity* **2008,** *18*, 31.
115. Izatt, R. M., Charles J. Pedersen: Innovator in macrocyclic chemistry and co-recipient of the 1987 Nobel Prize in chemistry. *Chemical Society Reviews* **2007,** *36* (2), 143-147.
116. Lehn, J.-M., Constitutional dynamic chemistry: bridge from supramolecular chemistry to adaptive chemistry. In *Constitutional Dynamic Chemistry*, Springer: 2011; pp 1-32.
117. Nangia, A.; Desiraju, G. R., Supramolecular synthons and pattern recognition. In *Design of Organic Solids*, Springer: 1998; pp 57-95.
118. Shattock, T. R.; Arora, K. K.; Vishweshwar, P.; Zaworotko, M. J., Hierarchy of supramolecular synthons: persistent carboxylic acid⋯ pyridine hydrogen bonds in cocrystals that also contain a hydroxyl moiety. *Crystal growth and design* **2008,** *8* (12), 4533-4545.
119. Adalder, T. K.; Sankolli, R.; Dastidar, P., Homo-or heterosynthon? A crystallographic study on a series of new cocrystals derived from pyrazinecarboxamide and various carboxylic acids equipped with additional hydrogen bonding sites. *Crystal growth & design* **2012,** *12* (5), 2533-2542.
120. Thomas, I. R.; Bruno, I. J.; Cole, J. C.; Macrae, C. F.; Pidcock, E.; Wood, P. A., WebCSD: the online portal to the Cambridge Structural Database. *Journal of applied crystallography* **2010,** *43* (2), 362-366.
121. Maharramov, A. M.; Mahmudov, K. T.; Kopylovich, M. N.; Pombeiro, A. J., *Non-covalent interactions in the synthesis and design of new compounds*. John Wiley & Sons: 2016.
122. Mukherjee, A., Building upon supramolecular synthons: some aspects of crystal engineering. *Crystal Growth & Design* **2015,** *15* (6), 3076-3085.
123. Hansen, C. L.; Quake, S. R.; Berger, J. M., High throughput screening of crystallization of materials. Google Patents: 2007.
124. Loschen, C.; Klamt, A., Solubility prediction, solvate and cocrystal screening as tools for rational crystal engineering. *Journal of Pharmacy and Pharmacology* **2015,** *67* (6), 803-811.
125. Sarkar, N.; Aakeröy, C. B., Evaluating hydrogen-bond propensity, hydrogen-bond coordination and hydrogen-bond energy as tools for predicting the outcome of attempted co-crystallisations. *Supramolecular Chemistry* **2019**, 1-10.
126. Macrae, C. F.; Bruno, I. J.; Chisholm, J. A.; Edgington, P. R.; McCabe, P.; Pidcock, E.; Rodriguez-Monge, L.; Taylor, R.; Streek, J.; Wood, P. A., Mercury CSD 2.0–new features for the visualization and investigation of crystal structures. *Journal of Applied Crystallography* **2008,** *41* (2), 466-470.
127. Bond, A. D., *The role of the Cambridge Structural Database in crystal engineering*. John Wiley & Sons, Ltd.: Chichester, UK: 2010.
128. Yamashita, H.; Hirakura, Y.; Yuda, M.; Terada, K., Coformer screening using thermal analysis based on binary phase diagrams. *Pharmaceutical research* **2014,** *31* (8), 1946-1957.
129. Kuleshova, L.; Hofmann, D.; Boese, R., Lattice energy calculation–a quick tool for screening of cocrystals and estimation of relative solubility. Case of flavonoids. *Chemical Physics Letters* **2013,** *564*, 26-32.
130. Mohammad, M. A.; Alhalaweh, A.; Velaga, S. P., Hansen solubility parameter as a tool to predict cocrystal formation. *International journal of pharmaceutics* **2011,** *407* (1-2), 63-71.
131. Musumeci, D.; Hunter, C. A.; Prohens, R.; Scuderi, S.; McCabe, J. F., Virtual cocrystal screening. *Chemical Science* **2011,** *2* (5), 883-890.
132. Price, S. L.; Price, L. S., Toward Computational Polymorph Prediction. *Polymorphism in the Pharmaceutical Industry: Solid Form and Drug Development* **2018**, 133-157.
133. Saganowska, P.; Wesolowski, M., Principal component and cluster analyses as supporting tools for co-crystals detection. *Journal of Thermal Analysis and Calorimetry* **2017,** *130* (1), 45-55.
134. Soares, F. L.; Carneiro, R. L., Green synthesis of ibuprofen–nicotinamide cocrystals and in-line evaluation by Raman spectroscopy. *Crystal growth & design* **2013,** *13* (4), 1510-1517.
135. Aaltonen, J.; Allesø, M.; Mirza, S.; Koradia, V.; Gordon, K. C.; Rantanen, J., Solid form screening–a review. *European Journal of Pharmaceutics and Biopharmaceutics* **2009,** *71* (1), 23-37.
136. Bernstein, J., Crystal polymorphism. In *Engineering of Crystalline Materials Properties*, Springer: 2008; pp 87-109.

137. Siraj, S. N.; Hiteshkumar, A. S.; Khan, G.; Jameelahmed, S. A., Pharmaceutical Cocrystals: Modern solubility enhancement approach based on crystal engineering. *Current Pharma Research* **2019,** *9* (3), 3078-3085.
138. Calvo, N. L.; Maggio, R. M.; Kaufman, T. S., Characterization of pharmaceutically relevant materials at the solid state employing chemometrics methods. *Journal of pharmaceutical and biomedical analysis* **2018,** *147*, 538-564.
139. Przybyłek, M.; Jeliński, T.; Słabuszewska, J.; Ziółkowska, D.; Mroczyńska, K.; Cysewski, P., Application of Multivariate Adaptive Regression Splines (MARSplines) Methodology for Screening of Dicarboxylic Acid Cocrystal Using 1D and 2D Molecular Descriptors. *Crystal Growth & Design* **2019,** *19* (7), 3876-3887.
140. Naik, G. R., *Advances in Principal Component Analysis: Research and Development*. Springer: 2017.
141. Jolliffe, I. T.; Cadima, J., Principal component analysis: a review and recent developments. *Philosophical Transactions of the Royal Society A: Mathematical, Physical and Engineering Sciences* **2016,** *374* (2065), 20150202.
142. Hopke, P. K., The evolution of chemometrics. *Analytica Chimica Acta* **2003,** *500* (1-2), 365-377.
143. Otto, M., *Chemometrics: statistics and computer application in analytical chemistry*. John Wiley & Sons: 2016.
144. Beebe, K. R.; Pell, R. J.; Seasholtz, M. B., *Chemometrics: a practical guide*. Wiley-Interscience: 1998; Vol. 4.
145. Wise, B. M.; Gallagher, N.; Bro, R.; Shaver, J.; Windig, W.; Koch, R. S., PLS Toolbox 4.0. *Eigenvector Research Incorporated: Wenatchee, WA, USA* **2007**, 99-162.
146. Hisada, H.; Okayama, A.; Hoshino, T.; Carriere, J.; Koide, T.; Yamamoto, Y.; Fukami, T., Determining the Distribution of Active Pharmaceutical Ingredients in Combination Tablets Using Near IR and Low-Frequency Raman Spectroscopy Imaging. *Chemical and Pharmaceutical Bulletin* **2020,** *68* (2), 155-160.
147. Soares, F. L. F.; Carneiro, R. L., Evaluation of analytical tools and multivariate methods for quantification of co-former crystals in ibuprofen-nicotinamide co-crystals. *Journal of pharmaceutical and biomedical analysis* **2014,** *89*, 166-175.
148. Shipp, D. W.; Sinjab, F.; Notingher, I., Raman spectroscopy: techniques and applications in the life sciences. *Advances in Optics and Photonics* **2017,** *9* (2), 315-428.
149. Das, R. S.; Agrawal, Y., Raman spectroscopy: recent advancements, techniques and applications. *Vibrational spectroscopy* **2011,** *57* (2), 163-176.
150. Hanlon, E.; Manoharan, R.; Koo, T. W.; Shafer, K.; Motz, J.; Fitzmaurice, M.; Kramer, J.; Itzkan, I.; Dasari, R.; Feld, M., Prospects for in vivo Raman spectroscopy. *Physics in Medicine & Biology* **2000,** *45* (2), R1.
151. Smith, E.; Dent, G., *Modern Raman spectroscopy: a practical approach*. John Wiley & Sons: 2019.
152. Raman, C. V., A new radiation. **1928**.
153. Kautek, W.; Roas, B.; Schultz, L., Formation of Y□ Ba□ Cu□ oxide thin films by pulsed laser deposition: A comparative study in the UV, visible and IR range. *Thin Solid Films* **1990,** *191* (2), 317-334.
154. Larkin, P., *Infrared and Raman spectroscopy: principles and spectral interpretation*. Elsevier: 2017.
155. Khan, M.; do Nascimento, G. M.; El-Azazy, M., Modern Spectroscopic Techniques and Applications. **2020**.
156. Stuart, B., Infrared spectroscopy. *Kirk-Othmer Encyclopedia of Chemical Technology* **2000**.
157. Smith, B. C., *Fundamentals of Fourier transform infrared spectroscopy*. CRC press: 2011.
158. Mohamed, M. A.; Jaafar, J.; Ismail, A.; Othman, M.; Rahman, M., Fourier transform infrared (FTIR) spectroscopy. In *Membrane Characterization*, Elsevier: 2017; pp 3-29.
159. McHale, J. L., *Molecular spectroscopy*. CRC Press: 2017.
160. Socrates, G., *Infrared and Raman characteristic group frequencies: tables and charts*. John Wiley & Sons: 2004.
161. Chauhan, A.; Chauhan, P., Powder XRD technique and its applications in science and technology. *J Anal Bioanal Tech* **2014,** *5* (5), 1-5.
162. Bunaciu, A. A.; UdriȘTioiu, E. G.; Aboul-Enein, H. Y., X-ray diffraction: instrumentation and applications. *Critical reviews in analytical chemistry* **2015,** *45* (4), 289-299.
163. Eckert, M., Max von Laue and the discovery of X-ray diffraction in 1912. *Annalen der Physik* **2012,** *524* (5), A83-A85.
164. McPherson, A., *Introduction to macromolecular crystallography*. John Wiley & Sons: 2011.

165. Kakudo, M.; Kasai, N., *X-ray Diffraction by Macromolecules*. Kodansha Limited and Springer-Verlag Berlin Heidelberg: 2005.
166. De Graef, M.; McHenry, M. E., *Structure of materials: an introduction to crystallography, diffraction and symmetry*. Cambridge University Press: 2012.
167. Ma, T.; Kapustin, E. A.; Yin, S. X.; Liang, L.; Zhou, Z.; Niu, J.; Li, L.-H.; Wang, Y.; Su, J.; Li, J., Single-crystal x-ray diffraction structures of covalent organic frameworks. *Science* **2018,** *361* (6397), 48-52.
168. Azároff, L. V.; Kaplow, R.; Kato, N.; Weiss, R. J.; Wilson, A.; Young, R., *X-ray Diffraction*. McGraw-Hill New York: 1974; Vol. 3.
169. Agilent, C. P., Agilent technologies. *Yarnton, England* **2010**.
170. Sheldrick, G. M., Crystal structure refinement with SHELXL. *Acta Crystallographica Section C: Structural Chemistry* **2015,** *71* (1), 3-8.
171. Dolomanov, O. V.; Bourhis, L. J.; Gildea, R. J.; Howard, J. A.; Puschmann, H., OLEX2: a complete structure solution, refinement and analysis program. *Journal of applied crystallography* **2009,** *42* (2), 339-341.
172. Farrugia, L. J., ORTEP-3 for Windows-a version of ORTEP-III with a Graphical User Interface (GUI). *Journal of Applied Crystallography* **1997,** *30* (5), 565-565.
173. Farrugia, L. J., WinGX and ORTEP for Windows: an update. *Journal of Applied Crystallography* **2012,** *45* (4), 849-854.
174. Macrae, C. F.; Edgington, P. R.; McCabe, P.; Pidcock, E.; Shields, G. P.; Taylor, R.; Towler, M.; Streek, J., Mercury: visualization and analysis of crystal structures. *Journal of Applied Crystallography* **2006,** *39* (3), 453-457.
175. Brown, M. E., *Introduction to thermal analysis: techniques and applications*. Springer Science & Business Media: 2001; Vol. 1.
176. Akash, M. S. H.; Rehman, K., Differential Scanning Calorimetry. In *Essentials of Pharmaceutical Analysis*, Springer: 2020; pp 199-206.
177. Zhang, S.; Li, L.; Kumar, A., *Materials characterization techniques*. CRC press: 2008.
178. Prime, R. B.; Bair, H. E.; Vyazovkin, S.; Gallagher, P. K.; Riga, A., Thermogravimetric analysis (TGA). *Thermal analysis of polymers: Fundamentals and applications* **2009**, 241-317.
179. Lothenbach, B.; Durdzinski, P.; De Weerdt, K., Thermogravimetric analysis. In *A practical guide to microstructural analysis of cementitious materials*, CRC Press Oxford, UK: 2016; pp 177-212.
180. Bhattacharya, S.; Brittain, H. G.; Suryanarayanan, R., Thermoanalytical and crystallographic methods. In *Polymorphism in Pharmaceutical Solids*, CRC Press: 2018; pp 330-358.
181. Šimek, M.; Grünwaldová, V.; Kratochvíl, B., Hot-stage microscopy for determination of API fragmentation: comparison with other methods. *Pharmaceutical development and technology* **2016,** *21* (5), 583-589.
182. Chadha, R.; Arora, P.; Bhandari, S.; Bala, M., Thermomicroscopy and its pharmaceuticals applications. In *Current Microscopy Contributions to Advances in Science and Technology*, Microscopy Book Series Badajoz, Spain: 2012; Vol. 2, pp 1013-1024.
183. Vitez, I. M.; Newman, A. W.; Davidovich, M.; Kiesnowski, C., The evolution of hot-stage microscopy to aid solid-state characterizations of pharmaceutical solids. *Thermochimica acta* **1998,** *324* (1-2), 187-196.
184. Vitez, I. M.; Newman, A. W.; Craig, D.; Reading, M., Thermal microscopy. *Thermal Analysis of Pharmaceuticals* **2007,** *6000*, 226-262.
185. Østergaard, J., UV imaging in pharmaceutical analysis. *Journal of pharmaceutical and biomedical analysis* **2018,** *147*, 140-148.
186. Sommer, L., *Analytical absorption spectrophotometry in the visible and ultraviolet: the principles*. Elsevier: 2012.
187. Calderone, R. A.; Clancy, C. J., *Candida and candidiasis*. American Society for Microbiology Press: 2011.
188. Castillo, C. G.; Kauffman, C. A.; Miceli, M. H., Blastomycosis. *Infectious Disease Clinics* **2016,** *30* (1), 247-264.
189. Anstead, G. M.; Graybill, J. R., Coccidioidomycosis. In *Hunter's Tropical Medicine and Emerging Infectious Diseases*, Elsevier: 2020; pp 666-670.
190. Flores-Genuino, R. N. S.; Ray, S.; Bigby, M.; Morales-Sánchez, M. A.; Arkoncel, M.; Realubit-Serrano, M. A. C.; Bamford, J. T., Interventions for the treatment of pityriasis versicolor. *The Cochrane database of systematic reviews* **2018,** *2018* (6).
191. Shiri, T.; Loyse, A.; Mwenge, L.; Chen, T.; Lakhi, S.; Chanda, D.; Mwaba, P.; Molloy, S. F.; Heyderman, R. S.; Kanyama, C., Addition of Flucytosine to Fluconazole for the Treatment of Cryptococcal

Meningitis in Africa: A Multicountry Cost-effectiveness Analysis. *Clinical Infectious Diseases* **2020,** *70* (1), 26-29.
192. Boniche, C.; Rossi, S. A.; Kischkel, B.; Barbalho, F. V.; Moura, Á. N. D.; Nosanchuk, J. D.; Travassos, L. R.; Taborda, C. P., Immunotherapy against Systemic Fungal Infections Based on Monoclonal Antibodies. *Journal of Fungi* **2020,** *6* (1), 31.
193. Ghannoum, M. A.; Salem, I.; Isham, N., Dermatophytosis. In *Antifungal Therapy, Second Edition*, CRC Press: 2019; pp 257-272.
194. Meenakshi, S.; Rani, R. V., Speciation of Candida Isolated among Immunocompromised Patients. *Int. J. Curr. Microbiol. App. Sci* **2019,** *8* (3), 1582-1586.
195. Sun, M.; Chen, C.; Xiao, W.; Chang, Y.; Liu, C.; Xu, Q., Increase in Candida parapsilosis candidemia in cancer patients. *Mediterranean journal of hematology and infectious diseases* **2019,** *11* (1).
196. Benedetti, V. P.; Savi, D. C.; Aluizio, R.; Adamoski, D.; Kava, V.; Galli-Terasawa, L. V.; Glienke, C., ERG11 gene polymorphisms and susceptibility to fluconazole in Candida isolates from diabetic and kidney transplant patients. *Revista da Sociedade Brasileira de Medicina Tropical* **2019,** *52*.
197. Lewis, R. E. In *Current concepts in antifungal pharmacology*, Mayo Clinic Proceedings, Elsevier: 2011; pp 805-817.
198. Dudley, M. N., Clinical pharmacology of fluconazole. *Pharmacotherapy* **1990,** *10* (6 part 3).
199. Govindarajan, A.; Aboeed, A., Fluconazole. In *StatPearls [Internet]*, StatPearls Publishing: 2019.
200. Van Cutsem, J., The antifungal activity of ketoconazole. *The American journal of medicine* **1983,** *74* (1), 9-15.
201. Hughes, C. E.; Beggs, W. H., Action of fluconazole (UK-49, 858) in relation to other systemic antifungal azoles. *Journal of Antimicrobial Chemotherapy* **1987,** *19* (2), 171-174.
202. Castagnola, E.; Machetti, M.; Bucci, B.; Viscoli, C., Antifungal prophylaxis with azole derivatives. *Clinical Microbiology and Infection* **2004,** *10*, 86-95.
203. Owoyemi, B. C. D.; da Silva, C. C.; Diniz, L. F.; Souza, M. S.; Ellena, J.; Carneiro, R. L., Fluconazolium oxalate: synthesis and structural characterization of a highly soluble crystalline form. *CrystEngComm* **2019,** *21* (7), 1114-1121.
204. Debruyne, D.; Ryckelynck, J.-P., Clinical pharmacokinetics of fluconazole. *Clinical pharmacokinetics* **1993,** *24* (1), 10-27.
205. Dayo Owoyemi, B. C.; da Silva, C. C.; Souza, M. S.; Diniz, L. F.; Ellena, J.; Carneiro, R. L., Fluconazole: Synthesis and Structural Characterization of Four New Pharmaceutical Cocrystal Forms. *Crystal Growth & Design* **2019,** *19* (2), 648-657.
206. Oversteegen, L.; Shah, M.; Rovini, H., HIV combination products. Nature Publishing Group: 2007.
207. Onono, M., Scotland approves dual therapy with dolutegravir/lamivudine (Dovato). *Final IAS 2019 reports: Scotland approves Dovato*.
208. Exchange, P.; OncNurse, T., Cannabis for Oncology Patients: A Clinical Review.

ANNEX I

CrystEngComm

PAPER

View Article Online
View Journal | View Issue

Cite this: *CrystEngComm*, 2019, 21, 1114

Fluconazolium oxalate: synthesis and structural characterization of a highly soluble crystalline form†

Bolaji C. Dayo Owoyemi,[a] Cecilia C. P. da Silva,[a] Luan F. Diniz,[b] Matheus S. Souza,[b] Javier Ellena[b] and Renato L. Carneiro*[a]

Received 10th October 2018,
Accepted 27th December 2018

DOI: 10.1039/c8ce01729h

rsc.li/crystengcomm

Fluconazole (FLZ) is one of the most used antifungal drugs worldwide and has been the focus of various investigations with the aim of enhancing its biomedical application. Most of the new solid forms achieved for this drug were determined by powder X-ray diffraction, and a few reports on polymorphs, solvates, cocrystals, and one salt–cocrystal by single-crystal X-ray diffraction (SCXRD) are available. By considering that FLZ is a very weak base (pK_a = 1.76, when protonated), salt formation with this drug is expected with the use of very strong organic acids, in order to dislocate the proton from the acid to the FLZ. To the best of our knowledge, only one organic salt of FLZ with picric acid (pK_a = 0.38) and one salt–cocrystal (maleate–maleic, pK_{a_1} = 1.92) were reported by SCXRD until now. Having in mind all the advantages that pharmaceutical salts have in drug delivery, in this work we depict the methodology and techniques employed to synthesize a new salt of FLZ using oxalic acid (pK_{a_1} = 1.23). The screening process was initially monitored using Raman spectroscopy, while further characterization by X-ray diffraction (powder and single crystal) and thermal analysis (DSC and TG) was performed to confirm the new salt fluconazolium oxalate (1 : 1). Finally, salt equilibrium solubility studies confirmed an improvement, about 7-fold, when compared to the commercialized active pharmaceutical ingredient (polymorph II). In addition, this is the first reported GRAS (generally regarded as safe) salt of the antifungal drug fluconazole.

Introduction

Fluconazole [FLZ, 2-(2,4-difluorophenyl)-1,3-bis(1*H*-1,2,4-triazole-1-yl)-2-propanol] (Scheme 1), known since 1983, is a triazole antifungal drug, formulated in oral tablets, suspensions, injectable vials, and topical cream. Its main mechanism of action involves the inhibition of cytochrome P-450-dependent 14a-sterol demethylase of lanosterol, an enzyme belonging to the heme protein. The inhibition of this enzyme leads to the depletion of ergosterol, a bioregulator of the membrane integrity in fungal cells. Due to the clinical efficacy and safety of FLZ, it has become one of the most used drugs worldwide, capable of curing several types of fungal infections, showing maximum inhibition against *Candida albicans*, and being used for treatment of dermatophyte infection (though not specifically indicated for this).[1–7]

Despite its intense use, according to Karanam and coworkers, FLZ is known to exhibit several polymorphic forms, solvates, and salts, with most of them, however, being characterized by powder X-ray diffraction (PXRD), Raman spectroscopy, and calorimetric techniques. A search in the Cambridge Structural Database (version 5.39, update, Aug 2018) showed 101 entries relative to metal complexes involving the FLZ structure against 14 entries concerning FLZ structures with organic molecules. These latter crystalline structures refer to five polymorphs, five cocrystals (2-hydroxybenzoic acid, malonic acid, fumaric acid, glutaric acid, and salicylic acid),

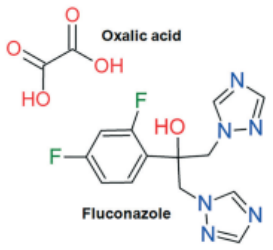

Scheme 1 Molecular structure of fluconazole and oxalic acid.

[a] *Department of Chemistry, Federal University of São Carlos – UFSCar, Rod. Washington Luís km 235, ZIP 13560-905 São Carlos – SP, Brazil*
[b] *Instituto de Física de São Carlos, Universidade de São Paulo, CP 369, 13.560-970, São Carlos, SP, Brazil. E-mail: renato.lajarim@ufscar.br*

† The CIF of this new salt structure was deposited in the CSD under the code CCDC 1838462 (fluconazole oxalic acid 1 : 1 salt). For crystallographic data in CIF or other electronic format see DOI: 10.1039/c8ce01729h

one solvate (ethyl acetate), one monohydrate, one salt (picric acid), and one salt–cocrystal (maleate–maleic).[8–15]

FLZ exhibits three main polymorphic forms, namely I, II, and III, and four more recent ones reported by Karanam and co-workers, namely IV, V, VI, and VII.[8] Among the three well-known polymorphic forms, FLZ form II is the commercialized one, form I is the most stable, and form III is the most soluble. Interconversion is observed to occur from form II to I under compression. Form I and the monohydrate are the most stable ones. The FLZ solubility is slightly pH dependent, in such a fashion that the most common forms of this drug are not very soluble in water (5 mg mL^{-1}).[10,16,17] By considering that the stability of the crystalline form and the low aqueous solubility for drugs are two of the main causes of bioavailability profile issues, together with low permeability, Kastelic and co-workers[12–14] reported new cocrystals of FLZ, in an attempt to enhance its aqueous solubility and to achieve a stable conformation. Only one study until now reported FLZ salt formation.[15] This lack of reports on organic salts can be associated with the fact that FLZ is a very weak base (pK_a = 1.76, conjugated acid, at 24 °C),[8] and therefore, salt formation could be observed only with the use of very strong acids, since the drug molecule will be essentially non-protonated at pH values above 3.5.

Having in mind that the use of salts of active pharmaceutical ingredients (APIs) or pharmaceutical salts has been, over the years, the primary approach applied by industries to improve the physicochemical properties of crystalline drugs, such as stability, solubility, and the dissolution rate,[18–24] our research group has devoted efforts toward finding suitable coformers capable of forming new FLZ organic salts. It is worth mentioning that by suitable we mean coformers not only exhibiting desirable hydrogen donor and acceptor groups, but also belonging to the list of substances generally regarded as safe (GRAS)[25] to be utilized in drug formulations, released by the Food and Drug Administration (FDA) or listed under EAFUS (everything added to food in the United States).[26] In this sense, the organic salt with picric acid reported in 2010 by Dutkiewicz and co-workers[15] does not fulfill the criteria for pharmaceutical application, since picric acid is not in the GRAS list. To accomplish our goal, crystal engineering (CE) principles,[27–30] the ΔpK_a rule,[31] and the tools available in the Mercury[32] program for multi-component screening were applied. The CE principles used were based on the context of supramolecular chemistry (synthon interaction of hydrogen bonding). Herein we considered all the reported crystalline structures of FLZ and studied the geometry of the molecule and the main functional groups capable of forming hydrogen bonds. The pK_a rule states that salts will be preferably formed when the ΔpK_a value ($\Delta pK_a = pK_{a(base)} - pK_{a(acid)}$) among the cocrystallizing agents is higher than 1; however, due to the low pK_a of FLZ, we considered for the experiments coformers having pK_a values below the FLZ pK_a (≤1.92).

The suitable coformers were selected from a predefined list available in the Mercury[32] program. This program belongs to the Cambridge Structural Database System and thus allows visualization and investigation of all crystalline structures deposited in the CSD.[9] In the CSD-materials package, it is possible to perform structural searches for identifying/quantifying motifs (predefined or drawn) occurring between specific functional groups, calculate crystal packing similarities (isostructural compounds), determine hydrogen bond propensities to assess polymorphism occurrence, analyze hydrate crystal structures, *etc.* For this work, the two tools used were the Generating Conformers, which allows assessment of the possible conformers (*i.e.* possible conformations of the FLZ molecule) to determine the crystalline structure based on geometrical statistics from the CSD, and the Multi-component Screening tool, which allows selection of the best coformers with basis in molecular complementarity. From the screening (depicted in detail in the Experimental screening section, see the Materials and methods section), three coformers emerged: oxalic acid, etidronic acid, and urea (pK_a values of 1.23,[33] 1.35,[34] and 0.1 (ref. 35) for the conjugated acid of urea, respectively). All the three coformers were tested for cocrystallization. Since the pK_a of urea is related to its conjugated acid, the formation of a salt was not expected. Only the salt with oxalic acid was obtained. The existence of the oxalate salt of FLZ was mentioned by Karanam and co-workers in 2011,[8] but no crystalline structure was depicted. Herein, we depict the methodologies and techniques employed to synthesize the 1 : 1 oxalate salt of FLZ. Raman spectroscopy was used to monitor the formation of new crystalline structures, while further characterization by X-ray diffraction (powder and single crystal) and thermal analysis (DSC and TG) was performed to confirm the salt properties and molecular structure. Finally, the salt equilibrium solubility study was performed and the result was compared with the values exhibited by other forms.

Materials and methods

Materials

A raw FLZ active pharmaceutical ingredient of pharmaceutical grade (form II, >99.0%, Brundavan Laboratories Ltd.) was purchased from a local drugstore in São Carlos, Sao Paulo (Brazil) and was used without further purification. However, FLZ form II rapidly converts to its monohydrate form when exposed to room temperature and humidity.[17] Oxalic acid dihydrate was purchased from Sigma-Aldrich Chemical Company with >99% purity (analytical reagent grade). Ultrapure deionized water was obtained from a Milli-Q system (18.2 mΩ cm), while HPLC grade solvents like acetonitrile and methanol were purchased from J.T Bakers Ltd.

Experimental screening

The possibility of achieving an ionic interaction between FLZ and a coformer towards synthesizing a salt of FLZ began with the coformer selection, using the Generating Conformers and the Multi-component Screening tools available in the Mercury[32] software, as mentioned in the Introduction section.

Firstly, we calculated the possible conformers for FLZ in the Generating Conformers tool, considering as the starting point the crystalline structure of the polymorph under refcode IVUQOF, reported by Caira and co-workers.[10] This initial calculation resulted in 171 possible configurations for the FLZ molecule. In sequence, the Multi-component Screening tool was applied, in such a fashion that each FLZ confomer generated was matched with the list of coformers available in the program. It is worth mentioning that the results obtained from the Multi-component Screening tool (hit rates ranging from 100% to 0%) were designed for cocrystal screening.[36] In this sense, as the main goal of this work was to select possible coformers for salt formation, then the coformers with minimum or no possibility of forming cocrystals (*i.e.* those with hit rates of 0% or close to it) were selected. These two tools were also applied for the other polymorphs deposited in the CSD and three coformers emerged: oxalic acid (OXL), etidronic acid (ETD), and urea. Here, solvent crystallization of different stoichiometric ratios of FLZ and the selected coformers was performed; 1 : 1, 1 : 2, 1 : 3, 2 : 1, 2 : 3, 3 : 1 and 3 : 2 were tested using solvent mixtures of acetonitrile/water (1 : 1 v/v) and methanol/water (1 : 1 v/v). Raman spectroscopy was employed as the first characterization tool in order to evaluate products with different spectra when compared to the reactants (FLZ, OXL, ETD, and urea), by comparing the fingerprint regions of the Raman spectra. Changes in the spectra were taken as evidence for the new chemical environment in the solids (new interactions). Only the 1 : 1 FLZ salt with OXL salt was successfully obtained.

Crystallization of fluconazolium oxalate salt (1 : 1)

The salt was synthesized from a 1 : 1 molar ratio of fluconazole (0.1 mmol) and oxalic acid dihydrate (0.1 mmol), dissolved in 3 mL of a water : methanol (2 : 3 v/v) solution, and stirred for 10 minutes, and the resulting solution was left at 25 °C to slowly evaporate. Suitable crystals for single crystal X-ray diffraction were obtained in the system after 48 hours. The crystals were filtered off, dried and stored in a plastic sample holder for further structural characterization use.

Raman spectroscopy

The Raman spectra were collected using a B&W Tek BWS 415-785H Raman spectrometer coupled to a B&W Tek BAC 151B microscope and an excitation laser with a wavelength of 785 nm, a spectral resolution of 3.5 cm^{-1}, an acquisition time of 120 s, a spectral range of 200–2180 cm^{-1}, and a laser power of 70 mW, managed by the BWSpec4.03 software. This vibrational spectroscopic technique aids in a quick screening and acts as the first tool for detecting evidence of new crystalline structures.

Powder X-ray diffraction (PXRD)

X-ray powder diffraction analysis of partially milled crystal powder was performed on a Multiflex X-ray diffractometer (Rigaku Corporation, Tokyo, Japan), using copper (Cu) Kα radiation (1.54 Å), a voltage of 40 kV and a current of 30 mA. The samples were scanned from 5° to 45° (2θ), with a step size of 0.2° θ per minute at a scan rate of 2° min^{-1} to provide structural information and the degree of crystallinity.

Single crystal X-ray diffraction

Crystallographic data collection for FLZ–OXL 1 : 1 was performed at 298 ± 2 K on a Bruker Super-Duo APEX II CCD diffractometer using MoKα radiation (0.71073 Å). The structure was solved by direct methods utilizing the WingX[37] and Olex2 (ref. 38) software packages, and the model obtained was refined by full-matrix least squares on F^2 (SHELXTL-2015 (ref. 39)). All the hydrogen atoms were placed in calculated positions and refined with fixed individual displacement parameters [U_{iso}(H) = 1.2U_{eq} or 1.5U_{eq}] according to the riding model (C–H bond lengths of 0.97 Å and 0.96 Å, for methylene and methyl groups, respectively). The O5 oxygen atom is disordered over two positions showing 50% occupancy each. Finally, the programs Mercury (version 3.10.2)[32] and ORTEP-3 (ref. 40) were also used within the WingX v1.70.01 (ref. 37) program package, to prepare the crystallographic information file (CIF) of the salt and its artwork representation for publication.

Thermal analysis (DSC and TG)

The thermal properties of the salt sample were evaluated on a differential scanning calorimeter Netzsch DSC 204 with the sample placed inside a 40 μL Al_2O_3 pan crucible with a pierced cover alongside an empty reference pan. The system was employed over a temperature range from 25 °C to 340 °C at a heating rate of 10 °C min^{-1} under N_2 gas (with a fixed flow rate of 2 ml min^{-1}), to determine the melting point and purity level of the new salts. Also, the thermogravimetric analysis (TGA) of the sample was performed using a Netzsch TG 209 F1 instrument, using an Al_2O_3 crucible with the sample and a reference pan under N_2 gas (flow rate of 2 ml min^{-1}), at a heating rate of 10 °C min^{-1} in a fixed range of 60 °C to 320 °C. The sample's melting and degradation points were both determined.

Hot-stage polarized optical microscopy

Hot-stage microscopy (HSM) was performed on a Linkam T95-PE device coupled to a Leica DM2500P optical microscope. Images were recorded using a CCD camera attached to the microscope at time intervals of 10–30 s. Single crystals of fluconazolium oxalate were heated at constant rates of 5 and 10 °C min^{-1} over a temperature range from 25 °C until the melting/decomposition of the crystals. Both heating and acquisition of the images were controlled using the Lynksys 32 software package (version 1.96).

Equilibrium salt solubility studies

The solubility of the FLZ oxalate salt was determined using a UV-vis 1800 Shimadzu spectrophotometer. The calibration curve was prepared using standard solutions of FLX–OXL from 0.067 to 0.539 mg ml^{-1}, analyzed at λ_{max} = 261 nm, which presented absorbance values between 0.103 and 0.969 A.U. and a determination coefficient (R^2) of 0.9966. In order to measure the solubility, an aqueous saturated solution of FLX–OXL (40.3 mg ml^{-1}, with precipitated solid) was left for 48 hours under magnetic stirring at room temperature and allowed to rest for 12 hours. The solution was centrifuged and filtered to remove the excess solid salt and a dilution (40 times) was performed until an appropriate absorbance value (0.443 A.U.) was obtained. After that, the absorbance measurement of the diluted solution from the saturated solution was used to quantify the amount of solubilized FLZ–OXL, considering the dilution factor.

Stability study

A sample containing 6.69 mg of fluconazolium oxalate was stored in a sealed glass desiccator with saturated sodium chloride solution at the bottom, placed inside an oven and kept at 40 °C. Under these conditions, the relative humidity (RH) is 75%. This system was kept at 40 °C for 7 days, in order to evaluate the stability of the crystalline structure. Every 24 h, the sample was weighed. At the end, the sample was subjected to PXRD analysis.

Results and discussion

Structure determination and description

Table 1 exhibits the main crystallographic data of fluconazolium oxalate (FLZ–OXL). Fig. 1 exhibits the ORTEP-3 (ref. 37) type view of the asymmetric unit.

The salt crystallizes in the monoclinic space group $P2_1/c$ with one $(FLZ)^+(oxalate)^-$ ionic pair in the asymmetric unit (Fig. 1). In this salt, each FLZ cation interacts with two oxalate anions through one N^+–H···O^- hydrogen bond, involving the triazlyl 4-nitrogen atom of the FLZ molecule and the C–O^- carboxylate group of the oxalate fragment, and one O–H···O hydrogen bond, involving the carbonyl group of the FLZ cation and the C–O hydroxyl group of the oxalate fragment (Fig. 2a). Here, these interactions result in the formation of a centrosymmetric ring with a graph-set notation $R_4^4(29)$, shown in blue in Fig. 2b. As a consequence of the 2_1-screw symmetry, these rings are stacked along the [010] direction, in such a fashion that strong non-classical hydrogen bonds of types C–H···N and C–H···F are the ones responsible for maintaining the crystalline packing (Table 2). In addition, because the oxalate anions are connected to each other *via* O–H···O intermolecular interactions, which are repeated along the [100] direction, the ring motifs are also stacked along this same direction (Fig. 2c). The π staking interactions are not observed between the aromatic rings of the FLZ molecule.

Table 1 Crystal data and structure refinement for fluconazolium oxalate

Empirical formula	$C_{13}H_{13}F_2N_6O^+$, $C_2HO_4^-$
Crystal system	Monoclinic
Space group	$P2_1/c$
a/Å	5.6109(6)
b/Å	14.9140(18)
c/Å	20.848(3)
β/°	96.566(6)
Volume/Å^3	1733.1(3)
Z	4
ρ_{calc} g cm^{-3}	1.519
Goodness-of-fit on F^2	1.047
Final R indices [$I \geq 2\sigma(I)$]	R_1 = 0.0551, wR_2 = 0.1279
Final R indices [all data]	R_1 = 0.1326, wR_2 = 0.1579
Largest diff. peak/hole/e Å^{-3}	0.21/−0.25

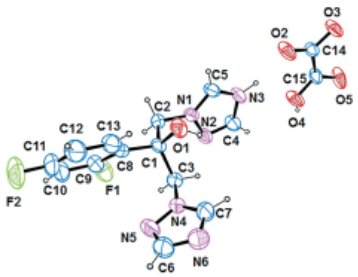

Fig. 1 ORTEP-3 (ref. 40) representation of fluconazolium oxalate.

Raman spectroscopy characterization

The FLZ salt reported here was prepared from 1 : 1 molar ratio of FLZ and oxalic acid dihydrate in a solution mixture of

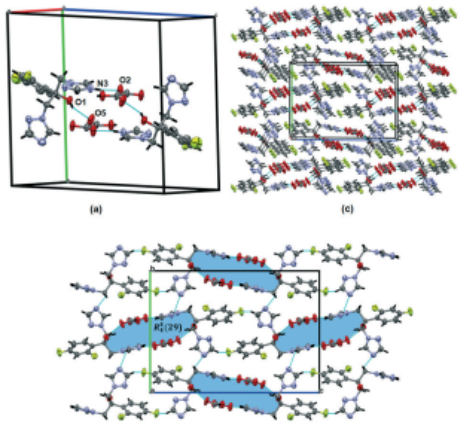

Fig. 2 (a) Unit cell fragment showing the main intermolecular interactions; (b) motif generated from the H-bonds; (c) crystalline packing of FLX–OXL along the *bc* plane.

Table 2 Hydrogen-bond geometry (Å, °) in the crystal structure of fluconazolium oxalate

Interaction	D···H (Å)	D···A (Å)	H···A (Å)	D–H···A (°)	Sym. code
N3H3···O2	1.030	2.650(3)	1.633	168.00	*x*, *y*, *z*
O1H1···O5	0.938	2.72(2)	1.930	140.89	−*x*, −*y*, −*z* + 1
O4H4···O3	0.938	2.517(3)	1.589	169.20	*x* + 1, +*y*, +*z*
C4H4···F2	1.080	3.522(5)	2.745	128.61	−*x* + 1, −*y*, −*z*
C6H6···N6	1.080	3.128(4)	2.455	119.25	−*x*, +*y* + 1/2, −*z* + 1/2
C6H6···N2	1.080	3.414(4)	2.450	148.01	*x* − 1, +*y*, +*z*

water and methanol. However, this crystallization process sometimes resulted in the formation of unwanted needle-like FLZ monohydrate (FLZ-HYD) crystals,[10] explaining the discrepancy encountered during the screening process for different stoichiometric ratios of FLZ/OXL. Raman spectroscopy serves as a quick characterization technique and allows monitoring of the synthesis of the homogenous yield.

The spectra obtained from Raman spectroscopy (Fig. 3) confirm the changes in the chemical environment of the FLZ oxalate salt when compared to the FLZ and oxalic acid dihydrate spectra in the fingerprint region of the Raman shift range 200–1500 cm^{-1}. The spectrum of the salt presents a shift in the peak position and the presence of new peaks, when compared to the FLZ-HYD and FLZ spectra, between the 270–370 cm^{-1} range and at 1000 cm^{-1}. Several peaks observed for the FLZ–OXL spectrum show shifts in their position and intensity, when compared to the FLZ-HYD (contaminant form encountered during crystallization steps), pure FLZ and OXL acid spectra. Hence, this vibrational behavior observed for the FLZ–OXL crystals strongly indicates the formation of new interactions and the possibility of the formation of an oxalate–FLZ multicomponent product.

Powder X-ray diffraction (PXRD)

The determination of the degree of crystallinity and phase identification of the fluconazolium oxalate were carried out by comparing its experimental powder diffraction pattern with the ones for FLZ and oxalic acid dihydrate. The calculated PXRD pattern obtained from the single-crystal study was also included (Fig. 4).

The experimental diffractograms of the starting materials are consistent with the ones reported in the literature, where the fluconazole diffractogram shows the presence of peaks of the monohydrate and form II, due to the fast interconversion.[17] The presence of characteristic reflections in the diffraction pattern of the fluconazolium oxalate reveals the newness of its crystalline phase, which is observed to be different from its precursors. In addition, the experimental and the calculated diffraction patterns are in good agreement with each other, thus confirming the newness and the purity of the synthesized salt.

Thermal characterization (DSC and TGA)

The results obtained from thermal characterization (DSC and TGA) confirm the newness of this oxalate salt of FLZ by unveiling the details of its physicochemical properties, like the melting point, thermal stability, composition, and degradation point. Fig. 5 shows the comparison of the DSC curves obtained for OXL, FLZ and the FLZ–OXL salt.

The dehydration of OXL acid presents a broad peak between 50 °C and 110 °C, as expected, and the melting point and degradation at 195.40 °C. The FLZ thermogram presents two peaks, at 102.8 °C and at 139.3 °C, with the initial peak indicating the presence of some amount of the hydrate form, since the hydrate collapses and starts to lose water around 90 °C.[17] Thus, the thermal results obtained for the starting materials (FLZ and oxalic acid dihydrate) were consistent with previous reports in the literature and observed to be different from the DSC curve presented by the fluconazolium oxalate, which exhibited a sharp peak at 188.5 °C, with a neck peak at 205 °C, and uniform degradation at 300 °C. This result indicates a higher stability of the fluconazolium oxalate when compared with that of the FLZ free base.

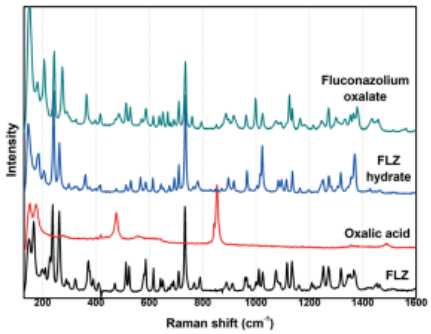

Fig. 3 Raman spectra of fluconazole, oxalic acid dihydrate, fluconazole monohydrate (contaminant) and fluconazolium oxalate.

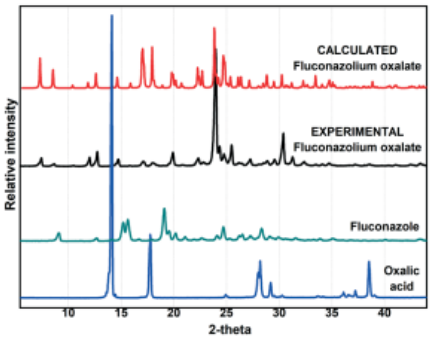

Fig. 4 Powder X-ray diffraction patterns of fluconazoliuum oxalate (calculated and experimental), FLZ and oxalic acid dihydrate.

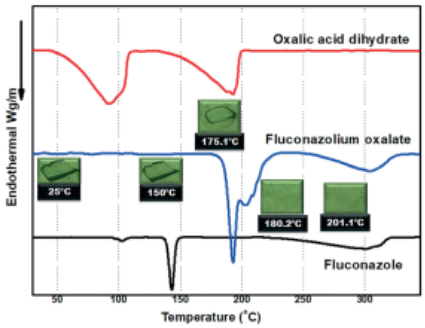

Fig. 5 DSC thermogram peaks observed for the fluconazolium oxalate, pure FLZ and oxalic acid dihydrate. Images at different temperatures were obtained by hot-stage analysis of the fluconazolium oxalate.

Fig. 6 shows the TGA curves of FLZ and the synthesized FLZ–OXL salt. The thermal instability of FLZ due to its hygroscopic nature was observed with about 5% mass loss due to the loss of water molecules from below 50 °C to 115 °C, and its stability was maintained uniformly until 225 °C before showing a steep degradation curve. This loss of water should be a combination of adsorption and crystallization water, since the DSC result shows a peak of the hydrate form at 102.8 °C, however the loss of water starts below 50 °C. The oxalate salt of FLZ presents a homogeneous composition with a better thermal stability and without a hygroscopic tendency compared to the pure FLZ, which forms hydrate easily. The fluconazolium oxalate shows around 1% mass loss from 50 °C to around 170 °C before showing a steep loss of mass and eventually starting to degrade uniformly. Comparing the TGA and DSC results it's possible to find that around 175 °C the crystal FLZ–OXL is collapsed followed by the degradation of the OXL at this temperature, as indicated by the hot-stage images in Fig. 5. The next loss of mass is related to the decomposition of the FLZ present in the FLZ–OXL, starting around 200 °C.

Table 3 Aqueous equilibrium solubility of the FLZ salt in comparison with the commercialized polymorph

	M.W. (g mol^{-1})	Water solubility (mg mL^{-1})	% of FLZ	Solubility in terms of FLZ (mg mL^{-1})
Form I	306.27	4.29	100	4.29 (ref. 17)
Form II	306.27	4.6	100	4.6 (ref. 17)
Form III	306.27	5.0	100	5.0 (ref. 16)
Monohydrate	324.27	3.56 (ref. 17)	94.44	3.36
FLZ sample	306.27	1.97	100	1.97
FLZ–OXL	396.30	17.87	77.28	13.81

Equilibrium aqueous solubility study

Solubility in water is an important physicochemical parameter to consider during the preparation of new chemical entity candidates for new APIs. Besides that, solubility often determines the bioavailability of the drug in the body and for this reason, it has a close relationship with pharmacological response.[41] For FLZ, the synthesis of new pharmaceutical salts is very attractive since this API is slightly soluble in water and also presents polymorphism and stability issues due to its hygroscopic character. Table 3 shows the aqueous solubility values exhibited for the most common forms of FLZ from the literature, namely, anhydrate forms I, II, and III, and the monohydrate one.[10,16,17]

The results from the solubility studies for the purchased sample of FLZ (equivalent to anhydrate form II) and the fluconazolium oxalate are also available in this table. As can be seen, the aqueous solubility value found for the raw FLZ used in the experiments was found to be smaller than the value found in the literature for form II. On the other hand, fluconazolium oxalate showed to be 7 times more soluble in water when compared with the raw material API used in the experiments, using the same methodology to measure the

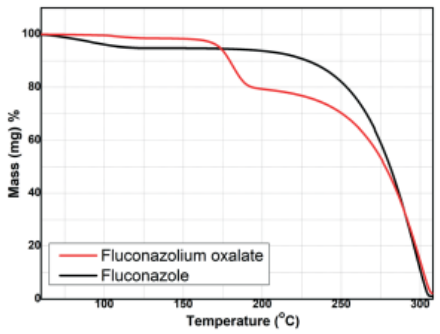

Fig. 6 TGA comparisons of pure FLZ and FLZ–OXL salt.

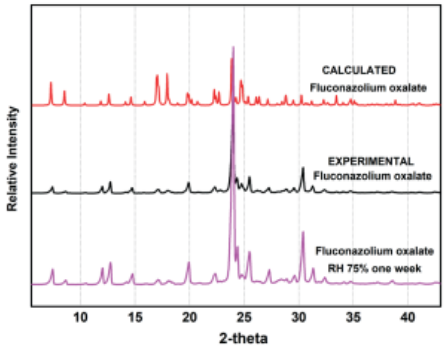

Fig. 7 PXRD of fluconazolium oxalate after one week under RH 75%.

solubility. Considering that oxalic acid fulfills the GRAS criteria for use in drug formulations, this result suggests that this salt could be a suitable candidate for novel FLZ pharmaceutical formulations with improved solubility.

Stability study

The one-week stability evaluation of fluconazolium oxalate does not show a significant mass increase, using a conventional hygroscopicity method.[42] As can be seen in Fig. 7, no changes in the PXRD pattern were observed after this study. In this way, it is possible to conclude that this salt is capable of avoiding the hygroscopicity associated with the pure FLZ polymorphs.

Conclusions

The fluconazolium oxalate reported in this paper is a great example of crystal engineering application. By making use of structural tools, it was possible to select coformers belonging to the GRAS/EAFUS list and find conditions to synthesize the first GRAS organic salt of the antifungal drug fluconazole. Although this drug presents several published polymorphs, solvates, and cocrystals, and also one organic salt with picric acid (not GRAS), because FLZ is a very weak base, it requires very strong acids to be able to perform its protonation and also requires that these acid molecules exhibit geometrical features that allow a suitable tridimensional crystalline arrangement. Although three potential coformers were found in the initial screening (oxalic acid, etidronic acid, and urea), only the oxalic acid generated suitable crystals. The salt reported herein meets the drug standards of the FDA, as shown through different characterization techniques using Raman spectroscopy, DSC, and TGA and structural descriptions using powder and single crystal XRD. The predicted aqueous solubility of the salt showed a better solubility (7 times higher) when compared to that of the commercialized FLZ. This solubility value is also the highest achieved at present, at least to the best of our knowledge, for FLZ structures.

Conflicts of interest

There are no conflicts to declare.

Acknowledgements

This study was financially supported in part by the Coordenação de Aperfeiçoamento de Pessoal de Nível Superior – Brasil (CAPES) – Finance Code 001 (C. C. P. S. and M. S. S.), CNPq (J. E. #305190/2017-2), and FAPESP (R. L. C. 2010/16520-5 and L. F. D. 2015/25694-0), and students of the LIEC UFSCar are acknowledged for their assistance in the facilities used in this research work.

References

1 J. N. Galgiani, Fluconazole, a new antifungal agent, *Ann. Intern. Med.*, 1990, **113**(3), 177–179.
2 M. A. Ghannoum and L. B. Rice, *Clin. Microbiol. Rev.*, 1999, **12**(4), 501–517.
3 R. H. Haubrich, D. Haghighat, S. A. Bozzette, J. Tilles, J. A. McCutchan and C. C. T. Group, High-dose fluconazole for treatment of cryptococcal disease in patients with human immunodeficiency virus infection, *J. Infect. Dis.*, 1994, **170**(1), 238–242.
4 Z.-W. Yao, X. Lu, C. Shen and D.-F. Lin, Comparison of flucytosine and fluconazole combined with amphotericin B for the treatment of HIV-associated cryptococcal meningitis: a systematic review and meta-analysis, *Eur. J. Clin. Microbiol. Infect. Dis.*, 2014, **33**(8), 1339–1344.
5 E. Nalintya, R. Kiggundu and D. Meya, Evolution of cryptococcal antigen testing: what is new?, *Curr. Fungal Infect. Rep.*, 2016, **10**(2), 62–67.
6 A. K. Gupta and E. A. Cooper, Update in Antifungal therapy of dermatophytosis, *Mycopathologia.*, 2008, **166**, 353–367.
7 A. K. Gupta, K. A. Foley and S. G. Versteeg, New antifungal agents and new formulations against dermatophytes, *Mycopathologia.*, 2017, **182**(1–2), 127–141.
8 M. Karanam, S. Dev and A. R. Choudhury, New polymorphs of fluconazole: Results from cocrystallization experiments, *Cryst. Growth Des.*, 2011, **12**(1), 240–252.
9 F. H. Allen, The Cambridge Structural Database: a quarter of a million crystal structures and rising, *Acta Crystallogr., Sect. B: Struct. Sci.*, 2002, **58**(3), 380–388.
10 M. R. Caira, K. A. Alkhamis and R. M. Obaidat, Preparation and Crystal Characterization of a Polymorph, a Monohydrate, and an Ethyl Acetate Solvate of the Antifungal Fluconazole, *J. Pharm. Sci.*, 2004, **93**(3), 601–611.
11 X. J. Gu and W. Jiang, Characterization of polymoprhic forms of fluconazole using fourier transform Raman spectroscopy, *J. Pharm. Sci.*, 1995, **84**(12), 1438–1441.
12 J. E. Kastelic, Z. I. Hodnik, P. Šket, J. Plavec, N. Lah, I. Leban, M. Pajk, O. PlaninŠek and D. Kikelj, Fluconazole cocrystals with dicarboxylic acids, *Cryst. Growth Des.*, 2010, **10**(11), 4943–4953.
13 J. Kastelic, N. Lah, D. Kikelj and I. Leban, A 1: 1 cocrystal of fluconazole with salicylic acid, *Acta Crystallogr., Sect. C: Cryst. Struct. Commun.*, 2011, **67**(9), o370–o372.
14 J. Kastelic, D. Kikelj, I. Leban and N. Lah, Fluconazole-malonic acid, *Acta Crystallogr., Sect. E: Struct. Rep. Online*, 2013, **69**, O378–O379.
15 G. Dutkiewicz, C. S. C. Kumar, H. S. Yathirajan, B. Narayna and M. Kubicki, Fluzonazolium picrate, *Acta Crystallogr., Sect. E: Struct. Rep. Online*, 2010, **66**(10), O2568.
16 N. Charoo, R. Cristofoletti, A. Graham, P. Lartey, B. Abrahansson, D. W. Groot, S. Kopp, P. Langguth, J. Polli, V. P. Shah and J. Dressman, Biowaiver monograph for immediate-release solid oral dosage forms: fluconazole, *J. Pharm. Sci.*, 2014, **103**, 3843–3858.
17 K. A. Alkhamis, A. A. Obaidat and A. F. Nuseirat, Solid-state chacarcterization of fluconazole, *Pharm. Dev. Technol.*, 2002, **7**(4), 491–503.

18 A. D. Bond, in *Pharmaceutical salts and cocrystals*, ed. J. Wouters and L. Quéré, Royal Society of Chemistry, Cambridge, UK, 2012, ch. 2, pp. 9–28.

19 A. Patel, S. A. Jones, A. Ferro and N. Patel, Pharmaceutical salts: a formulation trick or a clinical conundrum?, *Br. J. Cardiol.*, 2009, **16**(6), 281–286.

20 A. Samie, G. R. Desiraju and M. Banik, Salts and Cocrystals of the Antidiabetic Drugs Gliclazide, Tolbutamide, and Glipizide: Solubility Enhancements through Drug–Coformer Interactions, *Cryst. Growth Des.*, 2017, **17**(5), 2406–2417.

21 S. Hiendrawan, E. Widjojokusumo, B. Veriansyah and R. R. Tjandrawinata, Pharmaceutical Salts of Carvedilol: Polymorphism and Physicochemical Properties, *AAPS PharmSciTech*, 2017, **18**(4), 1417–1425.

22 G. Bolla and A. Nangia, Clofazimine mesylate: a high solubility stable salt, *Cryst. Growth Des.*, 2012, **12**(12), 6250–6259.

23 K. Suresh and A. Nangia, Lornoxicam salts: crystal structures, conformations, and solubility, *Cryst. Growth Des.*, 2014, **14**(6), 2945–2953.

24 S. Basavoju, D. Boström and S. P. Velaga, Pharmaceutical cocrystal and salts of norfloxacin, *Cryst. Growth Des.*, 2006, **6**(12), 2699–2708.

25 US-FDA Select Committee on GRAS Substances (SCOGS) Database: https://www.fda.gov/Food/IngredientsPackagingLabeling/GRAS/SCOGS/default.htm (access in Nov. 2018).

26 US-FDA, Everything added to food in the United States (EAFUS) list of chemicals published by the US-FDA: https://www.accessdata.fda.gov/scripts/fdcc/index.cfm?set=FoodSubstances&sort=Sortterm&order=ASC&showAll=true&type=basic&search= (access: Nov. 2018).

27 E. R. T. Tiekink, Adventures in crystal engineering, In: *Great thinkers, great minds: Sunway University Professional Lecture Series*, Sunway University Press, Sunway City, Malaysia, 2018, pp. 185–213.

28 G. R. Desiraju, Crystal Engineering: the design of organic solids, *J. Appl. Crystallogr.*, 1991, **24**, 265.

29 B. Moulton and M. J. Zaworotko, From molecules to crystal engineering: supramolecular isomerism and polymorphism in network solids, *Chem. Rev.*, 2001, **101**(6), 1629–1658.

30 C. B. Aakeroy and K. R. Seddon, The hydrogen bond and crystal engineering, *Chem. Soc. Rev.*, 1993, **22**(6), 397–407.

31 S. L. Childs, G. P. Stahly and A. Park, The salt-cocrystal continuum: the influence of crystal structure on ionization state, *Mol. Pharmaceutics*, 2007, **4**(3), 323–338.

32 C. F. Macrae, I. J. Bruno, J. A. Chisholm, P. R. Edgington, P. McCabe, E. Pidcock, L. Rodriguez-Monge, R. Taylor, J. van de Streek and P. A. Wood, Mercury CSD 2.0 - New Features for the Visualization and Investigation of Crystal Structures, *J. Appl. Crystallogr.*, 2008, **41**, 466–470.

33 M. F. Othman, N. Anuar, S. Ad. Rahman and N. A. A. Taifuddin, Corystal screening of ibuprofen with oxalic acid and citric acid via grinding method, *IOP Conf. Ser.: Mater. Sci. Eng.*, 2018, **358**, 1–6.

34 A. M. Pansuriya, M. M. Savant, C. V. Bhuva, J. Singh and Y. Y. Naliapara, One-pot synthesis of 5-carboxanilide-dihydropyrimidinones using etidronic acid, *ARKIVOC*, 2009, **7**, 79–85.

35 P. Das, A. Maity and U. K. Yelury, Co-crystals - a rising horizon for formulating poorly soluble drugs, *Journal of Pharmaceutical Advanced Research*, 2018, **1**(6), 292–305.

36 https://www.ccdc.cam.ac.uk/support-and-resources/ccdcresources/mercury.pdf.

37 L. J. Farrugia, WinGX and ORTEP for windows: an update, *J. Appl. Crystallogr.*, 2012, **45**, 849–854.

38 O. V. Dolomanov, L. J. Bourhis, R. J. Gildea, J. A. K. Howard and H. Puschmann, OLEX2: A complete structure solution, refinement and analysis program, *J. Appl. Crystallogr.*, 2009, **42**, 339–341.

39 G. M. Sheldrick, *Acta Crystallogr., Sect. A: Found. Adv.*, 2015, **71**, 3–8.

40 L. J. Farrugia, ORTEP-3 for Windows – a version of ORTEP-III with a graphical user interface (GUI), *J. Appl. Crystallogr.*, 1997, **30**, 565–565.

41 K. T. Savjani, A. K. Gajjar and J. K. Savjani, Drug Solubility: Importance and Enhancement Techniques, *ISRN Pharm.*, 2012, **2012**, 195727.

42 S. K. Nechipadappu, V. Tekuri and D. R. Trivedi, Pharmaceutical co-crystal of flufenamic acid: synthesis and characterization of two novel drug-drug co-crystal, *J. Pharm. Sci.*, 2017, **106**(5), 1384–1390.

ANNEX II

CRYSTAL GROWTH & DESIGN

Article

Cite This: *Cryst. Growth Des.* 2019, 19, 648−657

pubs.acs.org/crystal

Fluconazole: Synthesis and Structural Characterization of Four New Pharmaceutical Cocrystal Forms

Bolaji C. Dayo Owoyemi,[†] Cecilia C. P. da Silva,[†] Matheus S. Souza,[‡] Luan F. Diniz,[‡] Javier Ellena,[‡] and Renato L. Carneiro*[,†]

[†]Department of Chemistry, Federal University of São Carlos − UFSCar, Rod. Washington Luís km 235, 13.560-905, São Carlos, São Paulo, Brazil

[‡]Instituto de Física de São Carlos, Universidade de São Paulo, CP 369, 13.560-970, São Carlos, São Paulo, Brazil

Supporting Information

ABSTRACT: Pharmaceutical cocrystals have emerged over the past several decades as an alternative path for synthesizing stable and/or improved crystalline forms of active pharmaceutical ingredients. In this contribution, we developed a reproducible cocrystallization path for the supramolecular synthesis of four new pharmaceutical cocrystal forms of fluconazole (FLZ), an antifungal multifunctional drug: fluconazole−fumaric acid monohydrate (1:1:1), fluconazole−malic acid (1:1), fluconazole−dipicolinic acid (1:1), and fluconazole−adipic acid (1:1). All the new cocrystals were characterized by powder/single-crystal X-ray diffraction, Raman, Fourier transform infrared spectroscopy, differential scanning calorimetry/thermogravimetric analysis, and hot-stage polarized optical microscopy, and their water solubility was determined. Structurally, although the coformers were different, the same strong O−H···N hydrogen bond between the FLZ molecule and the coformers was observed. The aqueous solubility studies revealed that all the cocrystals were found to exhibit improved aqueous solubility when compared to the commercialized FLZ polymorph.

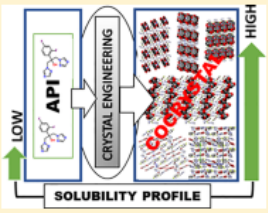

1. INTRODUCTION

Oral solid drug research, discovery, and development are challenging, expensive, and complex processes.[1] This is because the pharmaceutical industries seek active pharmaceutical ingredients (APIs)[2] with high therapeutic and clinical potential through preferable pharmacokinetic[3] and physicochemical properties, such as high permeability,[4] high aqueous solubility,[5] fast dissolution rate,[5] physical stability,[6] bioavailability,[7] and extended shelf life.[8] Obviously, not all marketed drugs achieve all of these parameters, and, for this reason, there is a vast scientific work toward finding new solid forms of APIs, in particular, for those exhibiting aqueous solubility issues. Drugs presenting low water solubility will pose low therapeutic effectiveness when orally administered.[9,10] In this sense, over the years, different techniques have been developed to enhance the final clinical/dosage efficiency of APIs in their solid-state form, such as formulation approaches; particle size reduction;[11] nanocrystal approach;[12] amorphization;[13] synthesis of an API salt[14] or cocrystal;[15] and use of different polymorphs.[16]

The rapid growth and establishment of crystal engineering (CE)[17−19] methodologies, in the context of the supramolecular chemistry[20,21] field, have stood out by providing a progressive contribution to the pharmaceutical industry. This success is based on the ability to apply CE's methodologies to manipulate and reorder crystal lattice of APIs, hence serving as an extremely useful tool for optimizing their physicochemical properties.[22] According to Desiraju, CE is defined "as the understanding of intermolecular interactions in the context of crystal packing and the utilization of such understanding to design new crystalline solids with desired physical and chemical properties".[23,24] In this view, apart from the aqueous solubility and dissolution rate improvement, the newly synthesized crystalline solid drug will still preserve its therapeutic activity, but it will be considered as a new entity with respect to the reference API. As consequence, the new form has a patentability right as disclosed by the regulations of the U.S. Food and Drug Administration (FDA) department.[19] The significance and effectiveness of CE methodologies are based on the idea that some physicochemical properties of solid APIs can be optimized by strategically rearranging their structure, usually by including guest molecule(s) in the crystal lattice. These guest molecules can be solvents, acids, bases, or any solid compound at room temperature, that belong, preferable, to the list of substances generally regarded as safe by the FDA (GRAS),[25] being chosen based on their physicochemical nature and probability to form supramolecular bonds.[26−28]

Fluconazole (FLZ, 2-(2,4-difluorophenyl)-1,3-bis(1*H*-1,2,4triazole-1-yl)-propan-2-ol), marketed as Diflucan (Scheme 1), is a triazole multifunction antifungal drug slightly soluble in water.[29] It has known potential and competence for inhibiting the synthesis of ergosterol, a main component in the fungal cell membrane, curing fungal infections like candidiasis, cryptococcal meningitis, and dermatophytic fungal infections like

Received: August 8, 2018
Revised: December 11, 2018
Published: January 4, 2019

DOI: 10.1021/acs.cgd.8b01194
Cryst. Growth Des. 2019, 19, 648−657

Scheme 1. Molecular Structure of FLZ and the Cocrystal Formers: Fumaric, Malic, Dipicolinic, and Adipic Acids

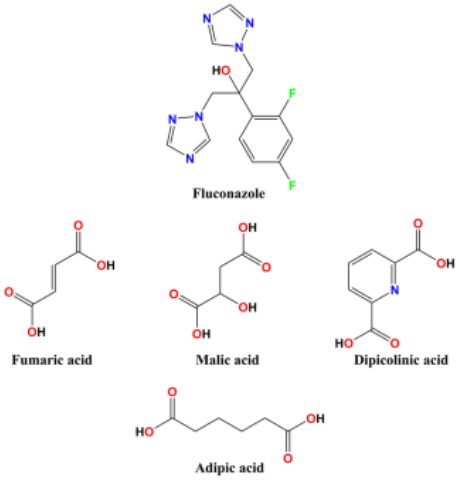

aspergillosis, coccidioidomycosis, histoplasmosis, and also for preventing their recurrences. It also prevents yeast infections in patients undergoing treatment for cancer and acquired immune-deficiency syndrome (AIDS).[30,31] However, due to the low aqueous solubility of this multifunction drug, the need arises for improving its physicochemical properties using CE strategies. Different research studies have reported successful breakthroughs in synthesizing different pharmaceutical solid forms of FLZ. Richardson et al.,[32] Gu and Jiang,[33] Lo et al.,[34] Dash and Elmquist[35] are among the earlier work that reported the synthesis of polymorphic forms of FLZ, while the solvate, monohydrate, and anhydrous forms were reported by Alkhamis et al.[36] A detailed summary and further synthesis of different crystalline solid forms of FLZ, including salts, was reported by Karanam et al.,[37] utilizing CE methodologies to enhance the physicochemical properties of FLZ with the crystallographic information file (CIF)[38] and X-ray diffraction data collections[39] (single crystal and powder) of previous contributions, all deposited in the Cambridge Structural Database (CSD).[40−43]

In this paper, we describe the supramolecular synthesis of four new pharmaceutical cocrystals of FLZ, as well as their respective solid state characterization, performed by vibrational spectroscopy (Raman and infrared), thermal analysis (differential scanning calorimetry, thermogravimetric analysis, hot-stage microscopy), and X-ray diffraction (powder and single crystal). In addition, their intrinsic aqueous solubility was carefully determined and compared with the solubility of the commercialized FLZ polymorph.

2. EXPERIMENTAL SECTION

2.1. Materials. Pure FLZ (pharmaceutical grade) was obtained from a local pharmacy in São Carlos, Brazil. The API was characterized by powdwe X-ray diffraction (PXRD) presenting the diffraction pattern corresponding to the FLZ form II, previously reported by Alkhamis et al.[42] The coformers fumaric (FUM), malic (MA), dipicolinic (DPA), and adipic (ADP) acids were purchased from Sigma-Aldrich at a purity greater than 99% (Analytical reagent grade). The ultrapure deionized water was obtained from a Milli-Q system (18.2 mΩ cm), while acetonitrile, ethanol, hexanol, and methanol were HPLC grade and purchased from J. T. Bakers Ltd. All materials were used without any further purification.

2.2. Experimental Design and Screening Exercise. First, the multicomponent screening wizard available in the MERCURY (version 3.10.1)[44] program was applied to match the functional groups and geometries of the FLZ molecule with similar multicomponent structures deposited in the CSD,[43] in order to select coformers candidates. In sequence, the analyses of the propensity of the selected coformers to achieve hydrogen bond interactions with FLZ were based on structural similarities with the reported cocrystals of this API, found in the CSD.[43] Such cocrystals exhibit chains or

Table 1. Crystallographic Data and Structure Refinement Parameters of the New Cocrystals FLZ−FUM-H_2O, FLZ−MA, FLZ−DPA, and FLZ−ADP

FLZ−FUM−H_2O	FLZ−MA	FLZ−DPA	FLZ−ADP
$C_{17}H_{18}F_2N_6O_6$ 1:1	$C_{17}H_{18}F_2N_6O_6$ 1:1	$C_{20}H_{17}F_2N_7O_5$ 1:1	$C_{19}H_{22}F_2N_6O_5$ 1:1
M = 440.37 g/mol	M = 440.37 g/mol	M = 473.40 g/mol	M = 452.42 g/mol
space group $P2_1/n$	space group $C2/c$	space group $P\bar{1}$	space group $C2/c$
monoclinic	monoclinic	triclinic	monoclinic
a = 17.053(3)	a = 16.5501(18)	a = 6.5699(6)	a = 17.083(3)
b = 5.5995(10)	b = 8.0980(7)	b = 11.495(10)	b = 8.1485(7)
c = 21.154(3)	c = 29.527(3)	c = 14.3991(12)	c = 31.195(3)
α = 90	α = 90	α = 102.382(7)	α = 90
β = 105.418(4)	β = 102.874(10)	β = 98.303(7)	β = 100.986(12)
γ = 90	γ = 90	γ = 96.740(7)	γ = 90
V = 1947.3(6) Å^3	V = 3857.8(7) Å^3	V = 1038.56(16) Å^3	V = 4262.8(9) Å^3
Z = 4	Z = 8	Z = 2	Z = 8
ρ_{calc} = 1.502 g/cm^3	ρ_{calc} = 1.516 g/cm^3	ρ_{calc} = 1.514 g/cm^3	ρ_{calc} = 1.410 g/cm^3
4492 unique refins	4789 unique refins	5130 unique refins	8290 unique refins
$R_{(int)}$ = 0.0781	$R_{(int)}$ = 0.0373	$R_{(int)}$ = 0.0264	$R_{(int)}$ = 0.0280
θ_{max} = 27.568°	θ_{max} = 28.282°	θ_{max} = 28.280°	θ_{max} = 27.482°
$R_{1[I>2\sigma(I)]}$ = 0.0617	$R_{1[I>2\sigma(I)]}$ = 0.0483	$R_{1[I>2\sigma(I)]}$ = 0.0488	$R_{1[I>2\sigma(I)]}$ = 0.0633
wR_2 = 0.1208	wR_2 = 0.1384	wR_2 = 0.1452	wR_2 = 0.1754
S = 1.032	S = 1.046	S = 1.020	S = 1.046

DOI: 10.1021/acs.cgd.8b01194
Cryst. Growth Des. 2019, 19, 648−657

dimers based on O−H···N or C−H···X (where X = N, O, or F) intermolecular interactions.[42] Thus, the experimental design consisted of applying different stoichiometric ratios between the FLZ and the selected coformers: 1:1, 1:2, 1:3, 2:1, 2:3, 3:1, and 3:2. A manual mechanochemical method of solid-state dry-grinding and solvent assisted grinding was initially employed for the cocrystal screening, while the cocrystallization methods by slow evaporation were performed in order to obtain regular crystals suitable for solid-state structural characterization by the single crystal X-ray diffraction technique.

2.3. Supramolecular Cocrystal Synthesis. *2.3.1. Fluconazole Fumaric Monohydrate Cocrystal (1:1:1, FLZ−FUM−H_2O).* This cocrystal was obtained from a 1:1 molar ratio of FLZ (30.63 mg, 0.1 mmol) and fumaric acid (11.61 mg, 0.1 mmol), both dissolved by sonication in 3 mL of a solvent mixture containing acetonitrile and deionized water (1:1, v/v). The solution was left at room temperature to slow evaporation. The formation of colorless homogeneous needle-like crystals, suitable yield, was observed in the solution after nearly 48 h.

2.3.2. Fluconazole Malic Acid Cocrystal (1:1, FLZ−MA). 30.63 mg (0.1 mmol) of FLZ and 13.41 mg (0.1 mmol) of malic acid were accurately measured and both dissolved in 4 mL of a solvent mixture containing acetonitrile and methanol (1:1, v/v). The system was sonicated and stirred for 10 min. The resulted solution was covered with aluminum foil with bored holes and left to slowly evaporate at room temperature. The formation of white clear crystals for SCXRD analysis was obtained after 48 h.

2.3.3. Fluconazole Dipicolinic Acid Cocrystal (1:1, FLZ−DPA). 30.63 mg (0.1 mmol) of FLZ and 16.71 mg (0.1 mmol) of dipicolinic acid were both dissolved in 3 mL of acetonitrile; 4−5 drops of water were added until a clear solution was achieved, using a sonicator bath. The resulting solution was allowed to slowly evaporate at room temperature, yielding white crystals after 48−72 h, suitable for SCXRD analysis.

2.3.4. Fluconazole Adipic Acid Cocrystal (1:1, FLZ−ADP). 30.63 mg (0.1 mmol) of FLZ and 14.61 mg (0.1 mmol) of adipic acid were both dissolved in 3 mL of a mixture of acetonitrile and acetone (v/v, 1:1), stirred on a magnetic stirrer for 15 min. The resulted solution (prepared in a 10 mL beaker) was then embedded into another 25 mL beaker containing 8 mL of hexanol. The system was sealed with aluminum foil, to promote a very slow evaporation process, at room temperature. The formation of lumpy crystals suitable for SCXRD analysis was observed after 48−72 h.

2.4. Single-Crystal X-ray Diffraction (SCRXD). The crystallographic data information for FLZ−MA, FLZ−DPA, and FLZ−ADP cocrystals (Table 1) were collected at 298(2) K on a Rigaku XtaLAB mini diffractometer with a CCD detector system equipped using a MoKα radiation (λ = 0.71073 Å). Data integration, Lorentz-polarization effects, and absorption corrections were performed using the CrysAlisPro[45] (version 171.38.43b) software. The structures were solved by direct methods utilizing the Olex2[46] software, and the models obtained were refined by full-matrix least-squares on F2 (SHELXTL-97).[47] All hydrogen atoms were placed in calculated positions and refined with fixed individual displacement parameters [U_{iso}(H) = 1.2U_{eq} or 1.5U_{eq}] according to the riding model (C−H bond lengths of 0.97 and 0.96 Å, for methylene and methyl groups, respectively). In addition, the crystallographic data collected for FLZ−FUM−H_2O cocrystal (Table 1) was performed at room temperature on a Bruker Super-Duo APEX II CCD diffractometer using MoKα radiation (0.71073 Å). The structure was solved by direct methods utilizing the WingX[48] and the Olex2[46] software, and the model obtained was refined by full−matrix least-squares on F^2 (SHELXTL-97).[47] All the hydrogen atoms were placed in their calculated positions and refined with fixed individual displacement parameters [U_{iso}(H) = 1.2U_{eq} or 1.5U_{eq}] according to the riding model (C−H bond lengths of 0.97 and 0.96 Å, for methylene and methyl groups, respectively).

The programs MERCURY (version 3.10.1)[44] and ORTEP-3[49] were used within the WinGX[48] to prepare the crystallographic information files (CIF) of the cocrystals and artwork representations for publication. Table 1 shows the crystallographic data of all cocrystals while the Table S1 (see the Supporting Information) presents their hydrogen bonds geometrical parameters. Crystallographic information on the new cocrystal structures were deposited in the CSD[43] under the codes CCDC 1831762 (fluconazole fumaric acid monohydrate cocrystal), CCDC 1831763 (fluconazole malic acid cocrystal), CCDC 1831761 (fluconazole dipicolinic acid cocrystal), and CCDC 1831760 (fluconazole adipic acid cocrystal). Copies of these files may be obtained free of charge from http:www.ccdc.cam.ac.uk.

2.5. Raman Spectroscopy. The Raman spectra were collected using a B&W Tek *i*-Raman BWS 415-785H spectrometer using excitation laser of 785 nm. Analyses were performed using a B&W Tek microscope BAC151A coupled to the spectrometer, spectral resolution of 3.5 cm^{-1}, 120 s of acquisition time, spectral range 200−2180 cm^{-1} and laser power of 70 mW. The equipment was managed by the BWSpec 4.03 software. The screening experiments and first characterization to evaluate the obtained crystals (i.e., changes in the chemical environment of solid forms) were performed quickly using Raman spectroscopy, by comparison with the API and coformer spectra. Slight changes in the spectrum are expected when a new structure is obtained due to the new supramolecular interactions, which changes the vibrational energies.

2.6. Fourier Transform Infrared Spectrophotometry (FT-IR). FT-IR characterizations were performed by a Shimadzu IRprestige-21 FT-IR using a potassium bromide (KBr) pellet technique. Spectra were acquired using 32 scans, wavenumber ranging from 4000 to 400 cm^{-1}, and a resolution of 4 cm^{-1}. Like Raman spectroscopy, IR spectra can be used to study the formation of new intermolecular interactions as well as changes in existing ones.

2.7. Powder X-ray Diffraction (PXRD). The X-ray diffraction studies of partially milled crystal powder were performed on a Multiplex X-ray diffractometer (Rigaku Corporation, Tokyo, Japan), using a copper (Cu) Kα radiation (1.54 Å), a voltage of 40 kV, and a current of 30 mA. The samples were scanned from 5° to 45° (2θ°), at a step size of 0.2° under a scan rate of 2°/min to provide structural information and degree of crystallinity.

2.8. Thermogravimetric (TGA) and Differential Thermal Analysis (DTA). The TGA/DTA analysis of the samples was performed on a Netzsch TG 209 F1 analyzer, using an Al_2O_3 crucible pan under $N_{2(g)}$ and a flow rate of 2 mL min^{-1}; heating rate conditions were set at 10 °C min^{-1} in the range of 25−325 °C. The samples were evaluated regarding the water/solvent content and decomposition profile.

2.9. Differential Scanning Calorimetry (DSC). Analyses were performed on a Shimadzu DSC-60 equipment. The cocrystal samples (about 2 mg) were weighed and heated from 25 to 350 °C at a heating rate of 10 °C min^{-1} in a crimped sealed aluminum pan, using nitrogen as a purge gas (50 mL min^{-1}). Data were processed using Shimadzu TA-60 thermal data analysis software (version 2.2).

2.10. Hot-Stage Polarized Optical Microscopy (HSM). The thermomicroscopy analyses were performed using a Leica DM2500P microscope connected to the Linkam T95-PE hot-stage accessory. Data were visualized using the Linksys 32 software for hot-stage control. One crystal was placed on a 13 mm glass coverslip, placed on a 22 mm diameter pure silver heating block inside of the stage. The sample was heated at a rate of 10 °C min^{-1} from room temperature up to 300 °C or stopped when the materials melted.

2.11. Equilibrium Solubility Studies. Aqueous solubility studies for pure FLZ and for each cocrystal were performed using a UV−vis 1800 Shimadzu spectrophotometer. Herein, the calibration curves were prepared using standard solutions of each cocrystal, which were analyzed at λ_{max} = 261 nm. In order to evaluate the solubility, saturated solutions of each cocrystal were obtained leaving weighted amounts/specific water volumes (FLZ: 76.91 mg/30 mL; FLZ−MA: 68.13 mg/5 mL; FLZ−FUM−H_2O: 69.75 mg/5 mL; FLZ−ADP: 30.9 mg/3 mL; FLZ−DPA: 74.64 mg/10 mL) of each sample, for 50 to 60 min under a magnetic stirrer at room temperature. The solutions were then centrifuged and filtered to remove the excess of solid, and dilutions were performed until obtain appropriate

DOI: 10.1021/acs.cgd.8b01194
Cryst. Growth Des. 2019, 19, 648−657

absorbance values. Finally, the absorbance measurements of the diluted solutions from the saturated ones were used to quantify the amounts of solubilized samples, considering the dilution factor.

2.12. Stability Studies. Stability of the cocrystals was tested at 75% relative humidity (RH). Samples of each cocrystal were weighted and stored in a desiccator filled with saturated sodium chloride solution to maintain the RH. This system was kept under 40 °C for 7 days, being weighted and submitted to PXRD analysis at the end.

3. RESULTS

3.1. Structural Description. ORTEP-3[49] type view showing the asymmetric units of the FLZ cocrystals depicted herein are shown in Figure 1. Hydrogen-bond geometric parameters for each cocrystal structure are described in Table S1 (see the Supporting Information).

3.1.1. Fluconazole Fumaric Acid Monohydrate Cocrystal (FLZ−FUM−H_2O). The FLZ−FUM−H_2O cocrystal crystallizes in the monoclinic space group $P21/n$ with one FLZ, one fumaric acid, and one water molecule in the asymmetric unit (Figure 1a). The FLZ molecule interacts with the fumaric acid and the water molecule through strong intermolecular O−H···N hydrogen bonds as shown in Figure 2a. Also, the water molecule is bonded to the carbonyl/hydroxyl groups of adjacent fumaric acid molecules through O−H···O hydrogen bonds, resulting in the formation of a $C_2^2(6)$ motif along the [010] direction (Figure 2b). In addition, when considering all the main O−H···N and O−H···O intermolecular interactions, the formation of a ring motif with $R_8^7(56)$ graph-set can be observed, shown in green also in Figure 2b. These rings are stacked along the [001] direction, being composed by two FLZ, three fumaric acid, and three water molecules. Due to the 2_1-screw axis, C−H···F hydrogen bonds (2.580 Å), red dashed lines in Figure 2c emerge among adjacent rings, giving stability to the structure, together with van der Waals and other C−H···O contacts. The π-stacking interactions were not observed between the aromatic rings of the FLZ molecules.

3.1.2. Fluconazole Malic Acid Cocrystal (FLZ−MA). The FLZ−MA cocrystal crystallizes in the monoclinic space group $C2/c$ with one FLZ and one malic acid in the asymmetric unit (Figure 1b). This cocrystal is formed through two O−H···N hydrogen bonds involving the ending hydroxyl groups of the malic acid as donors and the two triazlyl 4-nitrogen atoms of the FLZ molecule as acceptors (Figure 3a). In addition, one O−H···O hydrogen bond is observed between the hydroxyl group of the FLZ molecule and one carbonyl group of the malic acid. These three main intermolecular interactions result in the formation of two adjacent centrosymmetric $R_4^4(32)$ and $R_4^4(22)$ ring systems, orange/green shown in Figure 3a. Concerning the malic acid molecules, the remaining two carbonyl and hydroxyl groups interact via complementary O−H···O hydrogen bonds, constituting a centrosymmetric $R_2^2(12)$ homosynthon (shown in purple in Figure 3a). The ring systems lead to the formation of infinite zigzag chains along the [001] direction (Figure3b). These chains are connected to the adjacent ones via weak C−H···X (X = F, O, and N) contacts (magenta in Figure 3b). As a result, the crystal packing of FLZ−MA is composed by two-dimensional (2D) columns of FLZ molecules interspersed by 2D columns of malic acid molecules (Figure 3c).

3.1.3. Fluconazole Dipicolinic Acid Cocrystal (FLZ−DPA). The FLZ−DPA cocrystal crystallizes in the triclinic space group $P\bar{1}$ with one FLZ and one dipicolinic acid molecules in the asymmetric unit (Figure 1c). This cocrystal is formed

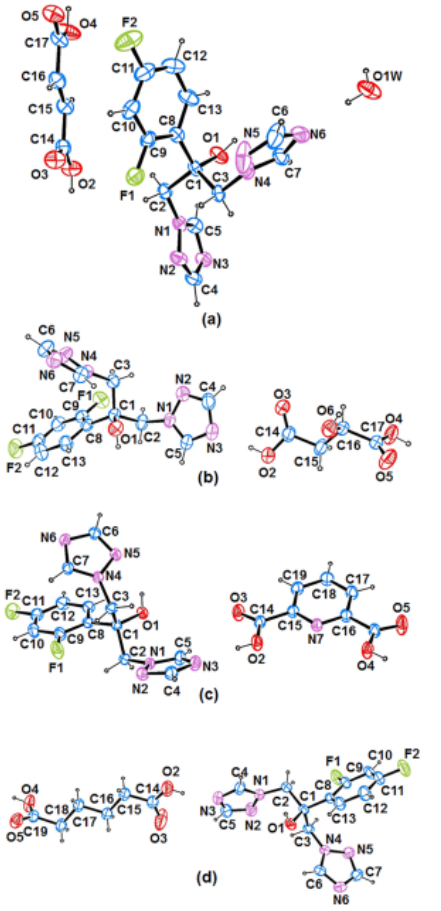

Figure 1. ORTEP-3[49] representation of the asymmetric unit of the cocrystals: (a) FLZ−FUM−H_2O, (b) FLZ−MA, (c) FLZ−DPA, and (d) FLZ−ADP.

through two O−H···N hydrogen bonds involving the hydroxyl groups of the dipicolinic acid as donors and the two triazlyl 4-nitrogen atoms of the FLZ molecule as acceptors (Figure 4a). In addition, one O−H···N hydrogen bond is observed to occur between adjacent FLZ molecules, leading to the formation of infinite FLZ chains along the [100] direction (Figure 4b). In addition, when considering all these main O−H···N intermolecular interactions, it can be observed the formation of a ring motif with graph-set notation $R_6^6(55)$, involving four FLZ and two dipicolinic acid molecules (green in Figure 4a). In this ring motif, the dipicolinic acid molecules are placed in a way to form columns along the [100] direction (Figure 4b). The planes passing through the six-membred ring of FLZ and through the dipicolinic acid ring have an angle of 15.08°. In this crystalline arrangement, a $R_2^2(8)$ motif (purple, in Figure

DOI: 10.1021/acs.cgd.8b01194
Cryst. Growth Des. 2019, 19, 648−657

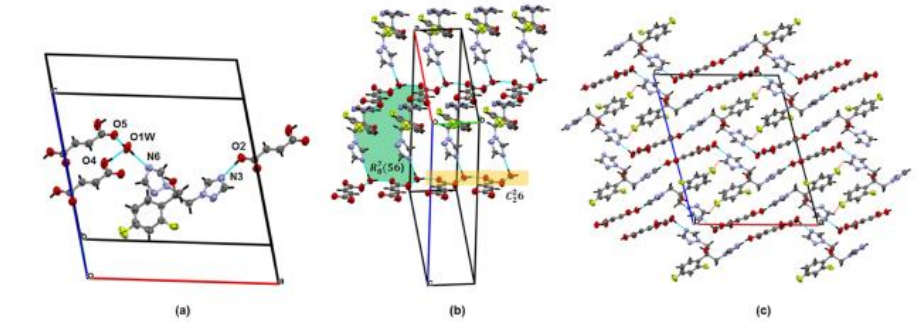

Figure 2. (a–c) Intermolecular interactions and crystalline packings of FLZ–FUM–H_2O.

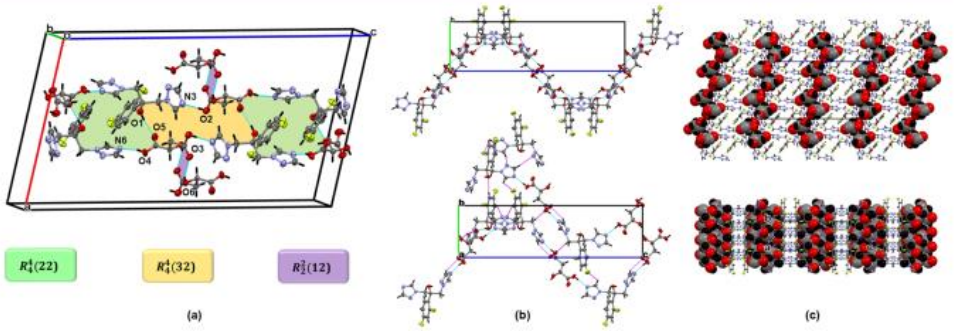

Figure 3. (a–c) Intermolecular interactions and crystalline packings of FLZ–MA. Magenta contacts in (b) indicate weak C–H···X (X= F, O, and N) contacts.

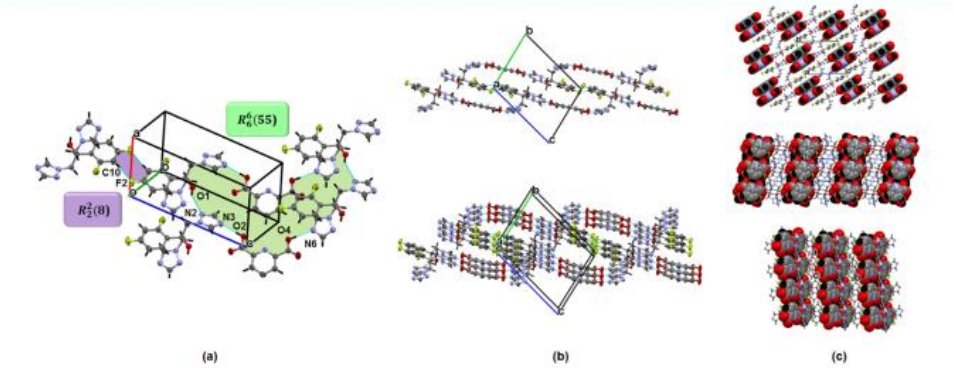

Figure 4. (a–c) Intermolecular interactions and crystalline packings of FLZ–DPA.

4a), assembled via complementary weak C10–H10···F2 hydrogen bonds, is responsible for connecting the adjacent $R_6^6(55)$ ring systems. Due to the inversion center inherent to the triclinic space group $P\bar{1}$, the final arrangement observed for this cocrystal is the generation of columns of FLZ molecules interspersed by columns of dipicolinic acid molecules (Figure 4c). As consequence of the close packing observed in this cocrystal system, several C–H···X (X = O, N, and F), C–H···π contacts, and weak π···π interactions are observed (see Table S2 in the Supporting Information).

3.1.4. Fluconazole Adipic Acid Cocrystal (FLZ–ADP). The FLZ–ADP cocrystal crystallizes in the monoclinic space group

DOI: 10.1021/acs.cgd.8b01194
Cryst. Growth Des. 2019, 19, 648–657

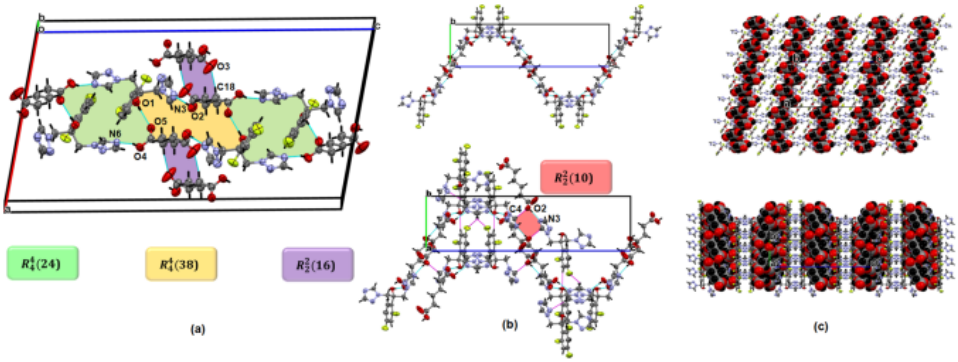

Figure 5. (a–c) Intermolecular interactions and crystalline packing of FLZ–ADP. Magenta contacts in (b) indicates weak C–H···X (X = F, O, and N) contacts.

*C*2/*c* with one FLZ and one adipic acid molecule in the asymmetric unit (Figure 1d). This cocrystal has a crystalline packing very similar to the FLZ–MA one, being formed through two O–H···N hydrogen bonds involving the hydroxyl groups of the adipic acid as donors and the two triazlyl 4-nitrogen atoms of the FLZ molecule as acceptors (Figure 5a). In addition, one O–H···O hydrogen bond is observed between the hydroxyl group of the FLZ molecule as donor and one carbonyl group of the adipic acid as an acceptor (Figure 5a). These three main intermolecular interactions result in the formation of two adjacent centrosymmetric $R_4^4(38)$ and $R_4^4(24)$ ring systems, orange/green shown in Figure 5a. Concerning the adipic acid molecules, the remaining carbonyl and one $-CH_2$ group interact through the complementary C18–H18A···O3 hydrogen bonds, constituting a centrosymmetric $R_2^2(16)$ homosynthon (shown in purple in Figure 5a). These ring systems lead to the formation of infinite zigzag chains along the [001] direction (Figure5b), these chains being connected to the adjacent ones via one strong nonclassical hydrogen bond C4–H4···O2 (magenta in Figure 5b) and other weak C–H···X (X = F, O, and N) contacts (magenta in Figure 5b). In particular, the nonclassical hydrogen bond leads to the formation of a fourth ring system with notation $R_2^2(10)$, red shown in Figure 5b. As a result, the crystal packing of FLZ–ADP is composed by 2D columns of FLZ molecules interspersed by 2D columns of adipic acid molecules (Figure 5c).

4. DISCUSSION

4.1. Solid-State Characterization. Solid-state characterization of the cocrystals was performed using vibrational spectroscopic techniques (Raman and infrared), X-ray diffraction (powder and single crystal), and thermal analysis (DSC, TG, and HSM) to verify the authenticity of the synthesized cocrystals.

4.1.1. Spectroscopic Analysis. Figure 6 shows a selected range of the Raman spectra of the four cocrystals, FLZ hydrate (FLZ–HYD), and the starting materials (FLZ, ADP, MA, DPA, and FUM acids). The Raman spectrum of pure FLZ form II presents characteristic intense peaks between 240–260 cm^{-1}, 730 cm^{-1}, and between 910–1020 cm^{-1} with similarities to the FLZ–HYD spectrum, found as an impurity during

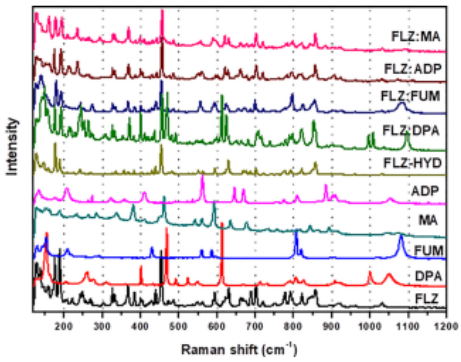

Figure 6. Raman spectra comparison of the FLZ cocrystals (FLZ–FUM–H_2O, FLZ–MA, FLZ–DPA and FLZ–ADP), pure FLZ drug, FLZ–HYD, and the pure cocrystal formers: (FUM, MA, DPA, and ADP).

screening experiments. Distinct spectral changes were observed in the cocrystals, especially the shift observed in the two characteristic peaks of FLZ between 180–200 cm^{-1} as well as the peaks at 380 cm^{-1}, 420 cm^{-1}, 800 and 1400 cm^{-1}. These shifts show the formation of bonding interaction, thus indicating changes in cocrystals chemical environment, which was further supported by SCXRD.

Figure 7 presents the FT–IR spectra (2400–400 cm^{-1}) of the coformers as well as the new cocrystals. The dicarboxylic acids coformers show peaks of varying broadness and intensity corresponding to the bonded and free C=O stretches between 1730–1700 and 1750 cm^{-1} in the malic acid. The multicomponent structures present a moderately broad peak around 1700 ± 10 cm^{-1}, except in the FLZ–DPA case, where it was observed with a sharp peak, indicating that the acids are protonated in the cocrystal structure.

4.1.2. Powder X-ray Diffraction. Figure 8 presents the experimental and calculated PXRD patterns of the synthesized cocrystals, from 5° to 45° (2θ), showing good agreements of peaks and suggesting a high purity level of the cocrystal

DOI: 10.1021/acs.cgd.8b01194
Cryst. Growth Des. 2019, 19, 648–657

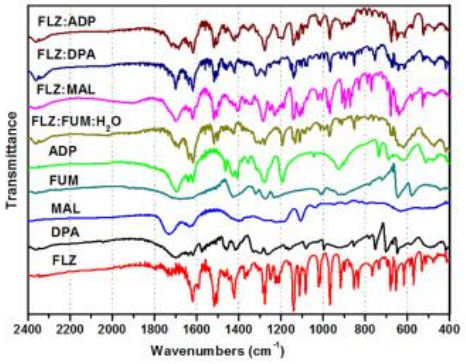

Figure 7. FT-IR spectra of the cocrystals (FLZ−FUM−H_2O, FLZ−MA, FLZ−DPA, and FLZ−ADP), pure cocrystal formers (FUM, MA, DPA and ADP), and pure FLZ drug.

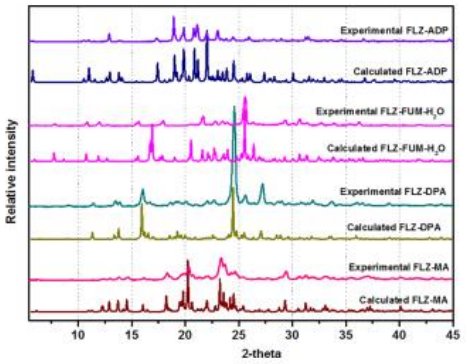

Figure 8. Comparison of the experimental and calculated PXRD patterns of the FLZ cocrystals (FLZ−FUM−H_2O, FLZ−MA, FLZ−DPA, and FLZ−ADP).

samples. Here, the novelty of the individual cocrystals is unquestionable because, apart from the similarities observed from the comparison of their experimental and calculated diffraction patterns, they are also observed to be different from their respective starting materials and other previously FLZ reported forms.

4.1.3. Thermal Analyses (DSC, TGA/DTA, and HSM). Figure 9 presents the DSC/TGA/HSM for the cocrystal systems. According to the literature,[35,36,50] the melting points (MP) of pure starting materials are FLZ (anhydrate Form I: 135−136 °C, anhydrate Form II: 138−140 °C, anhydrate Form III: 137−138 °C, monohydrate: 102.7 and 139.2 °C), ADP acid (152 °C), MA acid (130 °C), DPA acid (248−255 °C), and FUM acid (287 °C). Figure 9a shows the TGA events of the cocrystals, superposed with the DSC experiments to further support the previous results for the cocrystals.

The TGA for FLZ−FUM−H_2O (Figure 9a) shows a mass loss of about 4% to dehydration (4% wt loss = 18.0 g = 1 mol of water) in the 75−175 °C range, which supported the dehydration event of this monohydrate cocrystal. The

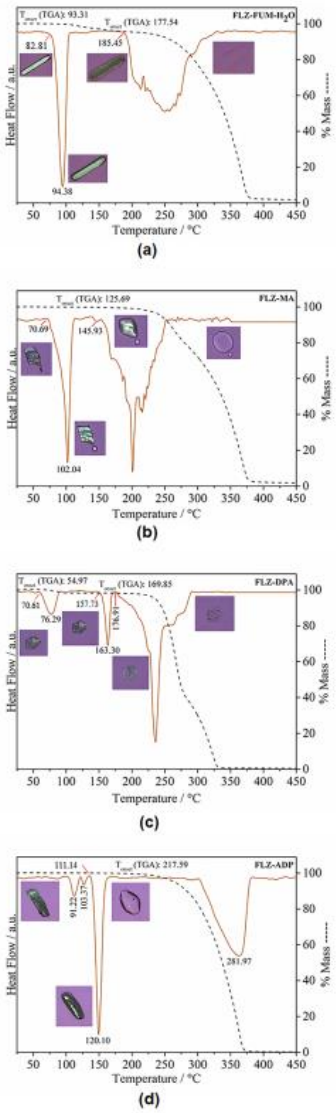

Figure 9. Superposed DSC/TG/HSM analysis obtained for (a) FLZ−FUM−H_2O, (b) FLZ−MA, (c) FLZ−DPA, and (d) FLZ−ADP, showing their melting points, degradation points, and the effect of temperature over one selected crystal.

dehydration is followed by the decomposition. The DSC for the FLZ−FUM−H_2O shows two endothermic peaks, related to the dehydration (94.38 °C) and melting/decomposition

DOI: 10.1021/acs.cgd.8b01194
Cryst. Growth Des. 2019, 19, 648−657

(starting at 185.42 °C) of the cocrystal. The results are compatible with that observed by HSM.

The FLZ−MA cocrystal system presents an endothermic melting peak for the system at onset 70.69 °C, which appears below the melting points of the FLZ and the MA. A broad endothermic peak from the degradation starts at 145.93 °C, promoting a loss of mass stating at 250 °C.

The FLZ−DPA cocrystal system presents two endothermic peaks, at onset 70.61 °C and onset 157.73 °C, and a broad degradation peak starting at onset 176.91 °C. According to the HSM experiment, the middle peak is the cocrystal melting point, with no correlation to the FLZ/DPA MP. On the other hand, the peak at 70.61 °C could be associated with some residual water, since there is a little loss of mass in this event, and neither SCRXD nor Raman present any difference before and after this endothermic event.

The FLZ−ADP cocrystal presents an endothermic peak with onset in 111.14 °C, taken as the melting temperature of this material, with no traces of FLZ/ADP peaks correlation observed in the thermogram. The degradation/ebullition starts around 220 °C. The two small endothermic peaks at 91.22 and 103.37 °C could not be associated with any known source, since there is no loss of mass at this temperature.

The HSM characterization allows the monitoring and mapping of thermal melting events of each cocrystal (unit crystal) showing their physical property transformation due to temperature changes, as also shown in Figure 9. The cocrystals stability and melting points previously confirmed using TGA/DSC were unveiled in these mapping.

4.2. Aqueous Equilibrium Solubility Determination. Solubility in aqueous media is a key parameter among other physicochemical properties for pharmaceutical cocrystals.[10] The FLZ solubility varies according to the polymorphic form used and is slightly pH dependent.[51] Usually, form II is the commercialized one, exhibiting an aqueous solubility range between 4.6 and 8 mg/mL.[36,51] On the other hand, Form I (solubility 4.26 mg/mL) and the monohydrate (solubility 3.56 mg/mL) are the most stable forms of this drug, being both less soluble and exhibiting slow dissolution rates when compared to Form II.[36,51] For Form III, the reported solubility values are 5, 14, and 5 mg/mL at 23 °C in water, 0.1 N HCL, and 0.1 M NaOH, respectively.[51] The aqueous equilibrium solubility for FLZ II bulk powder found in our experiments was around 2 mg/mL (Table 2). This value can be considered in agreement with the expected values for this API, taking into account that, in solution, the FLZ II can easily go to FLZ hydrate form, which is more stable and less soluble. In addition, when the FLZ was cocrystallized with different coformers, the aqueous equilibrium solubility (thermodynamic solubility) of all the cocrystals exhibited superior solubility, even considering only the soluble amount of fluconazole (Table 2): 3.82 mg/mL for the FLZ−ADP, 5.07 mg/mL for the FLZ−MA, 8.75 mg/mL for the FLZ−FUM−H_2O, and 3.22 mg/mL for the FLZ−DPA. This result was expected since the coformers are several times more soluble in water then the FLZ, despite the fact that they are weak acids.

Table 2. Aqueous Equilibrium Solubility of the FLZ Cocrystals in Comparison with the Commercialized Polymorph

structure	molar weight (g/mol)	water solubility mg/mL	% of fluconazole in the cocrystal	water solubility in terms of FLZ (mg/mL)
FLZ Form I[36]	306.27	4.29		4.29
FLZ Form II[36]	306.27	4.6		4.6
FLZ Form III[51]	306.27	5.0		5.0
FLZ monohydrate[36]	306.27	3.56		3.56
FLZ Form II	306.27	1.97		1.97
FLZ−MA	440.36	7.30	69.55	5.07
FLZ−FUM	440.34	12.59	69.55	8.75
FLZ−ADP	452.41	5.65	67.70	3.82
FLZ−DPA	473.39	4.98	64.70	3.22

4.3. Stability Check. Figure 10 shows the PXRD patterns for all the four cocrystals after 1 week under 40 °C and 75% RH, in order to perform an evaluation related to hygroscopicity and phase transition. The diffractograms of FLZ−FUM−H_2O and FLZ−DPA did not exhibit incompatible peaks when compared to the calculated ones. However, extra peaks appear in the FLZ−ADP (such as 29.3, 35.4, and 41.5 2θ°) and FLZ−MA cocrystals (25.9 2θ°), indicating the occurrence of new phases. Regarding the hygroscopicity, FLZ−DPA and FLZ−ADP presented a mass increasing below 1%, while FLZ−FUM−H_2O and FLZ−MA presented an increasing of 1.3% and 2.3%, respectively. The results indicate that all these cocrystals present a low hygroscopicity, but FLZ−ADP and FLZ−MA present a low stability regarding their crystalline phases. Even though FLZ−FUM−H2O and FLZ−DPA did not show changes in their crystalline phases after 1 week at 75% of R.H. and 40 °C, a longer stability study (as well as preformulation and formulation studies) would be needed in order to use them as APIs.

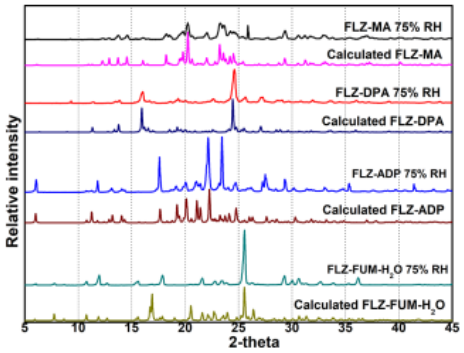

Figure 10. PXRD patterns for all the four cocrystals after 1 week under 40 °C and 75% RH.

5. CONCLUSIONS

In this study, four new cocrystals of the antifungal drug fluconazole were synthesized and characterized by single crystal and PXRD, Raman and FT-IR spectroscopies, thermogravimetric analysis, differential scanning calorimetry, HSM, aqueous solubility, and stability at 75% RH and 40 °C for 1 week. These cocrystals were prepared applying CE principles, aiming to enhance the FLZ water solubility. For achieving this, weak organic acids were selected after matching

DOI: 10.1021/acs.cgd.8b01194
Cryst. Growth Des. 2019, 19, 648−657

their functional groups and geometries in the multicomponent screening wizard available in the Mercury software. Analysis of the crystal structures and packing of these new entities revealed the formation of an O−H···N hydrogen bond between the FLZ molecule and the coformers. Interestingly, similar crystalline packings were observed to occur for the FLZ−MA and the FLZ−ADP cocrystals.

The TGA/DSC results showed that the FLZ−MA and FLZ−ADP exhibited melting points below the one of pure FLZ, and the other cocrystals exhibited melting points above the pure FLZ. On the other hand, the aqueous solubility experiments revealed an inverse relationship; i.e., the highest solubility was attributed to the most stable cocrystals. Nevertheless, all the cocrystals reported herein exhibited improved aqueous equilibrium solubility values when compared to the parent API. Stability studies under 75% RH for 1 week revealed that FLZ−ADP and FLZ−MA exhibited modifications in their PXRD, while FLZ−FUM−H_2O and FLZ−DPA remained unchanged. Further studies are needed in order to use these new structures as alternative choices for composing new pharmaceutical products derived from FLZ.

■ ASSOCIATED CONTENT

Supporting Information

The Supporting Information is available free of charge on the ACS Publications website at DOI: 10.1021/acs.cgd.8b01194.

Crystallographic data of the FLZ cocrystals, including hydrogen bonds and centroids. The calculated X-ray powder diffractograms files of FLZ, pure coformers, and previously reported FLZ forms can be accessed in the CSD via the Mercury program, for comparison (PDF)

Accession Codes

CCDC 1831760−1831763 contain the supplementary crystallographic data for this paper. These data can be obtained free of charge via www.ccdc.cam.ac.uk/data_request/cif, or by emailing data_request@ccdc.cam.ac.uk, or by contacting The Cambridge Crystallographic Data Centre, 12 Union Road, Cambridge CB2 1EZ, UK; fax: +44 1223 336033.

■ AUTHOR INFORMATION

Corresponding Author

*E-mail: renato.lajarim@ufscar.br.

Notes

The authors declare no competing financial interest.

■ ACKNOWLEDGMENTS

The authors acknowledge the Brazilian funding agencies CNPq (B.C.D.O. Grant No. 141901/2017-9 and J.E. No. 305190/2017-2), CAPES (C.C.P.S. and M.S.S), and FAPESP (L.F.D. Grant 2015/25694-0 and R.L.C. Grant 2010/16520-5) for financial support and the equipment support/access granted by the management of LIEC-UFSCar.

■ REFERENCES

(1) Shekunov, B. Y.; York, P. Crystallization processes in pharmaceutical technology and drug delivery design. *J. Cryst. Growth* **2000**, *211*, 122−136.

(2) Groom, C. R.; Bruno, I. J.; Lightfoot, M. P.; Ward, S. C. The Cambridge Structural Database. *Acta Crystallogr., Sect. B: Struct. Sci., Cryst. Eng. Mater.* **2016**, *72*, 171−179.

(3) Xu, Q.; Liu, K.; Lin, X.; Qin, Y.; Chen, L.; Cheng, J.; Zhong, M.; He, Q.; Li, Y.; Wang, T.; Pan, J.; Peng, M.; Yao, L.; Ji, Z. ADMETNet: The knowledge base of pharmacokinetics and toxicology network. *J. Genet. Genomics* **2017**, *44*, 273−276.

(4) Nel, A.; Ruoslahti, E.; Meng, H. New Insights into "Permeability" as in the Enhanced Permeability and Retention Effect of Cancer Nanotherapeutics. *ACS Nano* **2017**, *11*, 9567−9569.

(5) He, H.; Zhang, Q.; Li, M.; Wang, J.-R.; Mei, X. Modulating the Dissolution and Mechanical Properties of Resveratrol by Cocrystallization. *Cryst. Growth Des.* **2017**, *17*, 3989−3996.

(6) Clarke, H. D.; Arora, K. K.; Bass, H.; Kavuru, P.; Ong, T. T.; Pujari, T.; Wojtas, L.; Zaworotko, M. J. Structure−Stability Relationships in Cocrystal Hydrates: Does the Promiscuity of Water Make Crystalline Hydrates the Nemesis of Crystal Engineering? *Cryst. Growth Des.* **2010**, *10*, 2152−2167.

(7) Mannava, M. C.; Suresh, K.; Nangia, A. Enhanced Bioavailability in the Oxalate Salt of the Anti-Tuberculosis Drug Ethionamide. *Cryst. Growth Des.* **2016**, *16*, 1591−1598.

(8) Blessy, M.; Patel, R. D.; Prajapati, P. N.; Agrawal, Y. Development of forced degradation and stability indicating studies of drugs - a review. *J. Pharm. Anal.* **2014**, *4* (3), 159−165.

(9) Shugarts, S.; Benet, L. Z. The role of transporters in the pharmacokinetics of orally administered drugs. *Pharm. Res.* **2009**, *26*, 2039−2054.

(10) Savjani, K. T.; Gajjar, A. K.; Savjani, J. K. Drug solubility: importance and enhancement techniques. *ISRN Pharm.* **2012**, *2012*, 195727.

(11) Liversidge, G. G.; Cundy, K. C. Particle size reduction for improvement of oral bioavailability of hydrofobic drugs: I. Absolute oral bioavailability of nanocrystalline danazol in beagle dogs. *Int. J. Pharm.* **1995**, *125*, 91−97.

(12) Keck, C. M.; Müller, R. H. Drug nanocrystals of poorly soluble drugs produced by high pressure homogenisation. *Eur. J. Pharm. Biopharm.* **2006**, *62*, 3−16.

(13) Baghel, S.; Cathcart, H.; O'Reilly, N. J. Polymeric amorphous solid dispersions: a review of amorphization, crystallization, stabilization, solid-state characterization, and aqueous solubilizaion of Biopharmaceutical Classification System Class II drugs. *J. Pharm. Sci.* **2016**, *105*, 2527−2544.

(14) Serajuddin, A. T. M. Slat formation to improve drug solubility. *Adv. Drug Delivery Rev.* **2007**, *59*, 603−616.

(15) Aakeröy, C. Is there any point in making co-crystals? *Acta Crystallogr., Sect. B: Struct. Sci., Cryst. Eng. Mater.* **2015**, *71*, 387−391.

(16) Barich, D. H.; Zell, M. T.; Munson, E. J. In *Drug Delivery: Principles and Applications*, 2nd ed.; Wang, B., Hu, L., Siahaan, T. J., Eds.; John Wiley & Sons, NJ, 2016; Chapter 3, pp 35−48.

(17) Desiraju, G. R. Crystal engineering: structure, property and beyond. *IUCrJ* **2017**, *4*, 710−711.

(18) Desiraju, G. R. Crystl egineering and IUCrJ. *IUCrJ* **2016**, *3*, 1−2.

(19) Desiraju, G. R.; Nangia, A. Use of the term "crystal engineering" in the regulatory and patent literature of pharmaceutical solid forms. Some comments. *Cryst. Growth Des.* **2016**, *16*, 5585−5587.

(20) Cheney, M. L.; Weyna, D. R.; Shan, N.; Hanna, M.; Wojtas, L.; Zaworotko, M. J. Supramolecular architectures of meloxicam carboxylic acid cocrystals, a crystal engineering case study. *Cryst. Growth Des.* **2010**, *10*, 4401−4413.

(21) Desiraju, G. R. Supramolecular synthons in crystal engineering − a new organic synthesis. *Angew. Chem., Int. Ed. Engl.* **1995**, *34*, 2311−2327.

(22) Mishra, M. K.; Ramamurty, U.; Desiraju, G. R. Mechanical property design of molecular solids. *Curr. Opin. Solid State Mater. Sci.* **2016**, *20*, 361−370.

(23) Desiraju, G. R. Crystal engineering: a holistic view. *Angew. Chem., Int. Ed.* **2007**, *46*, 8342−8356.

(24) Desiraju, G. R. Designer crystals: intermolecular interactions, network structures and supramolecular synthons. *Chem. Commun.* **1997**, No. 16, 1475−1482.

(25) U.S. Food & Drug Administration. http://www.fda.gov/food/ingredientspackaginglabeling/gras/default.htm, 2018.

DOI: 10.1021/acs.cgd.8b01194
Cryst. Growth Des. 2019, 19, 648−657

(26) Desiraju, G. R. Hydrogen bonds in crystal engineering: interactions without borders. *Acc. Chem. Res.* **2002**, *35*, 565−573.
(27) Schultheiss, N.; Newman, A. Pharmaceutical cocrystals and their physicochemical properties. *Cryst. Growth Des.* **2009**, *9*, 2950−2967.
(28) Cheney, M. L.; Weyna, D. R.; Shan, N.; Hanna, M.; Wojtas, L.; Zaworotko, M. J. Coformer selection in pharmaceutical cocrystal development: a case study of a meloxicam aspirin cocrystal that exhibits enhanced solubility and pharmacokinetics. *J. Pharm. Sci.* **2011**, *100*, 2172−2181.
(29) *Martindale The Complete Drug Reference*, 38th ed.; Brayfield, A., Ed.; Pharmaceutical Press: London, UK, 2014.
(30) Ferreira, L. R.; Sousa, A. S.; Alvarenga, L. H.; Deana, A. M.; de Santi, M. E. O. S.; Kato, I. T.; Leal, C. R. L.; Ribeiro, M. S.; Prates, R. A. Antimicrobial photodynamic therapy on *Candida albicans* pre-treated by fluconazole felayed yeast inactivation. *Photodiagn. Photodyn. Ther.* **2016**, *15*, 25−27.
(31) Sungkanuparph, S.; Savetamornkul, C.; Pattanapongpaiboon, W. Primary prophylaxis for *Cryptococcosis* with fluconazole in human immunodeficiency virus − infected patients with CD4 T-cell counts < 100 cells/μL and receiving antiretroviral theraphy. *Clin. Infect. Dis.* **2017**, *64*, 967−970.
(32) Richardson, K.; Cooper, K.; Marriott, M.; Tarbit, M.; Troke, F.; Whittle, P. Discovery of fluconazole, a novel antifungal agent. *Clin. Infect. Dis.* **1990**, *12*, S267−S271.
(33) Gu, X.; Jlang, W. Characterization of polymorphic forms of fluconazole using Fourier Transform Raman spectroscopy. *J. Pharm. Sci.* **1995**, *84*, 1438−1441.
(34) Yang, Y.-L.; Ho, Y.-A.; Cheng, H.-H.; Ho, M.; Lo, H.-J. Susceptibilities of *Candida* species to amphotericin B and fluconazole: the emergence of fluconazole resistance in *Candida tropicalis*. *Infect. Control Hosp. Epidemiol.* **2004**, *25*, 60−64.
(35) Dash, A. K.; Elmquist, W. F. In *Profiles of Drug Substances, Excipients and Related Methodology*; Brittain, H. G., Ed.; Academic Press: San Diego, CA, 2001; Vol 27, pp 67−113.
(36) Alkhamis, K. A.; Obaidat, A. A.; Nuseirat, A. F. Solid-state characterization of fluconazole. *Pharm. Dev. Technol.* **2002**, *7*, 491−503.
(37) Karanam, M.; Dev, S.; Choudhury, A. R. New polymorphs of fluconazole: results from crystallization experiments. *Cryst. Growth Des.* **2012**, *12*, 240−252.
(38) Hall, S. R.; Allen, F. H.; Brown, I. D. The crystallographic information file (CIF): a new standard archive file for crystllography. *Acta Crystallogr., Sect. A: Found. Crystallogr.* **1991**, *47*, 655−685.
(39) Otwinowski, Z.; Minor, W. [20] Processing of X-ray diffraction data collected in oscillation mode. *Methods Enzymol.* **1997**, *276*, 307−326.
(40) Kastelic, J. e.; Hodnik, Z. i.; Šket, P.; Plavec, J.; Lah, N.; Leban, I.; Pajk, M.; PlaninŠek, O.; Kikelj, D. Fluconazole cocrystals with dicarboxylic acids. *Cryst. Growth Des.* **2010**, *10*, 4943−4953.
(41) Park, H. J.; Kim, M.-S.; Kim, J.-S.; Cho, W.; Park, J.; Cha, K.-H.; Kang, Y.-S.; Hwang, S.-J. Solid-state carbon NMR characterization and investigation of intrinsic dissolution behavior of fluconazole polymorphs, anhydrate forms I and II. *Chem. Pharm. Bull.* **2010**, *58*, 1243−1247.
(42) Caira, M. R.; Alkhamis, K. A.; Obaidat, R. M. Preparation and crystal characterization of a polymorph, a monohydrate, and an ethyl acetate solvate of the antifungal fluconazole. *J. Pharm. Sci.* **2004**, *93*, 601−611.
(43) Allen, F. H. The Cambridge Structural Database: a quarter of a million crystal structures and rising. *Acta Crystallogr., Sect. B: Struct. Sci.* **2002**, *58* (3), 380−388.
(44) Macrae, C. F. B.; Bruno, I. J.; Chisholm, J. A.; Edgington, P. R.; McCabe, P.; Pidcock, E.; Rodriguez-Monge, L.; Taylor, R.; van de Streek, J.; Wood, P. A. Mercury CSD 2.0 − new features for the visualization of crystal structures. *J. Appl. Crystallogr.* **2008**, *41*, 466−470.
(45) *CrysAlis PRO*; Agilent: Yarnton, England, 2010.
(46) Dolomanov, O. V.; Bourhis, L. J.; Gildea, R. J.; Howard, J. A.; Puschmann, H. OLEX2: a complete structure solution, refinement and analysis program. *J. Appl. Crystallogr.* **2009**, *42*, 339−341.
(47) Sheldrick, G. M. *Program for the Refinement of Crystal*; University of Gottingen: Germany. 1997.
(48) Farrugia, L. J. WinGX and ORTEP for Windows: an update. *J. Appl. Crystallogr.* **2012**, *45*, 849−854.
(49) Farrugia, L. J. ORTEP-3 for Windows − a version of ORTEP-III with a graphical user interface (GUI). *J. Appl. Crystallogr.* **1997**, *30*, 565−565.
(50) The Pubchem Project, https://pubchem.ncbi.nlm.nih.gov/, 2018.
(51) Charoo, N.; Cristofoletti, R.; Graham, A.; Lartey, P.; Abrahamsson, B.; Groot, D. W.; Kopp, S.; Langguth, P.; Polli, J.; Shah, V. P.; Dressman, J. Biowaiver monograph for immediate-release solid oral dosage forms: fluconazole. *J. Pharm. Sci.* **2014**, *103*, 3843−3858.

DOI: 10.1021/acs.cgd.8b01194
Cryst. Growth Des. 2019, 19, 648−657